

**SYNTHESIS AND CHARACTERIZATION OF
BIMETALLIC GOLD-SILVER (Au-Ag) NANOCATALYST
VIA SEED COLLOID TECHNIQUE**

NURAFALIANA BINTI BERAHIM

**DISSERTATION SUBMITTED IN FULFILMENT OF THE
REQUIREMENTS FOR THE DEGREE OF MASTER OF
ENGINEERING SCIENCE**

**FACULTY OF ENGINEERING
UNIVERSITY OF MALAYA
KUALA LUMPUR**

2020

UNIVERSITI MALAYA

ORIGINAL LITERARY WORK DECLARATION

Name of Candidate: Nurafaliana binti Berahim

Registration/Matric No: KGA150079

Name of Degree: Master of Engineering Science

Title of Project Paper/Research Report/Dissertation/Thesis ("this Work"):

Synthesis and characterization of bimetallic gold-silver (Au-Ag) nanocatalyst via seed colloid technique

Field of Study: Nanomaterials

I do solemnly and sincerely declare that:

- (1) I am the sole author/writer of this Work;
- (2) This Work is original;
- (3) Any use of any work in which copyright exists was done by way of fair dealing and for permitted purposes and any excerpt or extract from, or reference to or reproduction of any copyright work has been disclosed expressly and sufficiently and the title of the Work and its authorship have been acknowledged in this Work;
- (4) I do not have any actual knowledge nor do I ought reasonably to know that the making of this work constitutes an infringement of any copyright work;
- (5) I hereby assign all and every rights in the copyright to this Work to the University of Malaya ("UM"), who henceforth shall be owner of the copyright in this Work and that any reproduction or use in any form or by any means whatsoever is prohibited without the written consent of UM having been first had and obtained;
- (6) I am fully aware that if in the course of making this Work I have infringed any copyright whether intentionally or otherwise, I may be subject to legal action or any other action as may be determined by UM.

Candidate's Signature

Date:

Subscribed and solemnly declared before,

Witness's Signature

Date:

Name:

Designation:

SYNTHESIS AND CHARACTERIZATION OF BIMETALLIC GOLD-SILVER (Au-Ag) NANOCATALYST VIA SEED COLLOID TECHNIQUE

ABSTRACT

In the present study, unique catalysts of monometallic gold (Au), silver (Ag) and bimetallic gold-silver (Au-Ag) nanoparticles (NPs) were prepared with different size or diameters by the citrate-thermal reduction and the seed colloidal techniques, respectively. The catalytic nanoparticles were characterized by various advanced analytical techniques such as Ultraviolet-visible spectroscopy (UV-vis), zeta potential, electron dispersive X-ray spectroscopy (EDS), X-ray diffraction (XRD), high-resolution transmission electron microscopy (HRTEM), High-angle annular dark-field (HAADF) scanning transmission-electron microscopy (STEM) imaging and the energy dispersive spectroscopy (EDS) elemental mapping. The catalytic performance of the nanoparticles were ascertained through the reduction of 4-nitrophenol (4-NP) to 4-aminophenol (4-AP) in the presence of sodium borohydride (NaBH_4). The results of the study clearly showed that the rate of 4-NP reduction to 4-AP increased with a corresponding decrease in the size or diameter of the bimetallic NPs. The Au seed volume of 5.0 ml indicated relatively higher reduction rates as compared to that of 2.0 ml. However, the monometallic NPs showed relatively lesser catalytic activity in the reductive conversion of 4-NP to 4-AP. The catalytic properties of the bimetallic Au-Ag nanoparticles also reinforced with a direct impact of the size and composition of the bimetallic nanoparticles.

SINTESIS DAN PERCIRIAN DWI-LOGAM EMAS-PERAK (Au-Ag) PEMANGKIN NANO MELALUI BENIH KOLOID

ABSTRAK

Dalam kajian ini, nanozarah emas (Au), perak (Ag) dan dwi-logam emas-perak (Au-Ag) dengan saiz atau diameter berbeza sebagai pemangkin unik telah disintesis oleh pengurangan haba sitrat dan benih koloid teknik masing-masing. Zarah nano pemangkin telah dicirikan oleh pelbagai teknik analisis seperti spektroskopi sinar ultra ungu-dilihat (UV-vis), potensi zeta, spektroskopi sinar-X dispersi elektron (EDS), X-ray difraksi (XRD), mikroskop elektron penghantaran resolusi tinggi (HRTEM), pengitaran medan mikroskopi elektron penglihatan gelap sudut tinggi (HAADF-STEM) dan pemetaan unsur spektroskopi (EDS) penyebaran tenaga. Keupayaan pemangkin zarah nano telah ditentukan dalam pengurangan 4-nitrofenol (4-NP) kepada 4-aminofenol (4-AP) dengan kehadiran natrium borohidrida (NaBH_4). Hasil kajian dengan jelas menunjukkan bahawa kadar pengurangan 4-NP kepada 4-AP meningkat dengan pengurangan saiz atau diameter dwi-logam zarah nanopartikel. Isipadu bijih Au 5.0 ml menunjukkan kadar pengurangan yang lebih tinggi berbanding dengan 2.0 ml. Walau bagaimanapun, zarah nanopartikel satu logam menunjukkan aktiviti pemangkin yang lebih rendah terhadap penukaran pengurangan 4-NP kepada 4-AP. Sifat pemangkin nanopartikel dwi-logam Au-Ag diperkuat dengan kesan langsung terhadap saiz dan komposisi relatif zarah nanopartikel dwi-logam tersebut.

ACKNOWLEDGEMENTS

“In the Name of Allah, the Most Benevolent, the Most Merciful”

First of all, I would like to express my deepest appreciation to my supervisors; Professor Dr. Hj. Mohd Rafie bin Johan and Professor Dr. Wan Jeffrey bin Basirun for giving me the valuable opportunity to conduct this research. His continuing guidance and advice throughout this research are indeed valuable to me. Besides, they supported me in all stages of this work. They are the initiator of this project and always gave me constant encouragement and advice in spite of their tight schedule. Without their coherent and illuminating instruction, this thesis would not have reached its present form.

In addition, I would like to thank to my lab mates who helped me and shared their knowledge throughout this research. I also like to show my appreciation to lab assistants, which are Mrs. Norzirah, Mr. Said and others for helping me on the uses of equipment and machine. And also thank you to Centre for Research Grant Management for awarding this particular research, a Postgraduate Research Grant (PPP) (PG040-2016A) and MyBrain 15 which sponsored me.

Gracious thanks to my family for their support especially my parents, parent in laws, husband, siblings and daughter. With their support, I can achieve my goals. I love you all and thank you for your support.

Above all, I owe it all to Almighty God for granting me the wisdom, health and strength to undertake this research task and enabling me to its completion.

TABLE OF CONTENTS

ORIGINAL LITERARY WORK DECLARATION	II
ABSTRACT	III
ABSTRAK	IV
ACKNOWLEDGEMENTS	V
TABLE OF CONTENTS	VI
LIST OF FIGURES	IX
LIST OF TABLES	XII
LIST OF SYMBOLS AND ABBREVIATIONS	XIII
CHAPTER ONE	1
INTRODUCTION.....	1
1.1 BACKGROUND.....	1
1.2 PROBLEM STATEMENT.....	5
1.3 RESEARCH OBJECTIVES	6
1.4 SCOPE OF THE RESEARCH	7
1.5 OUTLINE OF THE THESIS	8
CHAPTER TWO.....	9
LITERATURE REVIEW.....	9
2.1 INTRODUCTION.....	9
2.2 GOLD NANOPARTICLES	111
2.3 SILVER NANOPARTICLES	13
2.4 BIMETALLIC NANOPARTICLES	16

2.4.1 BIMETALLIC GOLD-SILVER NANOPARTICLES	21
2.4.2 SYNTHESIS OF BIMETALLIC NANOPARTICLES	23
2.5 4-NITROPHENOL.....	27
CHAPTER THREE.....	333
RESEARCH METHODOLOGY	333
3.1 MATERIALS	333
3.2 SAMPLES PREPARATION.....	34
3.2.1 SYNTHESIS OF GOLD NANOPARTICLES	34
3.2.2 SYNTHESIS OF SILVER NANOPARTICLES	35
3.2.3 SYNTHESIS OF GOLD-SILVER NANOPARTICLES	36
3.2.4 CATALYTIC ACTIVITY REDUCTION OF 4-NP.....	38
3.3 CHARACTERIZATION TECHNIQUES.....	40
3.3.1 UV-VIS SPECTROSCOPY (UV-VIS).....	40
3.3.2 TRANSMISSION ELECTRON MICROSCOPY (TEM)	41
3.3.3 ENERGY DISPERSIVE X-RAY SPECTROSCOPY (EDS).....	42
3.3.4 X-RAY DIFFRACTION (XRD).....	44
3.3.5 HIGH RESOLUTION ELECTRON MICROSCOPY (HRTEM)	45
3.3.6 ZETA POTENTIAL.....	46
3.3.7 HIGH ANGLE ANNULAR DARK FIELD SCANNING TRANSMISSION ELECTRON MICROSCOPY	47
3.3.8 CATALYTIC ACTIVITY REDUCTION OF 4-NP.....	48
CHAPTER FOUR.....	49
RESULTS AND DISCUSSION	49
4.1 INTRODUCTION	49
4.2 UV-VISIBLE (UV-VIS) ANALYSIS	49

4.3 MORPHOLOGICAL AND PHYSICAL SIZE STUDIES	54
4.3.1 TRANSMISSION ELECTRON MICROSCOPY (TEM) ANALYSIS.....	54
4.3.2 ELECTRON DISPERSIVE X-RAY SPECTROSCOPY (EDS) ANALYSIS	59
4.3.3 ZETA POTENTIAL ANALYSIS	62
4.3.4 HIGH RESOLUTION TRANSMISSION ELECTRON MICROSCOPY (HRTEM) ANALYSIS	64
4.3.5 HIGH ANGLE ANNULAR DARK FIELD SCANNING TRANSMISSION ELECTRON MICROSCOPY (HAADF-STEM) ANALYSIS.....	65
4.4 STRUCTURAL STUDIES.....	70
4.4.1 X-RAY DIFFRACTION (XRD) ANALYSIS.....	70
4.5 CATALYTIC STUDIES	72
CHAPTER FIVE.....	88
CONCLUSION.....	88
5.1 CONCLUSION	88
5.2 FUTURE RECOMMENDATIONS	89
REFERENCES.....	90
LIST OF PUBLICATIONS	112
APPENDICES.....	113
APPENDIX A: FRONT PAGE OF PUBLISHED PAPER FROM THIS WORK.....	113
APPENDIX B: CALCULATION ON SURFACE AREA OF NANOPARTICLES.....	113

LIST OF FIGURES

Figure 2.1 Types of bimetallic nanoparticles.....	17
Figure 2.2 Schematic of core shell nanoparticles.....	19
Figure 2.3 Structures of bimetallic nanoparticles.....	20
Figure 2.4 TEM images of samples at different dropping time.....	26
Figure 2.5 Molecular structure of 4-NP.....	28
Figure 2.6 UV-vis absorbance for reduction nitrophenol using Pd nanowires, Au-Ag bimetallic nanocomposites, Ag nanoparticles, Pd/G and Au-Ag nanocages.....	29
Figure 3.1 Schematic diagram of Au nanoparticles preparation procedures.....	35
Figure 3.2 Schematic diagram of Ag nanoparticles preparation procedures.....	36
Figure 3.3 Seed colloid synthesis process routes for Au-Ag nanoparticles.....	37
Figure 3.4 Flowchart of sample preparation for Au, Ag and Au-Ag nanoparticles.....	39
Figure 3.5 UV-Visible spectrophotometer.....	41
Figure 3.6 TEM machine.....	42
Figure 3.7 FESEM machine equipped with EDS.....	43
Figure 3.8 Thin film by drop coating of the Au, Ag and Au-Ag nanoparticles on glass slide.....	44
Figure 3.9 XRD machine.....	45
Figure 3.10 HRTEM machine.....	46
Figure 3.11 Zeta-sizer instrument.....	47
Figure 4.1 UV-Vis absorption spectra for Au nanoparticles.....	50

Figure 4.2 UV-Vis absorption spectra for Ag nanoparticles.....	51
Figure 4.3 UV-Vis absorption spectra for Au-Ag nanoparticles.....	53
Figure 4.4 TEM image of Au nanoparticles.....	55
Figure 4.5 Particle size distribution of Au nanoparticles.....	55
Figure 4.6 TEM image Ag nanoparticles.....	56
Figure 4.7 Particle size distribution of Ag nanoparticles.....	56
Figure 4.8 TEM image of Au-Ag NPs with 2.0 ml Au seeds volume.....	57
Figure 4.9 Particle distribution of Au-Ag NPs with 2.0 ml Au seeds volume.....	57
Figure 4.10 TEM image of Au-Ag NPs with 5.0 ml Au seeds volume.....	58
Figure 4.11 Particle size distribution of Au-Ag NPs with 5.0 ml Au seeds volume.....	58
Figure 4.12 EDS spectra of Au NPs.....	60
Figure 4.13 EDS spectra of Ag NPs.....	60
Figure 4.14 EDS spectra of Au-Ag NPs at 2.0 ml Au seeds volume.....	61
Figure 4.15 EDS spectra of Au-Ag NPs at 5.0 ml Au seeds volume.....	61
Figure 4.16 Electro-kinetic parameters of Au, Ag and Au-Ag nanoparticles.....	63
Figure 4.17 HRTEM images of Au-Ag bimetallic NPs for different volume of Au seed.....	64
Figure 4.18 HRTEM images of lattice spacing of Au-Ag NPs.....	65
Figure 4.19 HAADF-STEM image of 2.0 ml Au seeds of Au-Ag NPs at magnification 100 nm.....	66
Figure 4.20 HAADF-STEM image of 2.0 ml Au seeds of Au-Ag NPs at magnification 200 nm.....	67
Figure 4.21 Elementals mapping 2.0 ml Au seeds of Au-Ag NPs	67
Figure 4.22 HAADF-STEM image of 5.0 ml Au seeds of Au-Ag NPs at	

magnification 100 nm.....	68
Figure 4.23 HAADF-STEM image of 5.0 ml Au seeds of Au-Ag NPs at	
magnification 200 nm.....	69
Figure 4.24 Elementals mapping 5.0 ml Au seeds of Au-Ag NPs	69
Figure 4.25 XRD patterns of Au NPs, Ag NPs, and Au-Ag NPs.....	71
Figure 4.26 Schematic illustration of the catalytic experiments of 4-NP with Au,	
Ag and Au-Ag nanoparticles.....	72
Figure 4.27 Absorption spectra of 4-NP without reducing agent.....	76
Figure 4.28 Absorption spectra of 4-NP reduced by NaBH ₄ only, Au,	
Ag and Au-Ag nanoparticles.....	79
Figure 4.29 Schematic surfaces of a metal in face-centered cubic (FCC).....	83
Figure 4.30 Plot of ln (A ₀ /A _t) versus time for the determination of rate constants for	
NaBH ₄ only, Au, Ag and Au-Ag nanoparticles.....	84

LIST OF TABLES

Table 2.1 Physical properties of 4-nitrophenol.....	28
Table 2.2 Comparison of rate constant, amount catalyst, and particle size of different catalyst for the 4-NP reduction.....	32
Table 3.1 Experimental conditions for the bimetallic Au-Ag nanoparticle.....	37
Table 4.1 Particle size and zeta potential for Au NPs, Ag NPs and bimetallic Au-Ag NPs.....	63
Table 4.2 Summary of the catalytic reduction of 4-NP by Au, Ag and Au-Ag catalysts.....	87

LIST OF SYMBOLS AND ABBREVIATIONS

$^{\circ}\text{C}$	Degree Celsius
$^{\circ}$	Degree
at. %	Atomic percent
aq	Aqueous
d	Spacing between the planes in the atomic lattice
E_0	Standard Electrode Potential
eV	Electron-Volt
g	Grams
k	Rate constant
kV	Kilo-Volt
M	Molality
Min^{-1}	Per minute
ml	Mililiter
mM	Milli-Molality
mV	Milli-Volt
nm	Nanometer
V	Volt
wt. %	Weight percent
θ	Angle between the incident ray and the scattered plane
λ	Wavelength of x-rays, and moving electrons, protons, and neutrons
μm	Micrometer
\AA	Angstrom

4-AP	4-aminophenol
4-NP	4-nitrophenol
A_0	Initial absorbance
A_t	Absorbance at specific time
Ag	Silver
Ag^+	Silver ion
$AgNO_3$	Silver nitrate
AP	Aminophenol
Au	Gold
Au^{3+}	Gold (III) ion
Au-Ag	Gold-silver
BF-STEM	Bright Field-Scanning Transmission Electron Microscopy
BH_4^-	Borohydride anion
BNPs	Bimetallic nanoparticles
$C_6H_8O_6$	L-ascorbic acid
EPA	Environmental Protection Agency, 1984
EDX	Energy Dispersive X-ray
FCC	Face-centered cubic
G	Graphene
GO	Graphene oxide
FESEM	Field Emission Scanning Electron Microscopy
HAADF	High Annular Angle Dark Field
$HAuCl_4$	Gold (III) chloride
HRTEM	High Resolution Transmission Electron Microscopy
LSPR	Localized Surface Plasmon Resonance
$Na_3C_6H_5O_7$	Trisodium Citrate

NaBH ₄	Sodium borohydride
NHE	Normal Hydrogen Electrode
NP	Nitrophenol
NPs	Nanoparticles
Pd	Palladium
Pt	Platinum
SERS	Surface Enhanced Raman-Scattering
SPR	Surface Plasmon Resonance
TEM	Transmission Electron Microscopy
UM	University of Malaya
UV-Vis	Ultraviolet Visible Spectroscopy
XRD	X-ray Diffraction
Z	Atomic number

CHAPTER ONE

INTRODUCTION

1.1 Background

In recent years, the field of nanomaterials becomes one of the most active areas in materials science with impressive developments. Examples of applications of nanomaterials are including in medicine, industry, defense and others sectors.

Nanomaterials can be defined as the synthesis, characterization, exploration and application of nanometer scale (1-100 nm) materials (Bhatia et al., 2018). It deals with the materials whose structures exhibit significantly novel and improved physical, chemical and biological properties, phenomena, and functionality due to their nano scaled size (Chen et al., 2017). In addition, nanomaterials have distinct properties compared to the bulk materials owing to larger surface-to-volume ratio, thus offering developments towards biosensors, biomedicine and bionanotechnology fields (Pandey et al., 2008).

Noble metal have attracted researchers due to their size-dependent optical, magnetic and catalytic properties. However, the combination between two different types of metals could enhance the physicochemical properties compared to the corresponding monometallic nanoparticles (Xu et al., 2005). Bimetallic nanoparticles (NPs) also have received increased attention due to their optical, electronic, magnetic and catalytic properties which are different from the individual metallic counterpart (Guha et al., 2011). Sanyal *et al.*, (2013) defined the structure of bimetallic nanoparticles as composed of two different elements which are organized in a core@shell structure or a randomly dispersed

alloy (Sanyal et al., 2013). A number of physical and chemical methods have been used to synthesize the bimetallic nanoparticles such as chemical reduction and seed growth (Zhang et al., 2012). Numerous kinds of bimetallic structures have been reported with different combinations; such as Au-Ag (Abood et al., 2018; Fauzia et al., 2019; Liu et al., 2016; Tanori et al., 2016; Yuan et al., 2015), Au-Cu (Barroso-Martin et al., Hsia et al., 2016; Shabani et al., 2016; Tanori et al., 2016), Ag-Cu (Shabani et al., 2016; Tanori et al., 2016; Tsuji et al., 2010; Zhang et al., 2017), Ag-Au (Cao et al., 2001; Emam et al., 2017; Shmarakov et al., 2017).

Among the bimetallic nanostructures, the Au-Ag system is of particular interest because of several reasons. First, the Au-Ag system has superior plasmonic response with tunable surface plasmon (SP) bands in the visible range between Au (520 nm) and Ag (400 nm) (Alshammari et al., 2006; Dai et al., 2017; Shore et al., 2011). Second, gold and silver have the same crystal structure which is face-centered cubic (FCC), with similar lattice constants of Au (0.479 nm) and Ag (0.486 nm) (Lu et al., 2013; Mahmud et al., 2019; Monga & Pal, 2015; Rodríguez-González et al., 2005; Xu et al., 2005; Zeng et al., 2015; Zhang et al., 2018). Therefore the preparation methods are quite facile and simple. In addition, silver has lower cost while gold possesses excellent chemical stability and ease of synthesis (Li et al., 2016; Liu et al., 2015; Pande et al., 2007). Both selected metallic nanoparticles also possess good catalytic activity towards reduction of the aromatic nitro compounds to amine derivatives (Rather et al., 2016).

There are various methods employed to prepare bimetallic Au-Ag NPs such as successive reduction (Zhang et al., 2018), laser ablation (Abood et al., 2018; Shukri et al., 2018), solvent extraction-reduction (Chen & Chen, 2002), microemulsion (Chen & Chen, 2002; Mahmud et al., 2019), galvanic replacement (Admala, 2017; Carrillo-Torres et al.,

2016; Sun & Li, 2018), seed-mediated growth (Wang et al., 2016; Yaseen et al., 2018), and colloidal synthesis (Arora et al., 2018; Zhang et al., 2012). Colloidal synthesis is one of the most commonly used because it offers a great variety of options for composition, size, crystal structure, shape and surface chemistry control due to the flexibility in selecting the reaction system and synthesis conditions (Arora et al., 2018; Zhang et al., 2012). In addition, this method also possesses an advantage towards surface catalysis reactions (McGilvray et al., 2012). Czaplinska and co-workers (2014) stated that the preparation procedures of bimetallic NPs can improve their catalytic reduction reaction by tuning the size, structure, composition and distribution. Fu *et al.*, (2018) prepared bimetallic Au-Ag NPs through the co-reduction method and their catalytic properties was tested by the reduction of 4-nitrophenol.

Apart from sensor and biomedical applications, catalytic applications of bimetallic nanoparticles is an interesting phenomenon due to the synergistic effects between the two metals (Alshammari et al., 2016; Hong et al., 2016; Knauer et al., 2014; Liu et al., 2015; Rodríguez-González et al., 2005; Shore et al., 2011; Tan et al., 2016; Yang et al., 2008; Zeng et al., 2015). In the structure of bimetallic nanoparticles, the type of elements used play important roles in the catalytic activity. Chen *et al.*, (2014) reported the catalytic activity of 4-NP reduction using Au-Pd on graphene nanosheets showed a higher rate in comparison with monometallic counterparts due to the synergistic effect of Au and Pd species. Tuo *et al.*, (2017) prepared bimetallic Pd-Pt for reduction 4-nitrophenol via reduction method and result shown the bimetallic Pd-Pt a higher catalytic activity than those of monometallic Pd and Pt. While Gopalakrishnan *et al.*, (2015) reported the influence of the bimetallic Au-Ag nanoparticles in catalytic applications with regards to the alloying element and concentration.

In chemical industries, 4-nitrophenol (4-NP) is widely utilized for the production of pesticides, drugs and synthetic dyes (Hong et al., 2016; Sun et al., 2014; Zhang et al., 2007; Zelekew & Kuo, 2016). 4-aminophenol (4-AP) which can be produced from the reduction of 4-NP, is widely used in manufacturing of many analgesics and antipyretic drugs, such as paracetamol, phenacetin and so on. From that, there is a great demand for aromatic amino compounds in the industry (Arora et al., 2018). Therefore, many researchers have fabricated efficient catalysts such as Au NPs (Dong et al., 2012; Ghosh et al., 2012; Li et al., 2014; Luo et al., 2014; Premkumar et al., 2011; Yang et al., 2013), Ag NPs (Kalantari et al., 2017; Yang et al., 2013), SiO₂@Au nanoring (You et al., 2012), trimetallic Ag-Au-Pd NPs (Suwannarat et al., 2018), Ag-TiO₂ (Gu et al., 2018), Ag-Pd nanoclusters (Zhu et al., 2018), Pd-P NPs (Zhao et al., 2018), Pd-Ni NPs (Revathy et al., 2018), Ag-Pd NPs (Feng et al., 2020), Cu₂O NPs (Rath et al., 2018), and Au-Ag nanocages (Hong et al., 2016) for the reduction of nitro compounds to amines.

In this work, the effect of the different type of nanoparticles (monometallic and bimetallic) on the 4-nitrophenols reduction in the presence of sodium borohydride was investigated. The model reaction of the reduction of 4-NP to 4-AP is selected as the reaction kinetics can be easily monitored by UV-Vis spectroscopy, via the color changes from the conversion of 4-nitrophenolate to 4-aminophenol. The reduction of 4-nitrophenols was further studied with different sizes of the bimetallic nanoparticles. The preparation of bimetallic Au-Ag NPs by seed colloidal technique was introduced to control the shape and size of nanoparticles through the temporal separation of the nucleation and growth processes (Kalantari et al., 2017; Ko & Chang, 2014; Wang et al., 2016). The pre-formed seeds of one metal act as nucleation sites for the further growth of the second metal NPs (Emam, 2019; Jana et al., 2001; You et al., 2012).

In addition, this method does not require expensive equipment but can be used to produce nanoparticles in a liquid dispersion, which is the desirable form for many applications (Zhang et al., 2012).

1.2 Problem Statement

As known, 4-nitrophenol could inflict damage to the central nervous system, liver, blood and kidney of living organisms. In addition, it can also induce the production of highly toxic and poorly degradable biological pollutants. However, it is widely used in chemical industries such as pesticides, synthetic dyes and drugs production. 4-AP also is extensively used in the manufacturing of many analgesics and antipyretic drugs (Sarmah et al., 2013). In this respect, numerous types of catalysts were fabricated from different materials for the reduction of 4-nitrophenol which resulted in different reaction rates in the reduction of 4-nitrophenol. The selection of a material is the most important factors in the 4-nitrophenol reduction. It has been widely reported that bimetallic nanoparticles has become an ideal material that possesses better catalytic properties compared to monometallic nanoparticles due to synergistic effects between the two distinct metal elements (Hareesh et al., 2019; Wu et al., 2013). The combination of gold and silver elements show better catalytic performance towards the reduction of the aromatic nitro compounds to amine derivatives compared to their single form (Hareesh et al., 2019; Seo et al., 2017). The bimetallic Au-Ag nanoparticles have been prepared using seed colloid method. This method has been selected because the produced nanoparticles in a liquid state which suitable for many application and easy to control the size of nanoparticles.

For solution-based technique, the nucleation and growth process of bimetallic nanoparticles can be easily controlled by adjusting the reaction parameters such as the reaction temperature, the concentration of precursors and the mole ratio precursors to surfactants (Dehghan Banadaki et al., 2014). Difference in size of bimetallic Au-Ag nanoparticles varies by changing the volume of Au seed volume. This will promise the tunable of size bimetallic nanoparticles may improve the reduction of 4-nitrophenol.

1.3 Research Objectives

Specifically, this research has the following objectives:

1. To synthesize Au, Ag and bimetallic Au-Ag nanoparticles via citrate thermal reduction and seed colloid techniques.
2. To characterize the Au, Ag and bimetallic Au-Ag nanoparticles using techniques such as UV-Visible (UV-Vis), Transmission Electron Microscopy (TEM), Energy Dispersive X-Ray Spectroscopy (EDS), X-ray Diffraction (XRD), High Resolution Transmission Electron Microscopy (HRTEM), Zeta Potential and High Angle Annular Dark-Field Scanning Transmission Electron Microscopy (HAADF-STEM).
3. To investigate the reduction of 4-nitrophenol using two different type of nanoparticles; monometallic (Au and Ag) and bimetallic (Au-Ag).

1.4 Scope of the research

The study of the study involves the synthesis and characterization of; (a) monometallic Au and Ag nanoparticles and (b) bimetallic Au-Ag nanoparticles. Initially, the gold and silver were prepared by citrate thermal reduction technique. This was followed by the preparation of gold-silver nanoparticles by a seed colloid method. Afterwards, the gold-silver nanoparticles were prepared at different volumes of HAuCl_4 solution but with a fixed volume of AgNO_3 solution. These samples were used as a catalyst for the reduction of 4-NP to 4-AP in the presence of sodium borohydride (NaBH_4) solution.

UV-visible (UV) spectroscopy, transmission electron microscopy (TEM), X-ray diffraction (XRD), energy dispersive X-ray spectroscopy (EDS), zeta potential, high resolution transmission electron microscopy (HRTEM), and high angle annular dark field scanning transmission electron microscopy (STEM) characterizations were performed to investigate the physical and chemical properties of the nanocatalysts.

This research investigates the preparation and characterization of monometallic Au, Ag and bimetallic Au-Ag nanoparticles for the 4-NP reduction. The monometallic particle consists of a single element, while the bimetallic consists of two different elements. The bimetallic nanoparticles is composed of two different elements which are organized in a core-shell structure or a randomly dispersed alloy. The bimetallic nanoparticles have better catalytic properties than the monometallic nanoparticles. In addition, the difference in the size of nanoparticles also influences the catalytic properties. The Au-Ag nanoparticles was prepared through the seed colloidal technique. This is an efficient method to control the size and shape of the bimetallic core-shell nanoparticles.

The bimetallic Au-Ag nanoparticles are prepared at different volumes of Au seed; 2.0 ml and 5.0 ml. The volume of silver nitrate, ascorbic solution and sodium solution are fixed through the experiment.

1.5 Outline of the thesis

In short, this thesis contains five chapters. In Chapter One, the background of this research work, research objectives, problem statement, the scope of research as the dissertation overview are briefly introduced. Chapter Two provides a better understanding of background literature review related to present work. Chapter Three describes the specifications of the raw materials, experimental procedures, and characterization methods employed in this research work. Chapter Four presents the findings of characterizations and the discussions on these results obtained from UV-Vis Spectroscopy (UV-Vis), Transmission Electron Microscopy (TEM), Energy Dispersive X-ray (EDS), X-Ray Diffraction (XRD), High Resolution Transmission Electron Microscopy (HRTEM), Zeta potential and High Angle Annular Dark Field Scanning Electron Microscopy. Lastly, in Chapter Five, conclusion and recommendation are presented for future studies.

CHAPTER TWO

LITERATURE REVIEW

This chapter describes the comprehensive review of nanoparticles, bimetallic nanoparticles, synthesis approach of monometallic and bimetallic nanoparticles, 4-nitrophenol and comparison reduction of the 4-nitrophenol in details.

2.1 Introduction

The history of nanomaterials is quite long. Nevertheless, some major developments in nanoscience have taken place during the past two decades. Research in nanomaterials is a multidisciplinary effort that involves interaction between researchers in the field of physics, chemistry, mechanics, material science, and even biology and medicine. The term nanoparticles, which refers to another form of nanomaterials, came into frequent use in early 1990's by the materials science community. The first nanoparticles which is a heterogeneous catalysis, was developed in the early nineteenth century (Khadzhiev, 2016; Somorjai, 1978; Stewart, 2017).

A nanoparticles is defined as a particle in the nanoscale size range measured in nanometers unit. A nanometer is a billionth of a meter equal to 10^{-9} m (Jeevanandam et al, 2018; Sudha et al., 2018). There are different shapes of nanoparticles i.e. spherical, hexagonal, ellipsoidal, pentagonal, cylindrical (rod-like), cubic, cuboid and triangular (Cao et al., 2016; Feng et al., 2017; Konar et al., 2016). They exhibit thermodynamic, catalytic, electronic and optical properties which are different from those of the corresponding bulk materials, thus are used as building blocks to construct complex

nanostructures such as nanowires, both by themselves and nanoparticles (Iqbal et al., 2007; Jain et al., 2007; Jana et al., 2001). The shape and crystallographic facets are the major factors which determine the catalytic and surface activities of the nanoparticles (Nikoobakht & El-Sayed, 2003). One of the important and challenging tasks in the synthesis of nanoparticles is the control of the shape and size (Nikoobakht & El-Sayed, 2003; Pérez-Juste et al., 2005; Raza et al., 2016). The size of the nanoparticle can be easily controlled but the control of the shape can be quite challenging. Nanoparticles (NPs) can be synthesized through physical method such as seeding growth, laser ablation, and pyrolysis, in addition to chemical methods such as chemical vapor deposition (CVD), sol gel technique and electrodeposition. In addition, biological synthesis methods can be done by using microorganisms and plants which are more eco-friendly and non-toxic (Ajitha et al., 2016; Kumar & Yadav, 2009; Nasrollahzadeh et al., 2016; Singh et al., 2016). For example, the synthesis of Au, Ag and Au-Ag nanoparticles using aqueous extract and dried powder of *Anacardium occidentale* leaf was accomplished by Noruzi and co-worker in 2012.

For transition metal nanoparticles, the decrease in the size to the nanoscale dimensions increases the surface-to-volume ratio. The preparation of nanoparticles in different shapes and sizes facilitates their utilization as catalysts in photochemical reactions (Jeevanandam et al., 2018; Khan et al., 2019; Mohamed et al., 1999). Nanoparticles have been shown to possess structural, electronic, dielectric, magnetic, optical and chemical properties that are different from the corresponding bulk materials. These properties exhibit strong size variations (Akita et al., 2008). The reaction parameters, such as reaction time, temperature, concentration and the selection of reagents and surfactants can be used to control the size and shape of the nanoparticles for systematic adjustments (Khan et al., 2019; Mohamed et al., 1999).

2.2 Gold Nanoparticles

Metal nanoparticles have become a continuous part in the current research in nanotechnology. They exhibit rare physical and chemical properties which are quite different from their macro scale (Jayalakshmi et al., 2014; Tyagi et al., 2011). Among the metal nanoparticles, gold nanoparticles (Au NPs) are the most commonly studied (Tyagi et al., 2011). Gold nanoparticles are also known as colloidal gold (Jayalakshmi et al., 2014). The reason for this is the relative ease of synthesis and wide range applications of colloidal gold i.e. catalysts, biomedicine and sensing (Patra & Baek; 2015). In addition, their ease towards surface modification reactions has made them a potential candidate for a variety of applications in catalysis, sensing and biomedicine. The first discovery of catalytic application of Au NPs is the oxidation of carbon monoxide by Au NPs supported on transition metal oxide (Seo et al., 2017). The high surface-area-to-volume ratio properties of Au NPs increases the chemical reactivity. Among the organic reactions that uses Au NPs as catalysts is the reduction of nitro groups such as in nitrophenol (Seo et al., 2017). The catalytic activity of nanoparticles can be enhanced by decreasing the particle size and changing the particle morphology (You et al., 2017). As Luo *et al.*, (2014) stated that gold nanoparticles is highly efficient catalyst for various reactions.

Gold nanoparticles have unique optical properties in the visible range, due to the surface plasmon oscillation of free electrons. This unique optical property of gold nanoparticles is known as Surface Plasmon Resonance. The unique optical property that arises from the localized surface plasmon resonance (LSPR) is sensitive to the size, shape and aggregation state of the nanoparticles. These properties have been recently investigated because play a role in catalytic activity (Li et al., 2014). The quasi-static approximation means that the gold nanoparticles are much smaller than the incidence wavelength. These oscillations in gold nanoparticles give rise to the SPR phenomenon,

which occur within visible frequencies and produce scattering and strong optical absorbance of the gold nanoparticles (Abdelhalim et al., 2012).

The special properties of gold nanoparticles depend on the size, therefore the synthetic methodology of gold nanoparticles with small and uniform size distribution play an important role in the physicochemical properties. The various synthetic strategies of gold nanoparticles include conventional and green technology techniques (Patra & Baek, 2015). The conventional synthetic methods involve the use of chemicals such as sodium citrate, sodium borohydride, hydroquinone, ascorbic acid and organic solvent (Alzoubi et al., 2015; Jayalakshmi et al., 2014; Mechler et al., 2010; Patra & Baek, 2015). While the green method utilizes plant or fruit extracts in the synthesis of Au NPs, which possesses advantages such as non-toxicity and environmentally friendly. For instance, banana peels, custard apple peels, citrulluslanatas rind and extract flower were utilized in the synthesis (Dwived and Gopal, 2010; Ghosh et al., 2012; Patra & Baek, 2015). However, the preparation of Au NPs using citrate is the best candidate due to several reasons such as inexpensive cost, non-toxic water solvent, and low pollution (Li et al., 2011). The reduction by citrate also known as the Turkevich method was introduced by Faraday in 1857. The Turkevich process is promising technique for the production of spherical gold nanoparticles. This method utilizes only three starting materials; auric acid, sodium citrate and distilled water. Sodium citrate acts as the capping and reducing agent. The function of both agents is to prevent the aggregation of gold nanoparticles and to reduce auric acid into gold nanoparticles. During the reaction, the citrate stabilizes the Au NPs through mutual electrostatic repulsion between neighboring gold nanoparticles; this occurs as a result of the negative surface charge of the citrate layer (Salcedo et al., 2013).

In 1973, Frens demonstrated that the size of gold nanoparticles can be controlled by changing the concentration of sodium citrate through the citrate reduction method. The structural characteristics of nanoparticles are controllable with such parameters such as additives, light and thermal energies, and their various combination. In order to achieve a desirable size control, gold nanoparticles are grown by a fast nucleation process followed by a diffusion-controlled growth. The control of size distribution of the nanoparticles is widely known as the LaMer model, or is also known as “focus in size distribution” in the field of non-aqueous solution synthesis of nanoparticles at elevated temperatures (Tyagi et al., 2016).

This nucleation-growth mechanism is affected by the temporal evolution of the nanoparticles sizes under certain conditions (Polte, 2015). Instead of a gradual growth of the nanoparticles was found that at the lower reaction temperature about 60-80 °C, as well as in boiling water (Babick, 2016; Ji et al., 2007; Shrestha et al., 2020). From this, Zukoski *et al.*, (1994) initiated a reversible aggregation of unstable primary particles, followed by a re-dispersion of the primary particles in the last stage of the reaction (Biggs et al., 1994).

2.3 Silver Nanoparticles

Nowadays, noble metal nanoparticles such as Au, Ag, Pd etc have received wide attention due to their amazing properties (Karthik et al., 2016). Among them, silver nanoparticles (Ag NPs) have attained special focus due to their enhanced properties in sensor, catalysis and electronic applications (Mott et al., 2010). Fundamental studies were carried out in the late 1980s and 1990s which showed that silver nanoparticles possess an interesting interaction with light due to dielectric constant which enables the occurrence of light resonances in the visible regions (Baba et al., 2014; Lee & Meisel, 1982).

Notably, silver is one of the metals which can be tailored to respond across the full visible spectrum.

There are two approaches for the synthesis of nanoparticles which is the bottom-up and top-down approach. Gaffet *et al.*, (1996) and Wang *et al.*, (2004) stated that the top-down approach includes chopping down the bulk metals by mechanical means. An example is the metal vapor methods (Blackborrow *et al.*, 1979; Klabunde *et al.*, 1991), which provides a versatile route for the production of a wide range of nanostructured metal colloids (Bradley, 1994). However, this technique has a few disadvantages such as the difficulty of obtaining a narrow particle size distribution, and sample contamination by impurities. While, the bottom-up approach such as the wet chemical nanoparticles preparation basically depends on the chemical reduction of metal salts, electrochemical pathways, or the controlled decomposition of metastable organo metallic compounds in solution. A variety of stabilizers in the form of polymers, donor ligands and surfactants are used in order to control the particle agglomeration (Cao, 2004).

The application of silver nanoparticles depends on the surface area of the silver nanoparticles, therefore, it is very important to control the particle size and dispersion precisely. For instance, when spherical metal particles are transformed into nanoscale disks or triangular prism, their surface plasmon resonance are strongly affected and are typically red shifted, splitting into distinctive dipole and quadruple plasmon modes (Jin *et al.*, 2001; Maillard *et al.*, 2002). Normally, silver nanoparticles dispersed in solution exhibits the Brownian motion. The activation energies between the nanoparticles determine whether the silver nanoparticles can be separated or agglomerated. The particles will agglomerate if the attractive forces between them are stronger than the repulsive forces. Therefore, the resultant forces between silver nanoparticles determine

whether they will separate or agglomerate (Lin et al., 2007). Therefore, a stabilizing agent is added together with the reducing agent to prevent the silver nanoparticles from agglomeration after the reduction of silver ion (Sondi et al., 2002). Ranoszek-Soliwoda *et al.*, (2017) utilized the same reducing and stabilizing agents for the preparation of Ag NPs.

Generally, silver nanoparticles can be fabricated using different techniques such as chemical reduction (Guzman et al., 2009; Kurihara et al., 1995), sonochemical (Zhang et al., 2004), photochemical (Henglein et al., 1998; Huang et al., 1996), electrochemical (Huang et al., 2006), and thermal decomposition (Kim et al., 2005). In addition, silver nanoparticles can be prepared by a natural method from plant origin using a non-toxic and environmentally friendly solvent (Dwivedi & Gopal, 2010). A preferable method to synthesize silver nanoparticles is the chemical reduction (Kalantari et al., 2017); where silver nitrate (AgNO_3) is reduced by a reducing agent. This is due to its large scale fabrication, simplicity and economical approach for nanoparticles production. Examples of reducing agents frequently used by previous researchers are sodium borohydride, sodium citrate, hydroxylamine hydrochloride and sodium hydroxide (Kalantari et al., 2017; Xin et al., 2014). The reducing agent not only reduces the silver ion, but also acts as a stabilizing agent and prevent aggregation.

The chemical reduction methods utilizes silver nitrate as the starting material. This method varies in the choice of reducing agent, the relative quantities and concentrations of reagents, temperature, mixing rate and duration of reaction. The diameters of the resulting particles are depends upon these conditions. One example is the greenish-yellow (maximum wavelength λ_{max} 430 nm) colloidal silver nanoparticle with sizes from 15 to

50 nm, from the reduction using sodium citrate at boiling temperature (Ranoszek-Soliwoda et al., 2017).

Previous studies have shown that reductants such as borohydride, citrate, ascorbate and elemental hydrogen are commonly used for the reduction of Ag^+ ions (Ahmad et al., 2003). The reduction of silver ions (Ag^+) in aqueous solution generally produces colloidal silver with particle diameters of several nanometers. When the colloidal particles are smaller than the wavelength of visible light, the solutions have a yellow brown color with an intense band in the 380 to 400 nm range and other less intense or smaller bands at longer wavelength in the absorption spectrum (Rosi et al., 2005; Tessier et al., 2000). This band is attributed to collective excitation of the electron gas in the particles, with a periodic change in electron density at the surface which also known as surface plasmon absorption (Bijanazadeh et al., 2012; Ershov et al., 1993; Henglein, 1989). The synthesis of nanoparticles by chemical reduction methods is therefore often performed in the presence of stabilizers in order to prevent unwanted agglomeration of the colloidal silver nanoparticles in the solution.

2.4 Bimetallic Nanoparticles

In recent years, bimetallic nanoparticles (BNPs) have received great attention due to their different optical, electronic, catalytic and magnetic properties relative to the monometallic nanoparticles. This is due to their novel chemical and physical characteristics resulting in the synergistic effects between the two metals. Furthermore, the combination of the properties related to the presence of two individual metals also attract more attention. BNPs composed of two different metal elements are of greater interest and importance than monometallic nanoparticles. The presence of the second

metal in a bimetallic alloy is of primary importance as it modifies the physical and chemical interactions among various atoms and induce changes on the structure and surface. These bimetallic nanocomposites have potential applications in biosensing, therapy and catalysis (Tojo & Vila-Romeu, 2014). The interaction between the two metals modifies the electronic states of the constituent metals. The properties of bimetallic nanoparticles can be tuned by adjusting the composition, morphology, size and atomic ordering. The stability and dispersion of nanoparticles, and regulating the magnetic and optical properties can be enhanced by tuning the surface plasmon band of BNPs (Srinoi et al., 2018). As shown in Figure 2.1, the structure of bimetallic nanoparticles can be broadly classified into two types which are mixed and segregated structures. In terms of atomic ordering, the bimetallic nanoparticles can be separated into four types: alloy, intermetallic, core-shells and sub-clusters (Srinoi et al., 2018).

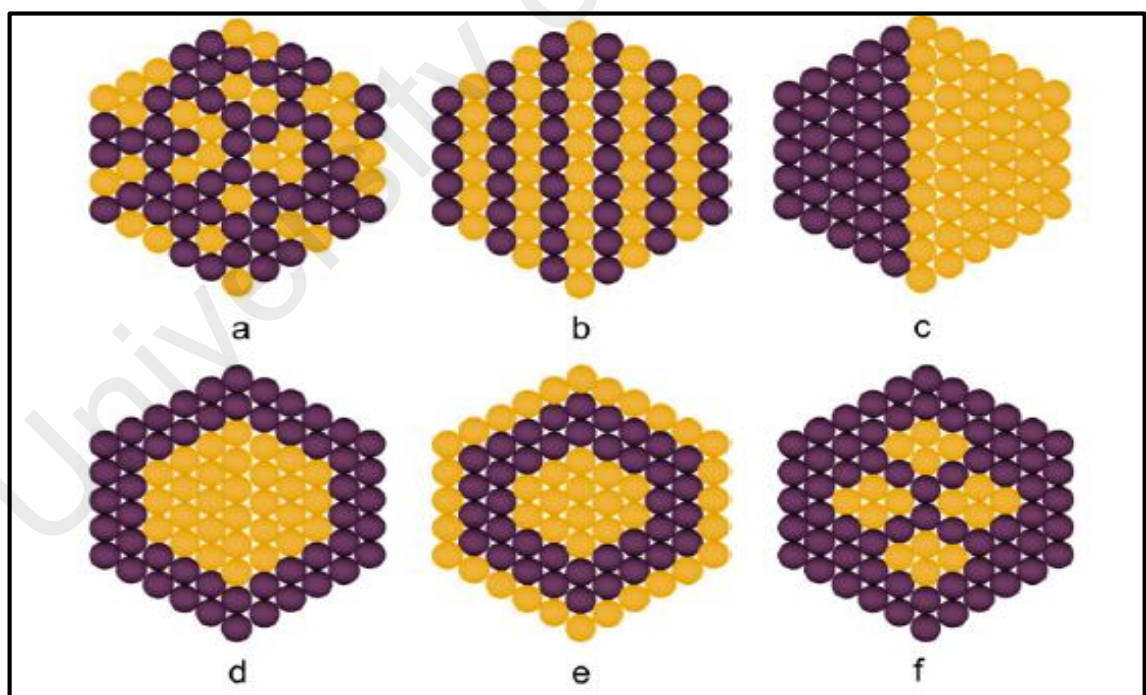


Figure 2.1: Types of bimetallic nanoparticles: (a) alloyed, (b) intermetallic, (c) subclusters, (d) core-shell, (e) multi-shell core-shell, and (f) multiple core materials coated by a single shell material. Purple and yellow spheres represent two different kinds of metal atoms (Srinoi et al., 2018).

The overall properties of the materials depends on the nature of the atomic ordering in the structures. The atomic ordering of mixed structures can be divided into random (Figure 2.1(a)) or an ordered configuration (Figure 2.1(b)). Alloyed and intermetallic structure are examples for mixed structure with random and ordered arrangement, respectively. Alloyed nanoparticles are composed of two metals are randomly mixed; while intermetallic structures are orderly mixed. Segregated structures (Figure 2.1(c)) are composed of two separate components with a shared interface; while core-shell structure (Figure 2.1(d)) consists of an inner metal core surrounded with a second metal as the outer shell. Examples of segregated structures are core-shell structure (Figure 2.1(d)), multi-shell core-shell structure, in which the shells are in an alternating arrangement (Figure 2.1(e)), and multiple small cores coated by a single shell (Figure 2.1(f)) (Srinoi et al., 2018).

The core-shell nanostructures as shown in Figure 2.2 have become an important research area since few decades ago, due to their potential applications in various fields such as catalysts, industrial and biomedical applications etc (Burda et al., 2005; Campbell et al., 2002; De Leeuw et al., 1997; Frederix et al., 2003; Kamat et al., 2002; Kanatzinis et al., 1990; Praharaj et al., 2004). The core-shell can be broadly defined as comprising a core (inner material) and a shell (outer layer material). The combinations of two kinds of metals and their fine structures, evolving new surface characteristics exhibits interesting physicochemical properties (Guha et al., 2011). The core-shell nanocomposites and nanostructures may consist of different sizes and different shapes of the core and shell thickness with different surface morphology. They may be spherical, centric, eccentric, star-like or tubular in shape. Their properties varies from one material to another depending on their size and shape. Whenever the surface of the nanoparticles is modified by functional groups or molecules or coated with a thin layer of another materials with

different constituents, they show enhanced properties compared to the non-functionalized uncoated particles. There are different types of core-shell structure such as metal-core and different metal shell, metal-core and non-metal shell, metal-core and polymer shell, non-metal-core and non-metal shell, polymer-core and non-metal shell and polymer-core and polymer shell, where the two polymers are different (Paik, 2013).

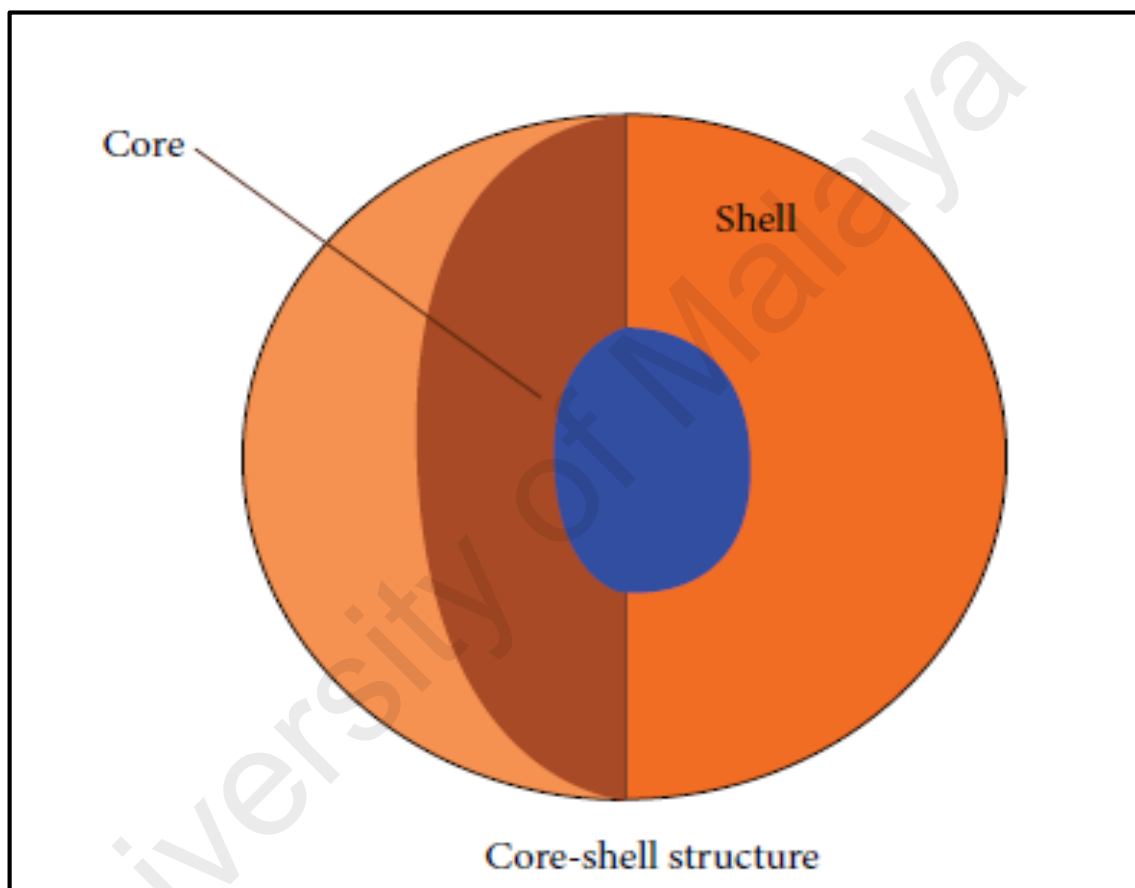


Figure 2.2: Schematic of core shell nanoparticles (Paik, 2013).

The core-shell nanostructures consist of a shell from a single type of metal atom surrounding a core from another metal. Different categories of the core-shell structures are shown in Figure 2.3 (a)-(d). Concentric core-shell nanoparticles are the most common (Figure 2.3(a)) where a core metal A is completely coated by a shell of a different material (metal B). Multiple nanoparticles may present an onion-like alternating of a –A–B–A– shell structures (Figure 2.3(b)) or multiple core-core/shell particles formed when a single

shell material is coated by many smaller core particles (Figure 2.3(c)). It can be demonstrated by dynamic simulation that onion-like structures, such as the A–B–A could be favored for Cu-Ag, Ni-Ag and Pd-Ag clusters, while the A–B–A–B arrangements could be formed in the case of Co-Rh and Pd-Pt clusters, respectively (Rossi et al., 2004). Three shell Pd-Au nanoparticles - made from an intermixed core, an Au-rich intermediate shell, and a Pd-rich outer shell were obtained by successive reduction of the corresponding metallic precursors by Ferrer et al. (2007). The synthesis a movable core particle within an uniformed hollow shell particle (Figure 2.3(d)) after the bilayer coating of the core material and removal of the first layer, could be done by using a suitable techniques such as dissolution (Lou et al., 2008) or thermal treatment (Zhang et al., 2011) to remove interior shell is possible. A movable core-shell structure could be also obtained by slow and fully controlled dissolution of melamine formaldehyde (MF) core encapsulated in silica shell, resistant for reaction conditions (Choi et al., 2008). The movable core of a noble metal (Ag, Au, Pt) is usually encapsulated in a polymer (Han et al., 2014; Heshmatpour et al., 2012) or silica shell (Choi et al., 2008; Nabid et al., 2016).

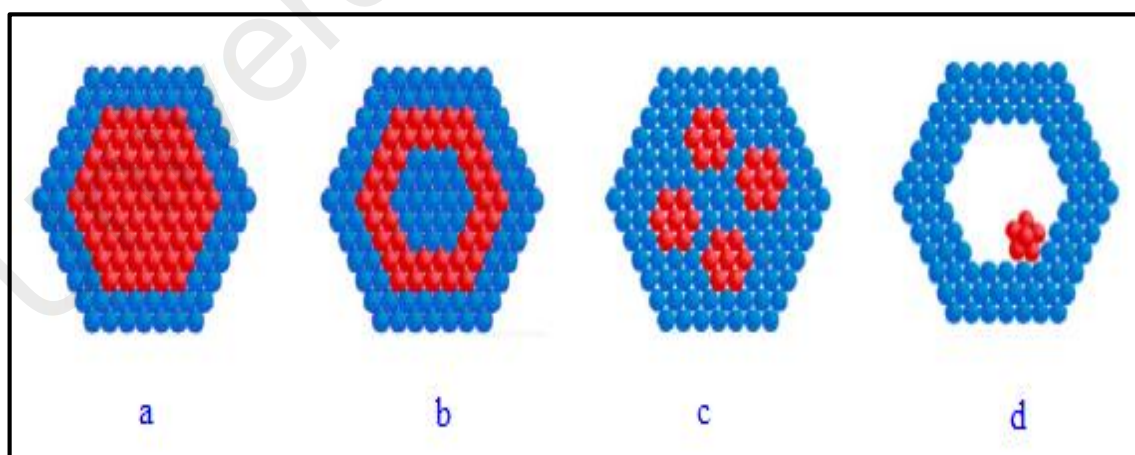


Figure 2.3: Structures of bimetallic nanoparticles (a) core-shell nanoparticles; (b) multishell core-shell nanoparticles; (c) multiple small core material coated by single shell material, (d) movable core within hollow shell material (Ghosh Chaudhuri & Paria, 2011; Pittaway et al., 2009).

2.4.1 Bimetallic Gold-Silver Nanoparticles

Bimetallic gold-silver (Au-Ag) nanoparticles have been reported by many researcher for different applications such as catalyst and surface enhanced Raman scattering (SERS) (Calagua et al., 2015; Ko & Chang, 2014; Lu et al., 2013; Monga & Pal, 2015). The combination of these two metals in core-shell entities offers the possibility to tune the localized surface plasmon resonance (LSPR) by varying the size of the core and the shell thickness (Lu et al., 2013). The localized surface plasmon resonance of the Au-Ag core-shell nanoparticles shows distinct geometry-dependence. This may lead to a new way to tune the surface plasmon resonance wavelength for enhancement of the surface electric field, which is suitable for detecting sensitive target molecules (Liu et al., 2015). Metallic Au and Ag have almost identical lattice constants (0.408 for Au and 0.409 for Ag). These characteristics reduces lattice strain at the gold-silver interface and leads to the formation of bimetallic structure (Monga & Pal, 2015; Rodríguez-González, 2005; Tsuji et al., 2006; Xu et al., 2005). In addition, the Au-Ag core-shell NPs have been exclusively explored due to the tunable surface plasmon bands in the visible region and similar face-centered crystal structure.

Recently, Haldar *et al.*, (2014) have reported the core size dependent catalytic properties of bimetallic Au-Ag core-shell nanoparticles. The catalytic properties can be tuned by tuning the size and shape of the nanoparticles. There are two parameters to fix the shell thickness of a core or shell with different core sizes, either by increasing the concentration of shell materials while keeping particle concentration constant, or by decreasing the particle concentration of the larger size core materials (Haldar et al., 2014). Monga and Pal, (2015) demonstrated the preparation of Au-Ag core-shell NPs for measuring the catalytic activity of nitrobenzene relative to their respective monometallic counterparts and the core-shell system shows higher catalytic activity than the

corresponding single metal due to the synergistic effect. In their core-shell system, the volume of silver nitrate solution was varied to control the thickness of the Ag shell (Monga & Pal, 2015). Albonetti *et al.*, (2010) also reported the synthesis of Au-Ag core-shell nanoparticles by microwave assisted eco-friendly method for catalytic applications. Yuan *et al.*, (2015) prepared bimetallic Au-Ag core-shell nanoparticles with different thickness of silver by adjusting the amount of silver nitrate solution for sensor application.

In catalytic applications, the core diameter and shell thickness could play an important role on the catalytic activity. By changing the nature of the core, the shell-thicknesses and the core/shell ratio, the surface properties and catalytic activity of Au-Ag core-shell NPs can be manipulated to be a consequence of different work functions of the Au and Ag metals. Since the electronic distribution of both Au and Ag is different, the catalytic activity of shell atoms (Ag) can be electronically affected by the core atoms (Au) and vice versa (Monga & Pal, 2015). Another factor that influence the catalytic activity of bimetallic core-shell NPs is the particle size (Gopalakrishnan *et al.*, 2015). In addition, Au as the core and Ag as the shell can enhance resistance to oxidation. Based on Shankar *et al.*, (2012) studied, the stability of bimetallic Au-Ag core-shell nanoparticles depend on the distance between the Ag-shell from Au-core. The thicker the Ag shell (the further the Ag from the Au core), the weaker the stability of the Au-Ag nanoparticles.

2.4.2 Synthesis of Bimetallic Nanoparticles

The synthesis of Au-Ag nanoparticles has been accomplished through several different techniques. The chemical synthetic methods which have been adopted for the past few years are the citrate reduction and polyol process. While the physical methods are such as sonochemical method, photolytic reduction and laser ablation (Tsuji et al., 2006). The green synthesis approach utilizes biological organisms such as plant extracts and microorganisms which is an eco-friendly method to prepare core-shell NPs. Gopalakrishnan *et al.*, (2015) reported the synthesis of Au-Ag core-shell nanoparticles using *Silybummarianum* seed extract for the reduction of 4-NP and methanol oxidation reactions. The extraction of *Silybummarianum* seed is the reducing and stabilizing agents (Gopalakrishnan et al., 2015). Kirubha and Palanisamy (2014) prepared Au-Ag core-shell NPs using gripe water for SERS application, where gripe water is the reducing and stabilizing agent. Since the catalytic activity of bimetallic core-shell NPs relies on the particle size, the biological method is not suitable due to difficulties to control the size distribution and crystal structure of the nanoparticles (Gopalakrishnan et al., 2015).

The most commonly used strategy is the seed-mediated growth method which involves a two-step seeding-growth method where the pre-synthesized metal nanoparticles are used as seeds for the overgrowth of the second metal (Calagua et al., 2015; Güzel et al., 2010; Ko et al., 2014; Sanyal et al., 2013). This method is much preferable for the synthesis of bimetallic nanoparticles due to the easiness of synthesis and ability to control their size, shape and composition. In this type of process, reducing agents play an important role to control the size distribution of the nanoparticles. For instance, strong reducing agents can create new nuclei in solution, which can lead to the formation of metal nanoparticles having with different sizes (Jana et al., 2001). The reducing agents which can be used through this technique are sodium borohydride

(Kumari et al., 2015; Zong et al., 2012), sodium citrate (Ko & Chang, 2014; Song et al., 2016; Yang et al., 2008), and polyvinylpyrrolidone (PVP) (Eisa et al., 2016) etc. Srnova-Sloufova *et al.*, (2000) prepared layered core-shell bimetallic Ag-Au nanocages through a seeded-growth method for surface enhanced Raman spectroscopy (SERS) applications. Park *et al.*, (2011) synthesized Au@Ag core-shell nanoparticles from spherical gold seeds with controllable shapes (Park et al., 2011). Hu *et al.*, (2005) developed an Au-seeding method by which bimetallic Au@Pd core-shell nanoparticles can be prepared with controllable sizes for use in SERS-based applications. This is due to their good potential in SERS activity, stability, and reversibility (Hu et al., 2005). Wang and coworkers have prepared sub-clustered PtAu nanoparticles with controllable morphologies by the overgrowth of gold onto platinum (Wang et al., 2010). The shape and size of the bimetallic nanoparticles were organized by tuning the size of Pt seeds or the solvent polarity in order to obtain nanoparticles with various shapes such as peanut-like, peer-like and clover-like shapes. This method to obtain certain morphologies is a potential candidate for different types of catalytic application. This is because the morphologies may influence the catalytic performance of the nanoparticles.

So far, to control the size, the composition and uniformity of nanoparticles possess some limitations even though the synthesis of bimetallic Au-Ag core-shell with spherical shape has been achieved. Furthermore, surfactants such as cetyltrimethylammonium bromide (CTAB) and polyvinylpyrrolidone (PVP) are needed in this synthetic method. However, these materials prevent reporter molecules from adsorbing onto the nanoparticles surface, which restrict the application in SERS and biosensors. The Au-Ag core-shell nanoparticles without surfactant are suitable for SERS application, but the size correlated and excitation wavelength dependent SERS studies have not been stated in detail due to restrictions of their size controlled synthesis, unlike gold nanoparticles

(Samal et al., 2013). On the other hand, Samal *et al.*, (2013) used the citrate as a stabilizer to prepare Au-Ag core-shell nanoparticles in water. This method could provide gradual coating of citrate stabilized gold nanoparticles with silver shells. In addition, citrate as a stabilizer can make gold and silver nanoparticles biocompatible and easy to be modified due to their loosely bound ligand layer. So that, citrate-capped Au-Ag nanoparticles could be well-organized towards catalysis, SERS and PEGylation applications.

Haldar *et al.*, (2014) have proposed a growth mechanism of bimetallic Au-Ag core shell nanoparticles by extracting aliquots of the reaction mixture at certain time intervals. The aggregation-based growth mechanism which includes the initial nucleation and growth of separate silver nanoparticles, which must be subsequently attached to the gold nanoparticles. Through this process, one should notice the progressive growth in the population of core-shell at the expense of the population of both the nanoparticles and the silver nanoparticles formed by homogeneous nucleation. At the early stage ($t= 5$ minutes), a few faceted primary shell thickness about 3-5 nm are formed (Figure 2.4(a)). But, these primary particles can aggregate through the Ostwald ripening process (Figure 2.4(b)). The shell thickness increases gradually as the reactant are added continuously. The thickness of silver shell is almost the same as the initially formed particles as shown in Figure 2.4 (c)). It assumed that the addition of the reactants at a constant flow rate does not induce the separate growth of silver nanoparticles. Unless it is ripening, the attachment of primary gold nanoparticles to form bimetallic gold-silver core shell nanoparticles. All the precursors are added to the reaction system after 30 minutes and precise bimetallic Au-Ag core shell nanoparticles are formed.

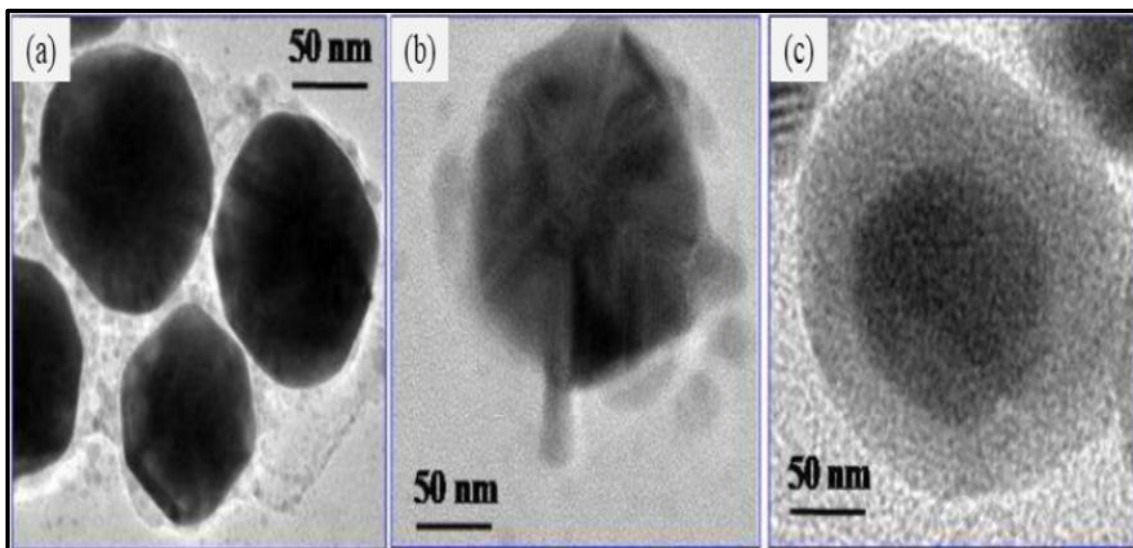


Figure 2.4: TEM images of samples at different dropping time. (a) initial reaction stage ($t = 5$ minutes), (b) primary particles had some tendency to aggregate through Ostwald ripening and (c) addition of reactant continuously to form shell thickness (Haldar et al., 2014).

In this research, the precursors used were silver nitrate as a source of silver ion, gold (III) chloride trihydrate as the source of gold ion, citrate and ascorbic are the reducing and stabilizing agents. Distilled water was used in the preparation of aqueous solutions. The chemical composition was determined based on previous study (Yang et al., 2008). The variation in composition of gold seeds was needed in order to provide an ultimate condition for reducing 4-NP. The concentration of silver nitrate solution was constant throughout the experiment. The presence of mild reducing agent which was aqueous ascorbic acid solution was used to reduce the silver ions at the metallic surface only. The silver ions that are reduced by the ascorbate ions are deposited onto the surface of gold nanoparticles to form the Au-Ag nanoparticles. The citrate solution was used to prevent the nanoparticles from agglomeration to form larger nanoparticles.

2.5 4-nitrophenol

The concern for public health and environmental safety has been increasing over the past few decades. Chemical pollution of surface threaten the aquatic life such animals and plants with hazardous effects. As we know, nitroaromatic compounds have been used in industry and agriculture fields for instance, pesticides, pharmaceuticals and intermediates in the synthesis of dyes. Nitrophenols (NP) is the one of the nitroaromatic compounds and considered as dangerous substance that invades the body through the respiratory system, digestive system and skin (Tang et al., 2015). Therefore, the removal of nitrophenol are essential to protect the human being and the environment. The simplest way to remove nitrophenol from the environment is the reduction into aminophenol (AP) (Ghorai, 2015). On the other hand, the product of nitrophenol reduction can be used for antipyretic drugs, photographic developer, corrosion inhibitor etc. There are several synthesis routes which have been developed for the removal of nitrophenols in aqueous solutions such as the Fenton process, photodegradation and ozonation. Recently, metal-based catalysts have been used for the reduction of nitrophenols such as gold, silver, platinum, nickel and cobalt nanoparticles (Lin & Doong, 2014).

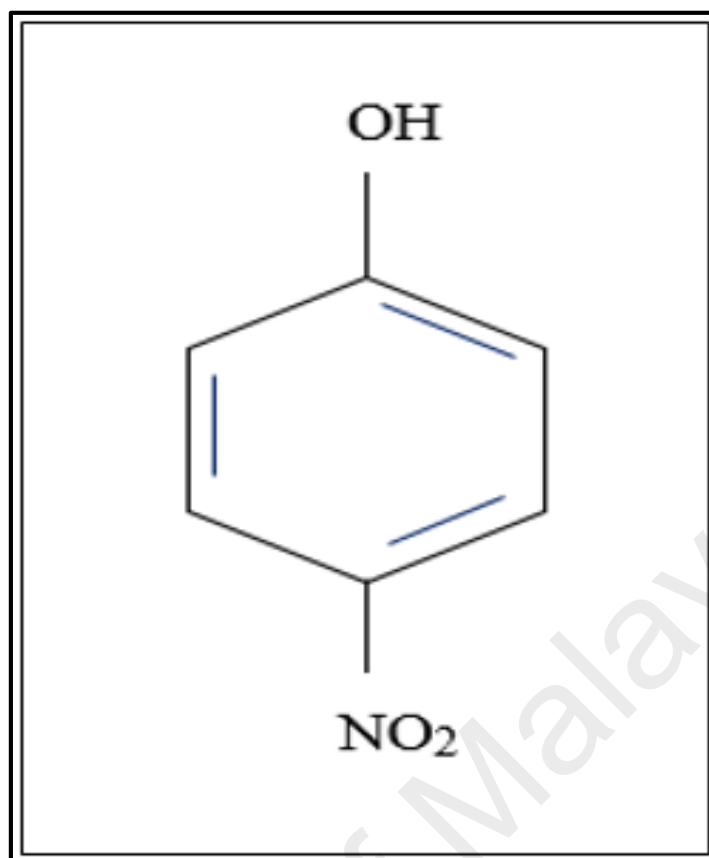


Figure 2.5: Molecular structure of 4-NP (Open chemistry database. Retrieved from <https://pubchem.ncbi.nlm.nih.gov/compound/4-Nitrophenol#section=Top>)

Table 2.1: Physical properties of 4-NP

Chemical formula	$C_6H_5NO_3$
Appearance	Colorless
Molar mass	139.11 g/mol
Melting point	113.8 °C
Boiling point	279.0 °C
Solubility in water	15,600 mg/L at 25 °C

The most common method to reduce nitrophenol to aminophenol is by catalytic reduction by various noble metal nanoparticles, such as monometallic and bimetallic nanoparticles. Noble metals are much preferable due to the higher catalytic rates and faster catalytic induction (Hong et al., 2016). There are several examples of researchers who synthesized catalyst for the reduction of 4-NP such as palladium/graphene nanocomposites (Sun et al., 2014), Au-Ag nanocages (Hong et al., 2016), palladium nanowires (Chawla et al., 2016), silver nanoparticles (Liang et al., 2013), Au-Ag bimetallic nanocomposites (Gopalakrishnan et al., 2015), and titania (Ghorai, 2015). Different types of catalyst will require different reaction times to reduce nitrophenol to aminophenol as shown in Figure 2.6 (a-e).

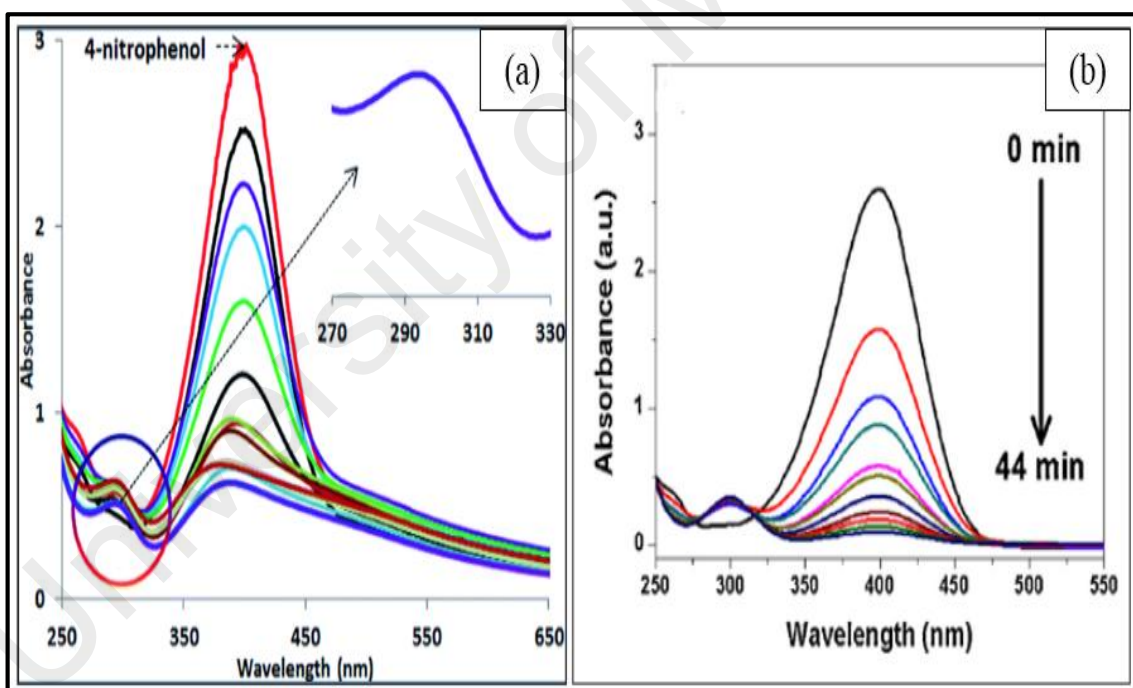


Figure 2.6: UV-vis absorbance for reduction nitrophenol using (a) Pd nanowires (Chawla et al., 2016), (b) Au-Ag bimetallic nanocomposites (Gopalakrishnan et al., 2015)

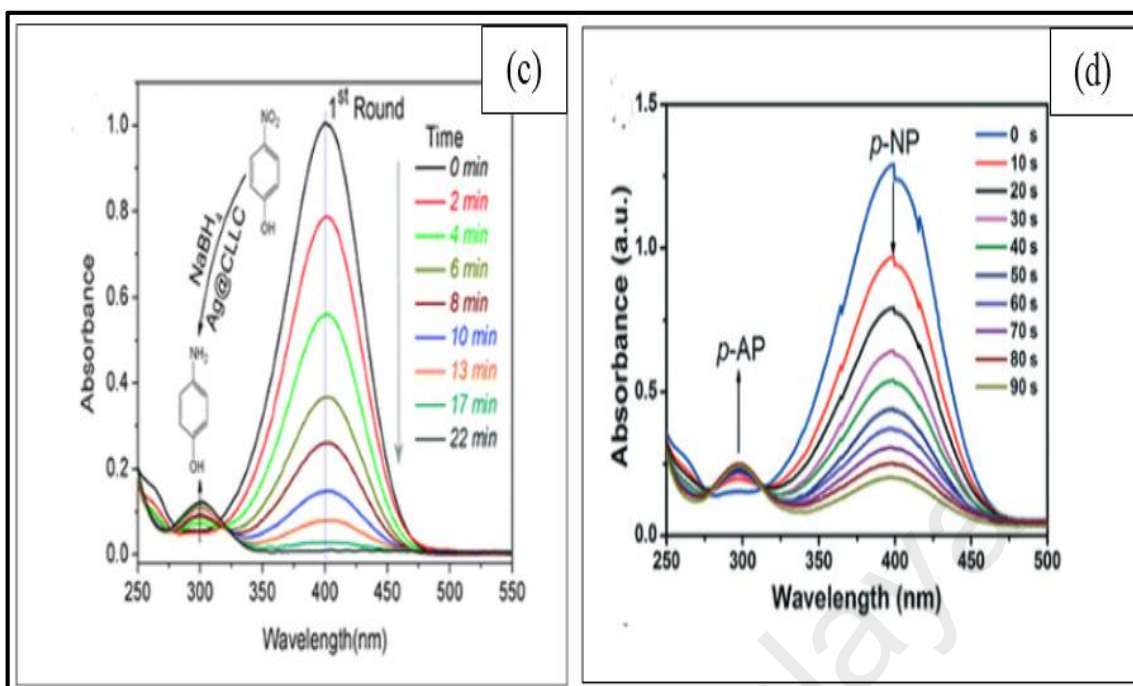


Figure 2.6: UV-vis absorbance for reduction nitrophenol using (c) Ag nanoparticles (Liang et al., 2013), (d) Pd/G (Sun et al., 2014)

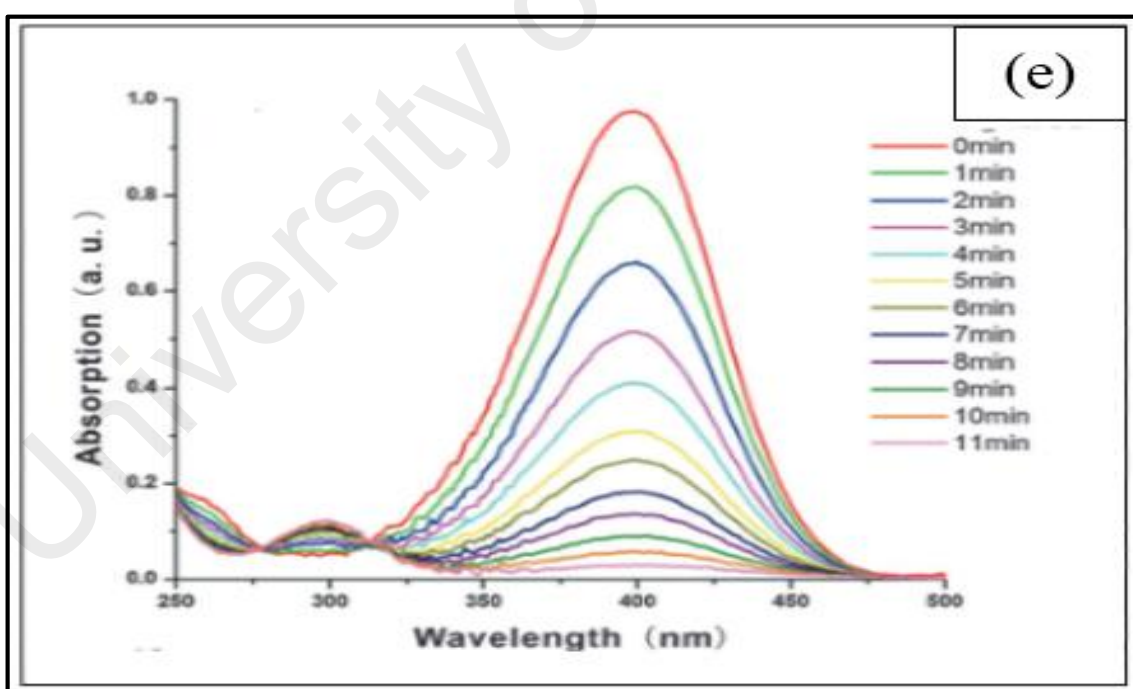


Figure 2.6: UV-vis absorbance for reduction nitrophenol using (e) Au-Ag nanocages (Hong et al., 2016).

In this study, 4-NP was reduced by the Au-based catalyst. Even though, Au-based systems may lead higher cost but the combination of gold with silver can reduce the usage of gold by forming bimetallic gold-silver nanoparticles. In addition, bimetallic nanoparticles intensively impacts the catalytic activities (Hong et al., 2016; Sun et al., 2014). According to Hong *et al.*, (2016), metal nanoparticles have been studied extensively in the field of catalysis due to the unique catalytic role in various electron-transfer reactions which results from their possession of a higher Fermi potential. It may causes the lowering of the redox potential value, which becomes more negative and allows them to act as catalysts.

Table 2.2 presents rate constant, amount catalyst, and particle size of different catalyst for the 4-NP reduction. Clearly, the bimetallic nanoparticles shows the higher rate of 4-NP reduction compare to their single element. This is due to the synergistic effect between the two elements. Wu *et al.*, (2013) prepared Au, Ag and Au-Ag NPs onto graphene oxide (GO). GO is used as a stabilizing agent and a support. From that, it will prevent the nanoparticles from aggregation. In addition, GO has a large surface area and abundant functional group on its surface so that, the nanoparticles can be anchored to its surface (Wu et al., 2013). While the performance of Au/GO over Ag/GO due to the particle sizes since small NPs have higher catalytic activities than larger ones; the size of the Au/GO particles was smaller than that of Ag/GO. The Au, Ag and Au-Ag NPs synthesized on the poly(cyclotriphosphazene-co-polyethyleneimine) (PCP) microspheres also for avoiding the nanoparticles from aggregation (Fu et al., 2018). According to Sun's report (Sun et al., 2018), different amount of Au-Ag NPs used for 4-NP reduction which are 0.1, 0.4 and 0.8 ml. Compare with these three amount, the rate of reaction of 0.8 ml catalyst has an obvious high. It indicates that the amount of catalyst also play an important role towards the catalytic activity.

Table 2.2: Comparison of rate constant, amount catalyst, and particle size of different catalyst for the 4-NP reduction

Catalysts	Shape of NPs	Reducing Agents	Amount catalyst (ml)	Rate (min^{-1})	Time (min)	Particle Size (nm)	Ref.
Ag/GO NPs	Spherical	NaBH ₄	0.1	0.208	25	7.5	Wu et al., 2013
Au/GO NPs	Spherical	NaBH ₄	0.1	0.368	10	5.0	Wu et al., 2013
Au-Ag/GO alloy NPs	Spherical	NaBH ₄	0.1	0.761	5	6.0	Wu et al., 2013
Au/PCP	Spherical	NaBH ₄	0.2	0.023	44	3.7	Fu et al., 2018
Ag/PCP	Spherical	NaBH ₄	0.2	0.023	44	2.6	Fu et al., 2018
Au-Ag/PCP	Spherical	NaBH ₄	0.2	0.083	12	4.0	Fu et al., 2018
Au-Ag NPs	Spherical	NaBH ₄	0.1	0.161	6	16.8	Sun et al., 2018
Au-Ag NPs	Spherical	NaBH ₄	0.4	0.373	3	16.8	Sun et al., 2018
Au-Ag NPs	Spherical	NaBH ₄	0.8	0.598	2	16.8	Sun et al., 2018

CHAPTER THREE

RESEARCH METHODOLOGY

This chapter designates materials and experimental procedures, as well as the parameters considered in this work. Section 3.1 describes the materials used through this work. Section 3.2 describes the preparation of gold (Au) nanoparticles, followed by the preparation of silver (Ag) and gold-silver (Au-Ag) nanoparticles and finally, gold, silver and gold-silver were used as the catalyst for the reduction of the 4-NP to 4-AP. While Section 3.3 describes the characterization techniques used to analyze the samples.

3.1 Materials

All the chemical reagents were used as-received without any further purification. Gold (III) chloride trihydrate (99.9 %, $\text{HAuCl}_4 \cdot 3\text{H}_2\text{O}$), trisodium citrate ($\text{Na}_3\text{C}_6\text{H}_5\text{O}_7$), silver nitrate (AgNO_3), L-ascorbic acid ($\text{C}_6\text{H}_8\text{O}_6$), sodium borohydride (99.0 %, NaBH_4), and 4-nitrophenol (98.0 %, $\text{C}_6\text{H}_5\text{NO}_3$) were purchased from Sigma-Aldrich. Distilled water was used in the preparation of nanoparticles throughout the experiments.

3.2 Samples preparation

3.2.1 Synthesis of gold nanoparticles

The synthesis of colloidal gold was performed by using the citrate thermal reduction technique (Yang et al., 2006). Briefly, an aqueous solution of $\text{HAuCl}_4 \cdot 3\text{H}_2\text{O}$ (1.0 ml of 1.0 wt. %) was added to 90.0 ml distilled water and a light yellow solution was formed. Then, the above solution was stirred vigorously along with heating until reaching boiling point at 100 °C. An aqueous solution of sodium citrate (2.0 ml, 38.8 mM) was added drop-wise into the reaction solution. Sodium citrate does not only function as the reducing agent, but also to prevent particle aggregation and as a stabilizing agent during the synthesis process. The successive color changes of the Au solution upon the addition of the citrate can be described as follows: light yellow to clear, to purple (after 3 minutes), to dark purple and finally to maroon (after 10 minutes). The solution was quickly cooled in an ice bath after it turned maroon after 10 minutes. The ice bath was required at final step in order to maintain a constant temperature during the process which is essential for obtaining the uniform size of gold nanoparticles. The solution was then centrifuged at 6,000 rpm and washed with distilled water three times to remove impurities. The synthesis process of Au nanoparticles is illustrated in Figure 3.1.

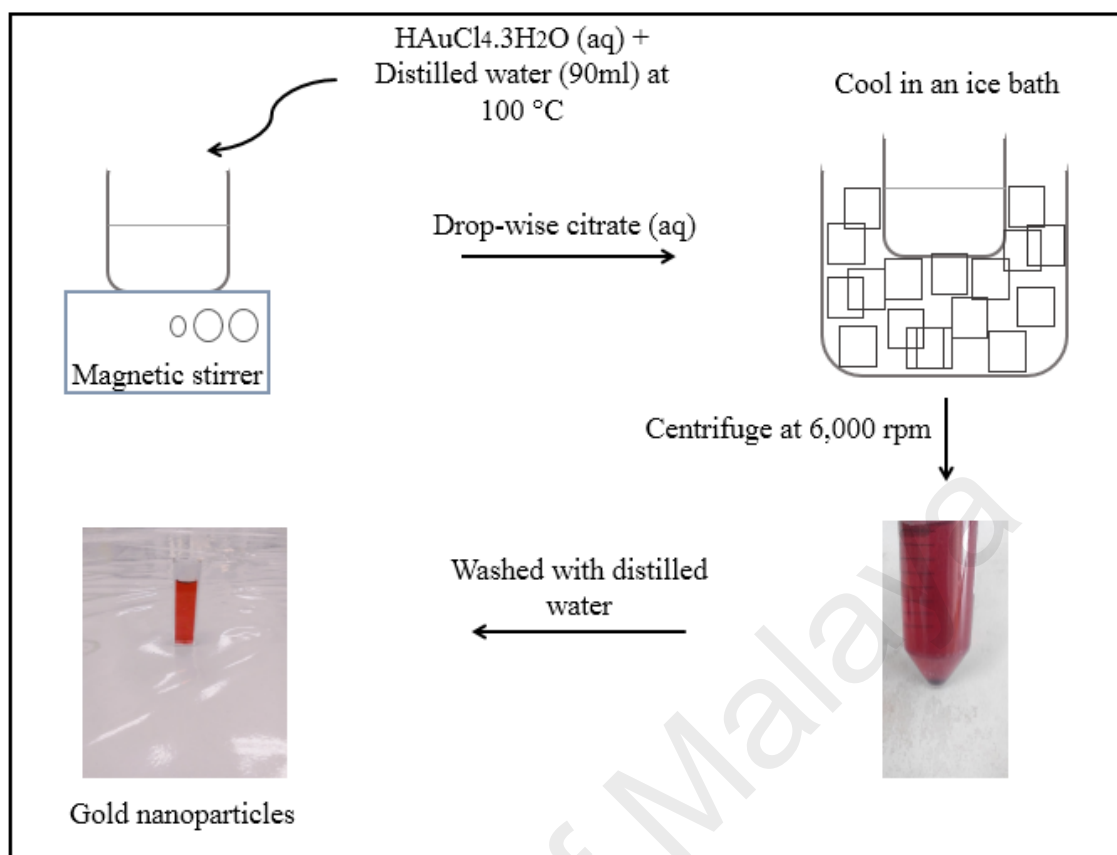


Figure 3.1: Schematic diagram of Au nanoparticles preparation procedures

3.2.2 Synthesis of silver nanoparticles

Figure 3.2 shows the preparation of silver nanoparticles. Silver nanoparticles were prepared using citrate thermal reduction method, the same method to prepare gold nanoparticles. Firstly, 0.018 g of silver nitrate was weighed and diluted into 100.0 ml distilled water. The silver nitrate solution was heated to boiling point at $100\text{ }^\circ\text{C}$. Then, 2.0 ml of 38.8 mM sodium citrate aqueous solution was added drop-wise and the solution turned chrome yellow after 10 minutes. The solution was cooled at room temperature. Finally, the solution was then centrifuged at 6,000 rpm and washed with distilled water.

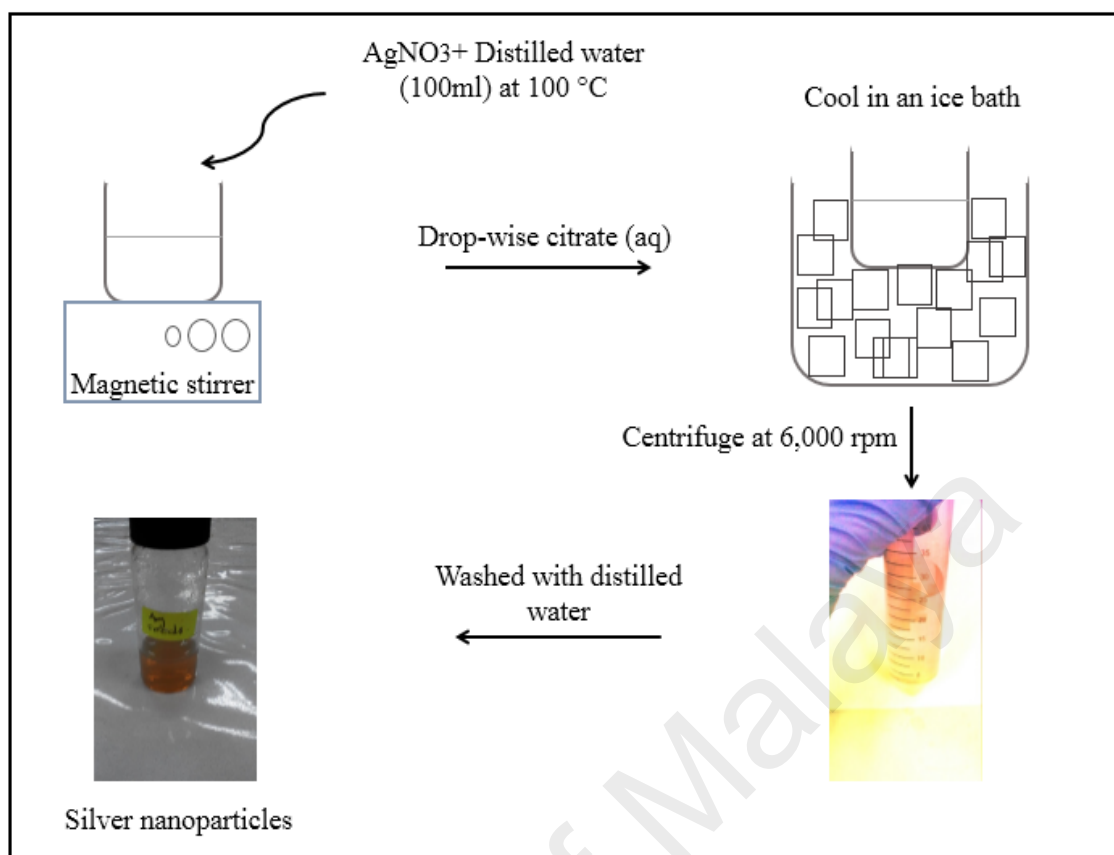


Figure 3.2: Schematic diagram of Ag nanoparticles preparation procedures

3.2.3 Synthesis of gold-silver nanoparticles

Figure 3.3 shows the bimetallic Au-Ag nanoparticles which were prepared using the seed colloidal technique (Yang et al., 2008). The as-synthesized citrate-capped Au NPs were used as the seed in the formation of the bimetallic Au-Ag NPs. The different volume of Au NPs (2.0 and 5.0 ml) and 1 ml of sodium citrate solution (38.8 mM) were added to 30 ml of distilled water and stirred for 10 minutes. Then, 1.2 ml of silver nitrate aqueous solution (10.0 mM) and 0.4 ml of ascorbic aqueous solution (100.0 mM) were added drop-wise to the above mixture. The reaction mixture was stirred continuously for 30 minutes to ensure a homogeneous solution at room temperature. The solution was then

centrifuged at 6,000 rpm and washed with distilled water. The details of the experimental conditions used are listed in Table 3.1.

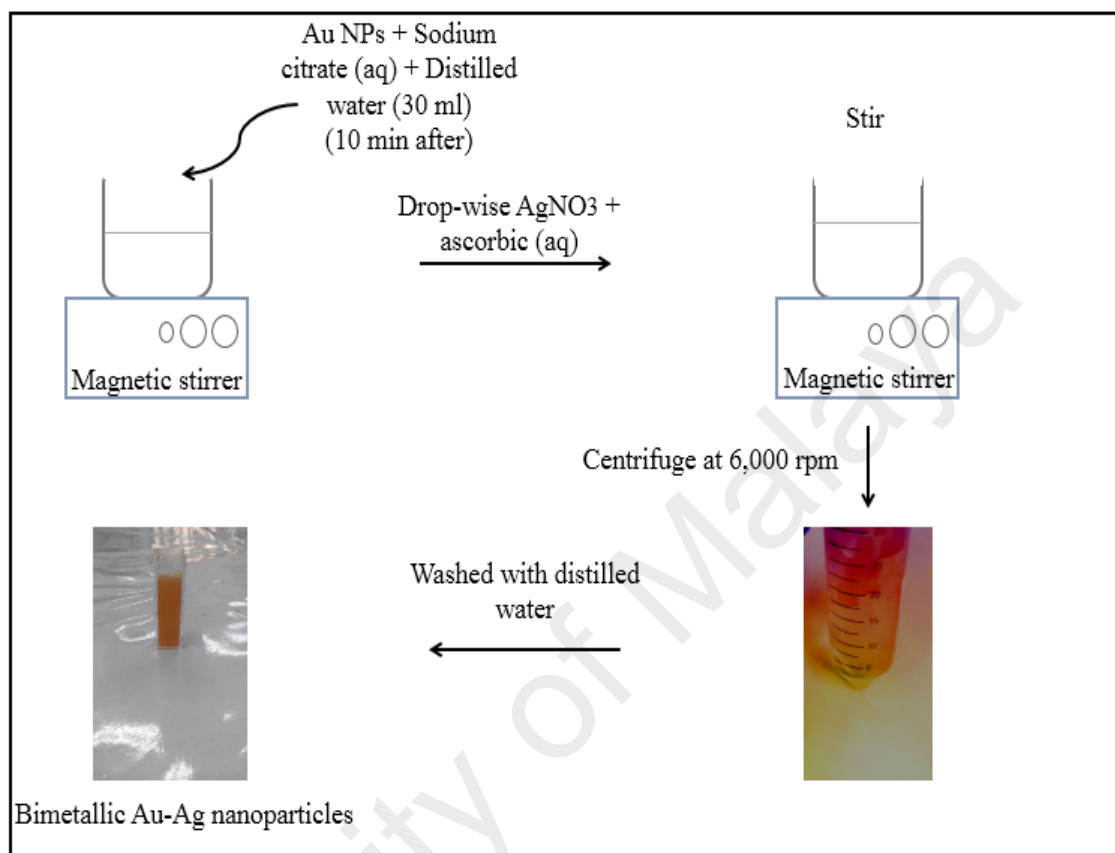


Figure 3.3: Seed colloid synthesis process routes for Au-Ag nanoparticles

Table 3.1: Experimental conditions for the synthesis of bimetallic Au-Ag nanoparticles

Molar ratio of Au:Ag	Au NPs (ml)	Silver nitrate (ml)	Citrate solution (ml)	Ascorbic solution (ml)
1.7:1.0	2.0	1.2	1.0	0.4
4.2:1.0	5.0	1.2	1.0	0.4

3.2.4 Catalytic activity reduction of 4-NP

The reduction of 4-NP to 4-AP was performed to evaluate the catalytic activity of the Au, Ag and bimetallic Au-Ag nanoparticles. The reaction was carried out in a standard quartz cuvette. For the reduction process, the 4-NP solution (3.0 ml, 0.2 mM) was added with 1.0 ml of distilled water. This was followed by the addition of aqueous NaBH₄ (0.5 ml, 0.4 M) solution, resulting in the color change from light yellow to bright yellow. Finally, 0.2 ml of the Au-Ag nanoparticles was added to the reaction mixture. After the addition of the Au-Ag nanocatalyst, the UV-vis spectral absorbance was recorded at every 1 minute interval in the range of 200-800 nm at room temperature using a CARY 50 UV-vis spectrophotometer. Figure 3.4 shows the flowchart of sample preparation.

University of Malaya

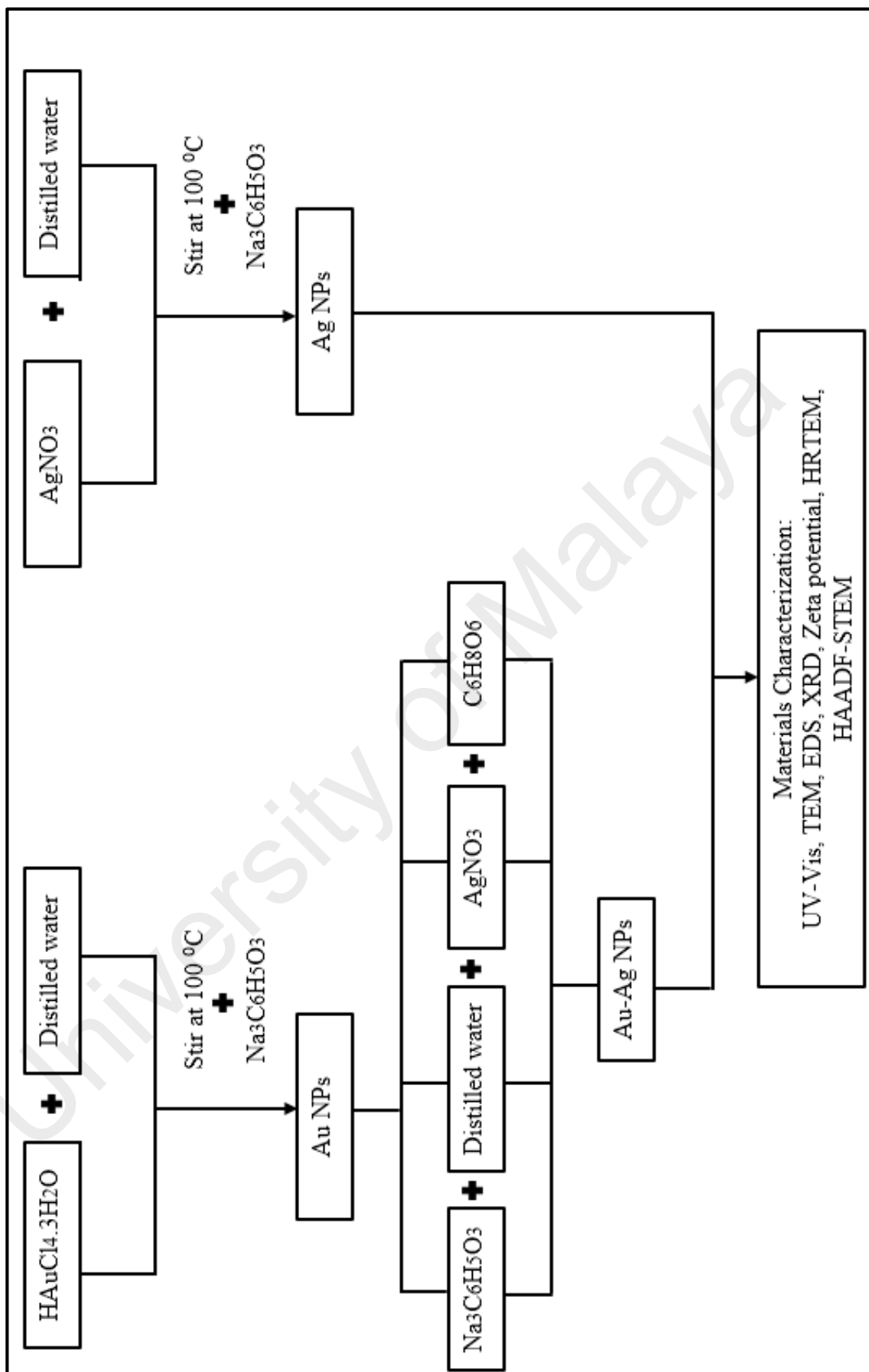


Figure 3.4: Flowchart of sample preparation for Au, Ag and Au-Ag nanoparticles

3.3 Characterization techniques

Several characterizations were performed through this project from the preparation of gold, silver and gold-silver nanoparticles until the catalytic reduction of 4-NP to 4-AP. The characterizations methods were UV-vis spectroscopy (UV-Vis), transmission electron microscopy (TEM), energy dispersive X-ray spectroscopy (EDS), X-ray diffraction (XRD), high resolution transmission electron microscopy (HRTEM), zeta potential and high angle annular dark field scanning transmission electron microscopy (HAADF-STEM).

3.3.1 UV-Vis Spectroscopy (UV-Vis)

Figure 3.5 shows the CARY-50 UV-Visible spectrophotometer (Varian) used for optical characterization of Au, Ag and Au-Ag nanocatalysts. The wavenumber range for this equipment is 180-900 nm, and the wavenumbers considered in this work is within the range 200 to 800 nm. The samples were run in the absorption mode. The samples were placed in an ultrasonic bath for 10 minutes to ensure the particles were dispersed evenly in the solution. Before running the samples, the baseline correction was carried out by using distilled water for gold, silver and gold-silver nanoparticles in the quartz cuvette. The optical properties of the samples were studied by the plot of graph absorbance versus wavelength. The surface plasmon resonance (SPR) peaks for each samples were investigated.



Figure 3.5: UV-Visible spectrophotometer

3.3.2 Transmission Electron Microscopy (TEM)

TEM is used for nanostructural analysis by providing the information related to morphology and crystallographic information of a sample. The TEM is utilized to determine the approximate size of the gold, silver and gold-silver nanoparticles, at the same time the morphology of nanoparticles were observed. The TEM measurement was performed by Zeiss LEO LIBRA 120 transmission electron microscope (TEM) with an electron beam source. The accelerating voltage and magnification were 120 kV and 40 k respectively.

The nanoparticles samples were sonicated in an ultrasonic bath for 10 minutes to break the agglomeration. Then, the samples were drop-casted onto copper grids (Formvar/carbon on mesh copper) and dried in a vacuum desiccator. After that, the copper grids were inserted into the TEM holder for analysis. The TEM images particle size distribution of each sample was measured using *image-J* software and represents as size distribution histogram.



Figure 3.6: TEM machine

3.3.3 Energy Dispersive X-ray Spectroscopy (EDS)

Energy Dispersive X-Ray Spectroscopy (EDS) is a chemical microanalysis technique used in conjunction with field emission scanning electron microscopy (FESEM). The FESEM (HITACHI SU8220) was attached with EDX Oxford Instruments model XMX1011. The EDX technique detects X-rays emitted from the sample during bombardment by the electron beam and leads to the characterization of the elemental

composition of the analyzed sample. The sample images were captured from a bright-fringe scanning electron microscopy (BFSTEM) mode at an accelerating voltage of 30 kV.

In this project, the EDS analysis was carried out to investigate the composition of the gold, silver and bimetallic gold-silver nanoparticles. Before running testing, the synthesized Au, Ag and Au-Ag nanoparticles were sonicated for 10 minutes, drop-casted onto copper grids and dried in a vacuum desiccator.

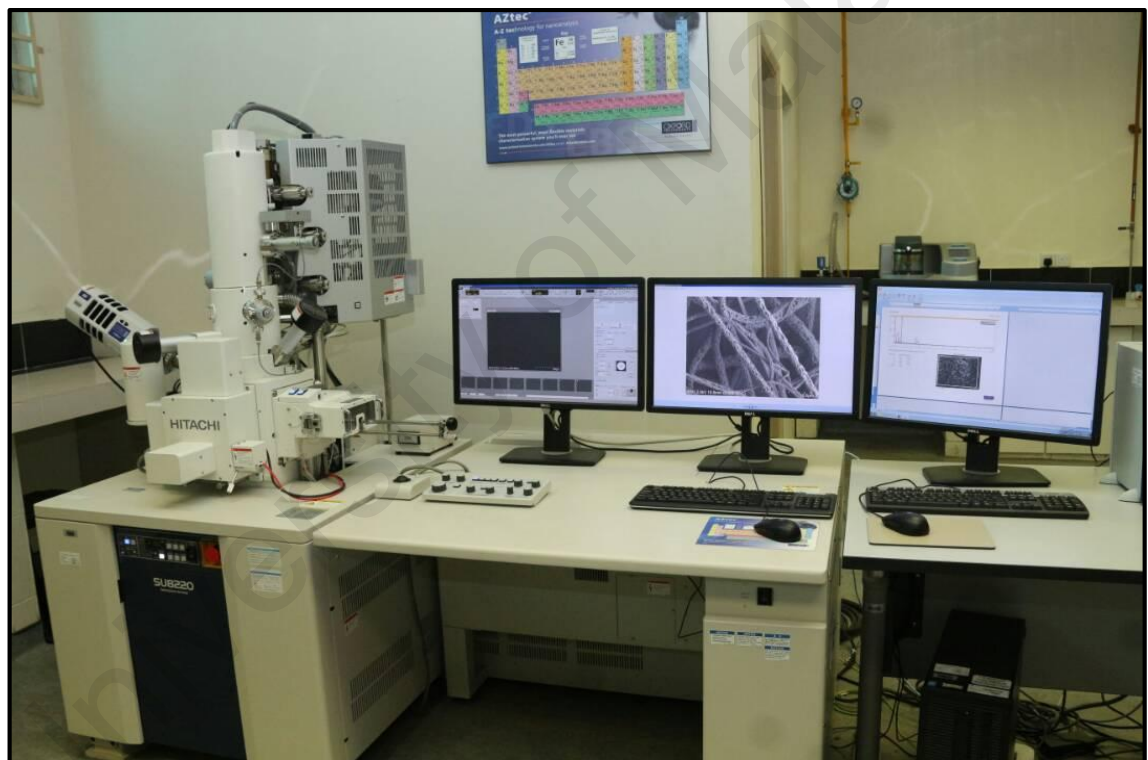


Figure 3.7: FESEM machine equipped with EDS

3.3.4 X-ray Diffraction (XRD)

X-ray diffraction is a useful technique in determine the structure, composition as well as state of polycrystalline materials. In this work, X-Ray Diffraction was performed to determine the structure and planes of the synthesized Au, Ag and Au-Ag nanoparticles between 20° to 90°. The XRD pattern of the samples were recorded with a PANalytical Empyrean X-ray diffractometer using Cu K_α radiation of $\lambda = 1.54060 \text{ \AA}$. Throughout these experiments, the samples were thin films, prepared by drop coating of the solution on glass slides as shown in Figure 3.8 and followed by drying at room temperature. The scan parameters of the diffractometer was set with step size of 0.02°. The voltage and current used are 40 kV and 40 mA, respectively.

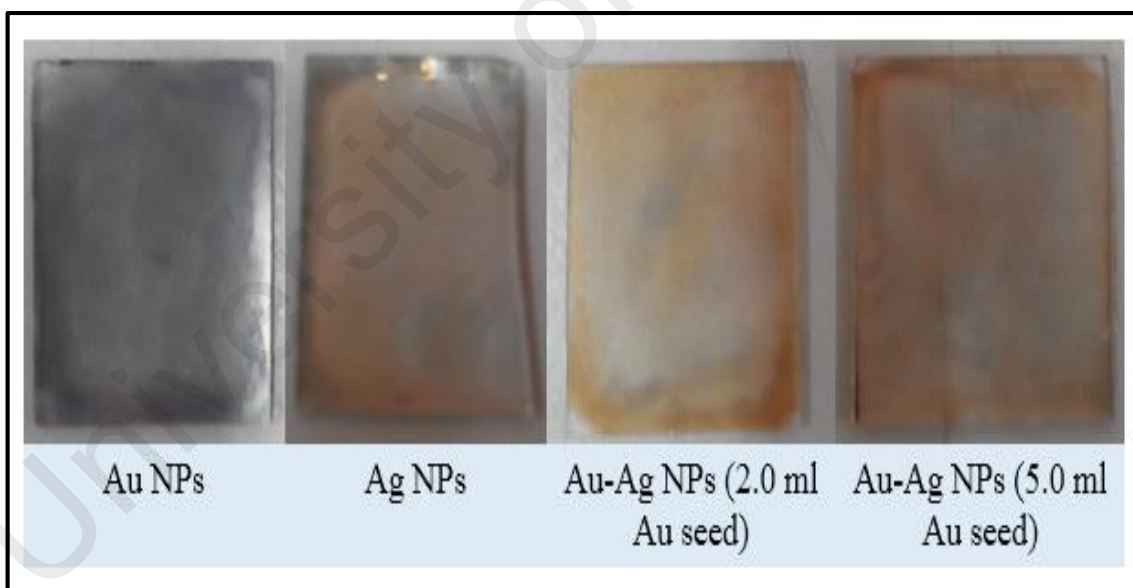


Figure 3.8: Thin film by drop coating of the Au, Ag and Au-Ag nanoparticles on glass slide



Figure 3.9: XRD machine

3.3.5 High Resolution Electron Microscopy (HRTEM)

High resolution electron microscopy provides high resolution images at the atomic scale level. The high resolution transmission electron microscopy (HRTEM) uses both the transmitted and scattered beams to create an interference image. It is a phase contrast image and can be as small as the unit cell of a crystal. The HRTEM model is TECNAI TF20 X-Twin FEI at accelerating voltage of 200 kV.

Sample preparation for HRTEM analysis was similar with the sample preparation of TEM in previous section. The nanoparticles samples were sonicated in an ultrasonic bath for 10 minutes to break the agglomeration. Then, the samples were drop-casted onto copper grids and dried in a vacuum desiccator. After that, the copper grids were inserted into the holder for analysis.



Figure 3.10: HRTEM machine

3.3.6 Zeta Potential

Zeta potential (ζ) is a measure of the surface electrostatic potential of the nanoparticles. It is related to the electrophoretic mobility and stability of the nanoparticles suspension (Dougherty et al., 2007). In this research, zeta potential analysis was performed to measure the potential stability and surface charge of the synthesized Au, Ag and Au-Ag nanoparticles by using Zetasizer Nanoseries ZS (Malvern, UK) instrument at room temperature. The procedure for sample preparation, started with the sample solutions were injected into a disposable capillary cell. Next, the sample cell was inserted into the instrument and the measurement was started after the sensors have equilibrated. The measurement was run and results were collected, and represented as a graph of total counts versus zeta potential. The sign value whether positive or negative determines the

state of charge at the particle surface. Particles with zeta potentials more positive than +30 mV or more negative than -30 mV are normally considered stable (Zhang & Yang, 2008).



Figure 3.11: Zeta-sizer instrument

3.3.7 High Angle Annular Dark Field Scanning Transmission Electron Microscopy

The HAADF-STEM analysis were conducted by TECNAI TF20 X-Twin FEI with an accelerating voltage of 200 kV. This testing was done to reveal the elemental distributions of Au and Ag in Au-Ag nanoparticles. The signal in HAADF-STEM mode depends on the atomic number of the elements. Samples for HAADF-STEM observations were prepared on copper grid and dried in a vacuum desiccator, which is same way with TEM analysis sample preparation.

3.3.8 Catalytic Activity Reduction of 4-NP

The reduction of 4-NP to 4-AP was performed to evaluate the catalytic activity of the Au, Ag and Au-Ag nanoparticles. The reaction was carried out in a standard quartz cuvette. For the reduction process, the 4-NP solution (3.0 ml, 0.2 mM) was added with 1.0 ml of distilled water. This was followed by the addition of aqueous NaBH₄ (0.5 ml, 0.4 M) solution, resulting in the color change from light yellow to bright yellow. Finally, 0.2 ml of the nanoparticles catalyst (Au, Ag and Au-Ag) was added to the reaction mixture. After the addition of the nanocatalyst, the UV-vis spectral absorbance was recorded at every 1 minute interval in the range of 200 to 800 nm at room temperature.

CHAPTER FOUR

RESULTS AND DISCUSSION

4.1 Introduction

In this chapter, the monometallic Au, Ag and bimetallic Au-Ag nanoparticles synthesized via the citrate thermal reduction and seed colloidal techniques, respectively are obtained. After that, the nanoparticles are used for catalytic reduction of 4-NP to 4-AP. The details of results are discussed throughout this chapter.

4.2 UV-visible (UV-Vis) Analysis

The UV-vis measurement was performed to obtain the surface plasmon resonance (SPR) of the Au, Ag and Au-Ag nanoparticles. The absorption spectra of the colloidal solution of gold nanoparticles are shown in Figure 4.1-4.3. The UV-vis absorbance spectra of the resultant Au and Ag nanoparticles appeared at 523 and 428 nm, respectively.

Gold nanoparticles are known to exhibit a range of surface plasmon resonance between 500 to 600 nm (Kumari et al., 2016). During heating, the color of the HAuCl_4 solution changed from yellow to maroon due to the reduction of Au^{3+} to Au NPs after the addition of citrate aqueous solution.

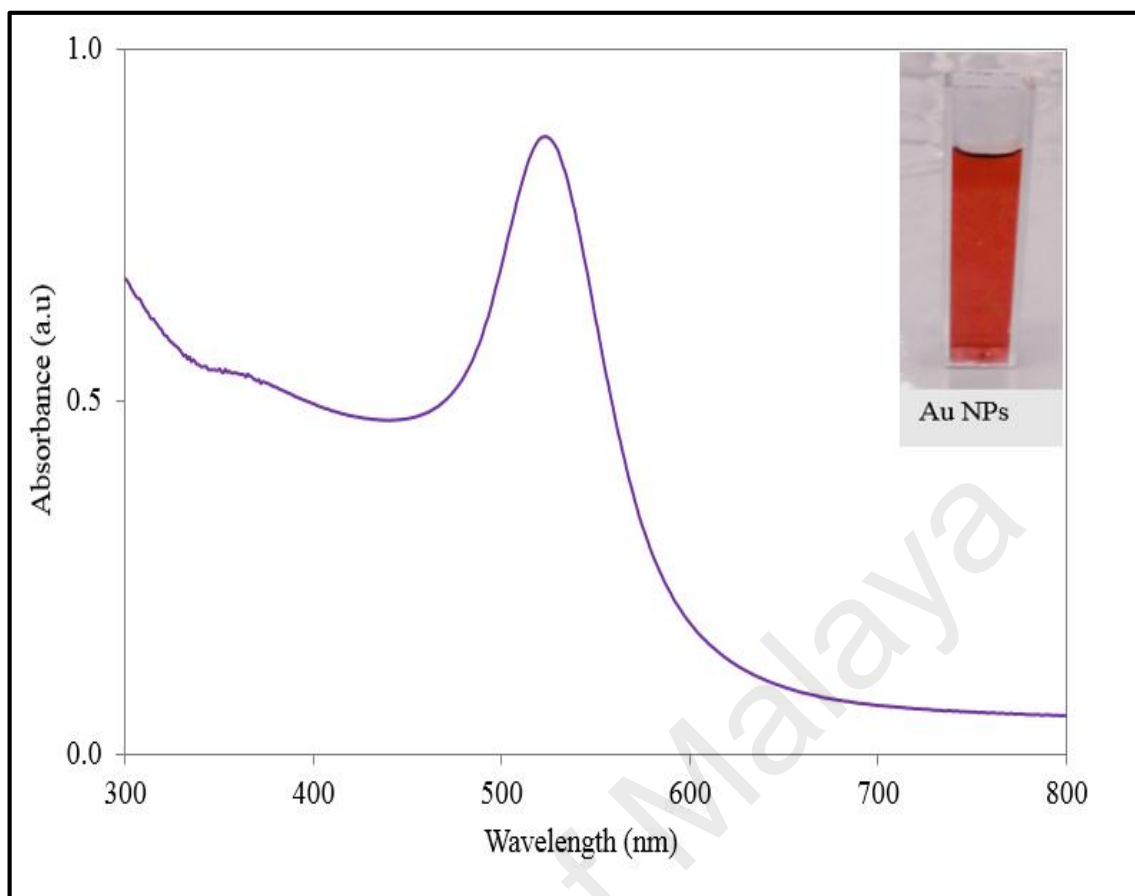


Figure 4.1: UV-Vis absorption spectra for Au nanoparticles

The absorbance spectra between 350 nm to 450 nm region is typical of the silver nanoparticles (Mamun Ur Rashid, 2013). The absorption spectra of the colloidal solution of Ag nanoparticles are shown in Figure 4.2. The color of the synthesized silver colloidal is a chrome yellow solution (Basavaraj Udupudi, 2012). The source of the Ag NPs is the AgNO_3 salt.

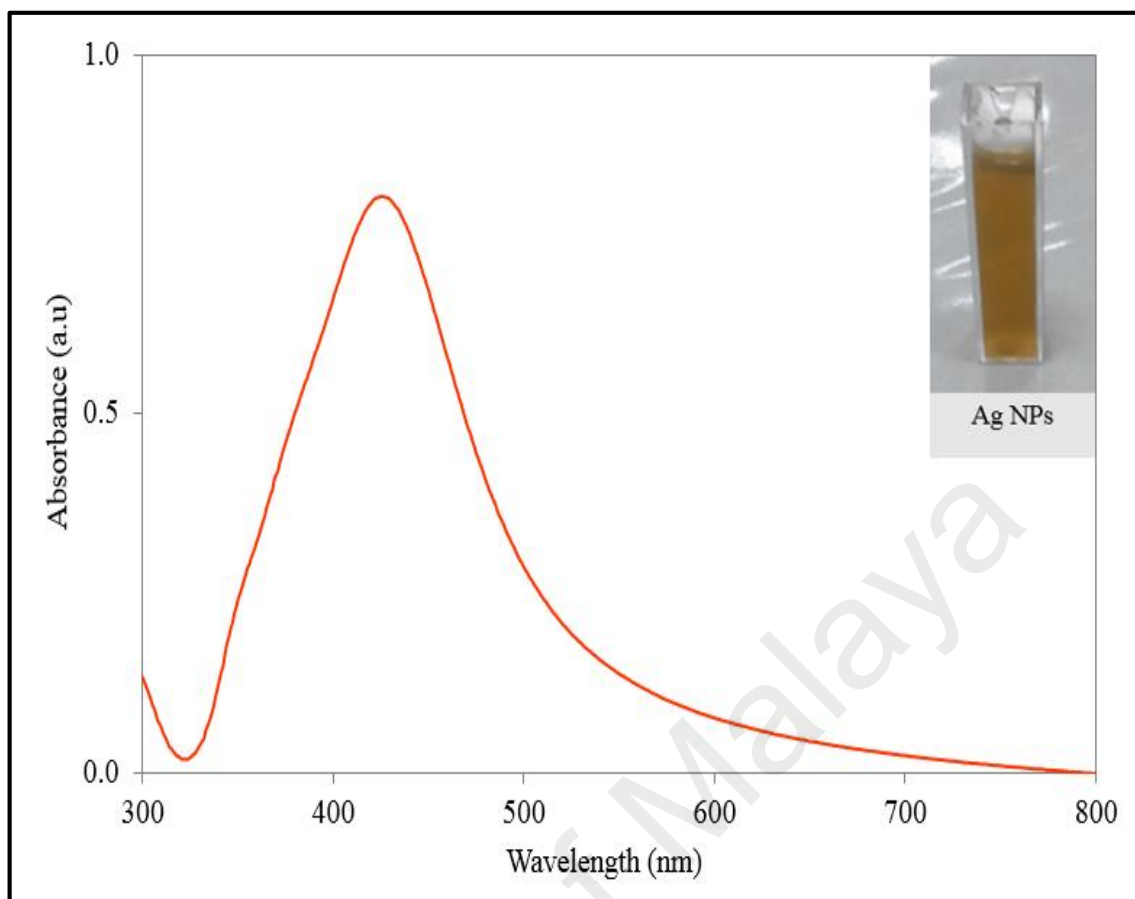


Figure 4.2: UV-Vis absorption spectra for Ag nanoparticles

The UV-Vis absorbance spectra of the Au-Ag bimetallic NPs of 2.0 ml and 5.0 ml Au seeds volumes showed SPR peaks at 450 nm and 435 nm, respectively as shown in Figure 4.3. The maximum absorbance spectra of bimetallic NPs shows a single peak suggesting a homogeneous colloidal mixture of the Au and Ag nanoparticles without signifying formation of independent particles (Kalantari et al., 2017; Yang et al., 2008). The solution color changes from light pink to yellow-orange with the addition of AgNO_3 and ascorbic acid solution indicating the deposition of Ag layer onto the surface of Au NPs. The ascorbic acid and citrate solutions serve as a weak reducing agent for the reduction of Ag ions and also as a stabilizing agent (Yang et al., 2008). The stabilizing agents prevented the agglomeration of the newly formed nanoparticles. The SPR band gives useful information about the size of the synthesized nanoparticles. This is because

the frequency and width of SPR rely on the size of the nanoparticles as well as on the dielectric constant of the metal itself and the surrounding medium (Huang et al., 2007). In addition, Yong *et al.*, (2008) stated the surface plasmon resonance depends on the particle size, shape and its surrounding environment. Thus, the surface plasmon band for the bimetallic core shell nanoparticles can evaluate by its polarizability. The equation as follows:

$$\alpha = R_3 \frac{(\epsilon_s - \epsilon_m)(\epsilon_c + 2\epsilon_s) + (1-g)(\epsilon_c - \epsilon_s)(2\epsilon_s + \epsilon_m)}{(\epsilon_s - 2\epsilon_m)(\epsilon_c + 2\epsilon_s) + (1-g)(\epsilon_c - \epsilon_s)(2\epsilon_s - \epsilon_m)} \quad (4.1)$$

$$g = 1 - \frac{R_1^3}{R_2^3} \quad (4.2)$$

where ϵ_m is the dielectric constant of the matrix, ϵ_c is the dielectric function of the core, ϵ_s is the dielectric functions of the shell materials, g is the volume fraction of the shell layer, R_1 is the radius of the core and R_2 is the radius of the total particle.

According to Equations 4.1 and 4.2, the plasmon band gradually shift to the longer wavelength (red-shift) as the seed volume is decreased, suggesting the formation of bimetallic core shell nanoparticles with larger diameter (Yang et al., 2008). From the UV-Vis absorbance spectra, it was observed that the SPR band gradually shifted to higher wavelengths region as the seed volume decreased, signifying the formation of bimetallic Au-Ag nanoparticles with relatively larger diameters. The optical properties of the Au-Ag NPs exhibited a plasmon resonance at 450 nm and 435 nm which corresponded to

particles that are mostly in Ag character. Generally, it is known that Ag NPs have plasmon absorbance at about 400 nm (Chen et al., 2002).

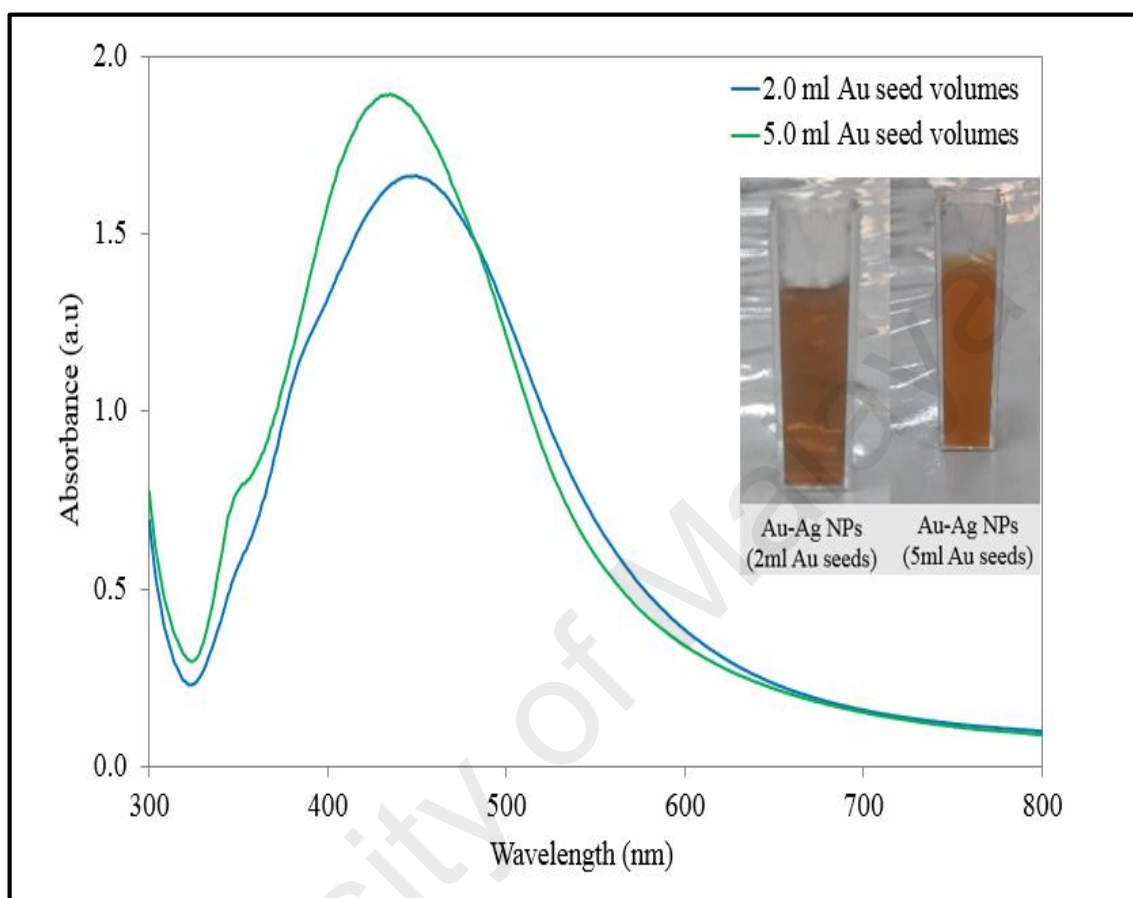


Figure 4.3: UV-Vis absorption spectra for Au-Ag nanoparticles

4.3 Morphological and Physical Size Studies

4.3.1 Transmission Electron Microscopy (TEM) Analysis

TEM was utilized to investigate the size and morphology of the resulting Au, Ag and Au-Ag nanoparticles. The TEM analysis of the nanoparticles were performed at scales of 100 nm.

The mean diameter of Au NPs was around 24.0 ± 2.7 nm. The Au nanoparticles synthesized by citrate thermal reduction method are monodispersed with spherical shape and broad size distribution. The TEM micrograph of the gold nanoparticles can be seen in Figure 4.4.

The mean diameter of the Ag nanoparticles is about 27.5 ± 4.0 nm. The size is larger than the gold nanoparticles. Figures 4.6-4.7 shows a typical TEM image of the Ag NPs with its corresponding size distribution histogram. The TEM analysis shows that the Ag NPs are more polydispersed in appearance.

Figures 4.8 and 4.10 demonstrate the TEM images of bimetallic Au-Ag NPs at different volume of Au seeds. TEM images of the NPs revealed that most of the bimetallic Au-Ag NPs were about spherical in shape and well dispersed. The mean diameter of the bimetallic Au-Ag NPs is approximately 75.2 ± 5.3 nm and 55.2 ± 6.0 nm, corresponding to 2.0 ml and 5.0 ml of Au seed, respectively. The mean diameter of bimetallic Au-Ag NPs is larger than pure Au and Ag NPs, indicating that the gold nanoparticles are mixed by silver (Yang et al., 2008). The TEM is a well-known method to confirm the bimetallic structures of nanoparticles between gold and silver due to the contrast difference caused by the atomic number Z of gold and silver (79 for Au; 47 for Ag) (Zhang et al., 2011).

From the mean diameter values of Au-Ag NPs, particle size for 2.0 ml Au seed was larger than the 5.0 ml Au seed which is in good agreement with the UV-vis results.

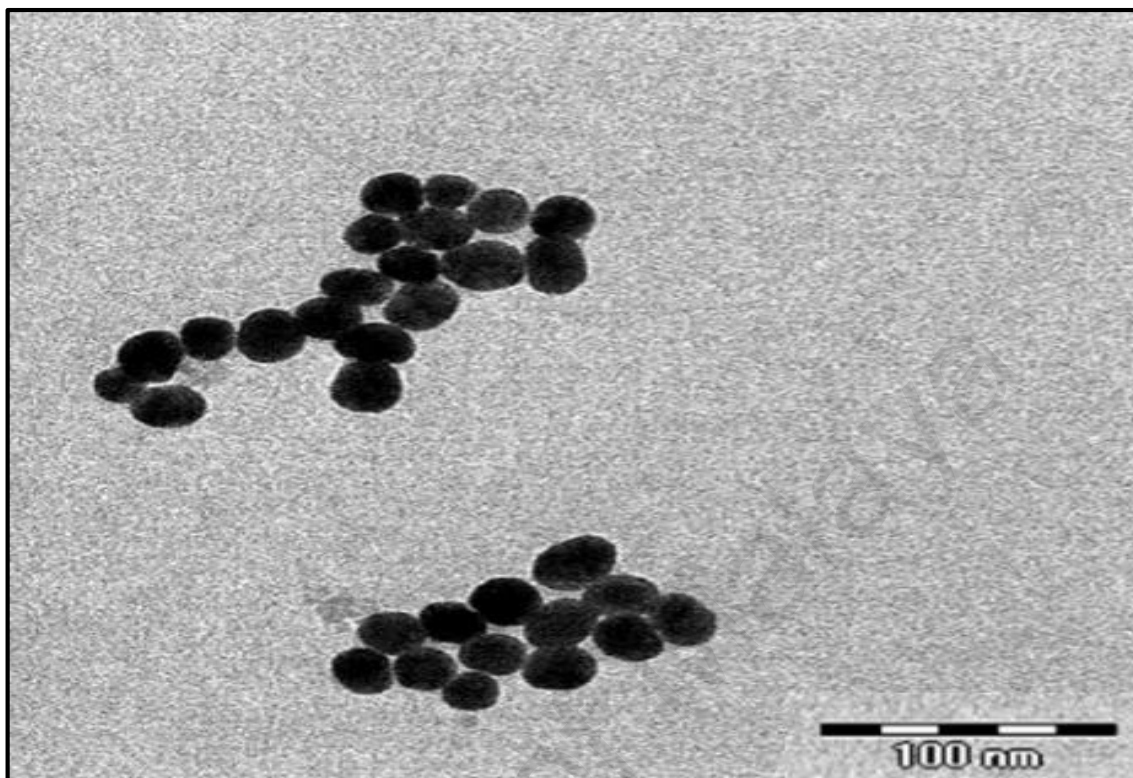


Figure 4.4: TEM image of Au nanoparticles

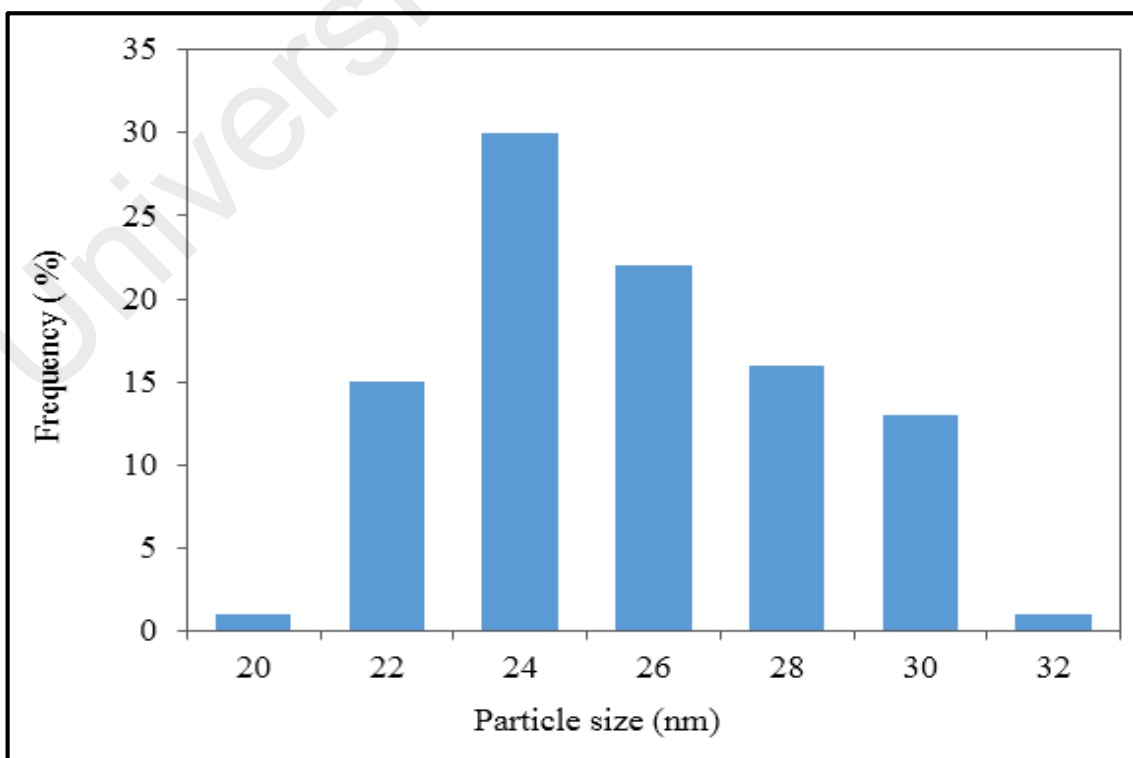


Figure 4.5: Particle size distribution of Au nanoparticles

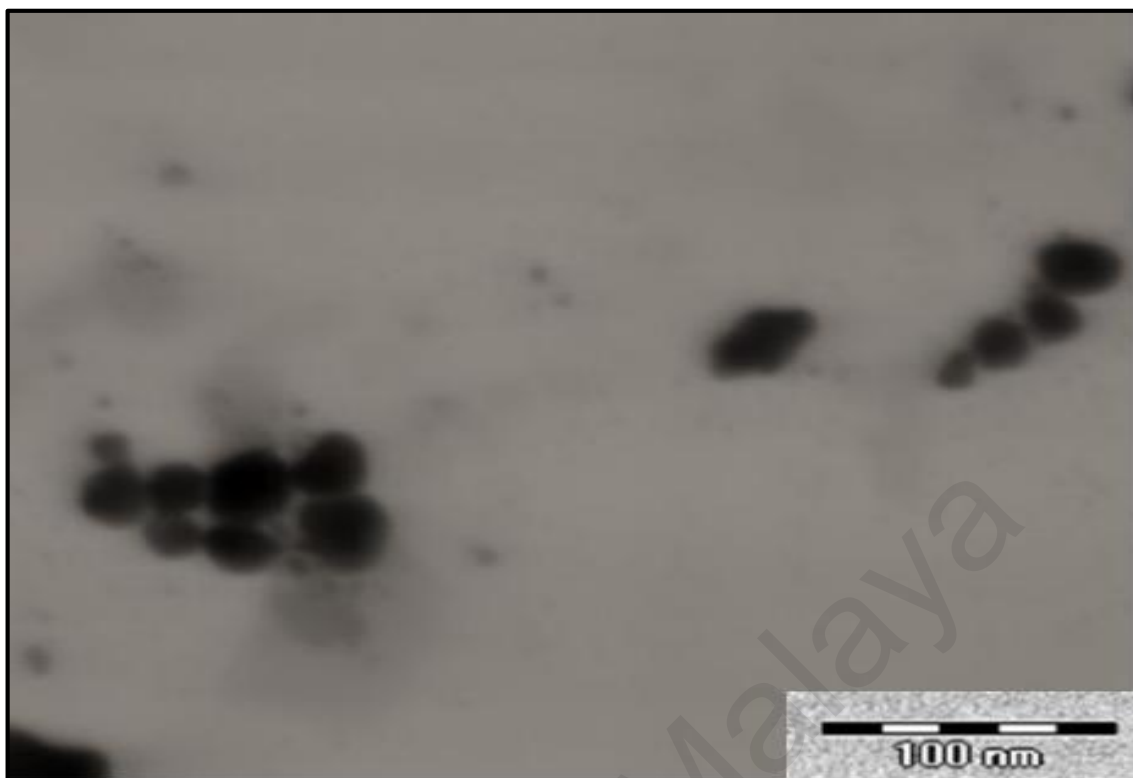


Figure 4.6: TEM image of Ag nanoparticles

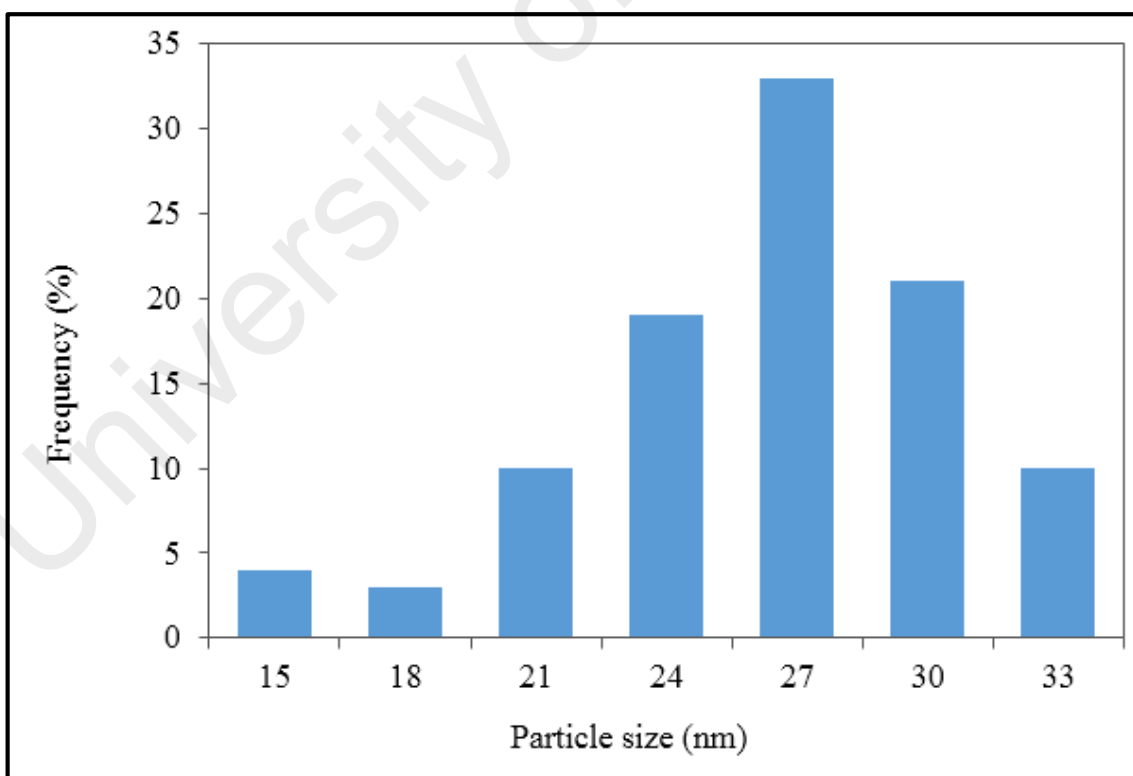


Figure 4.7: Particle size distribution of Ag NPs

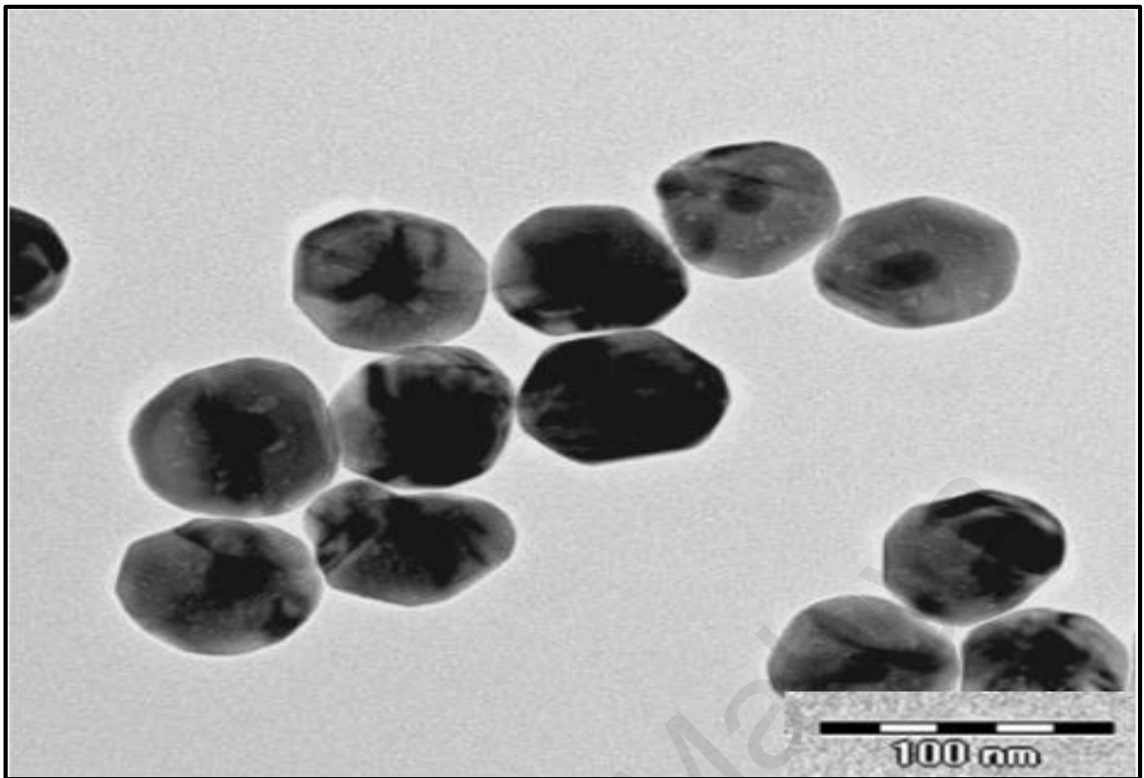


Figure 4.8: TEM image of Au-Ag NPs with 2.0 ml Au seeds volume

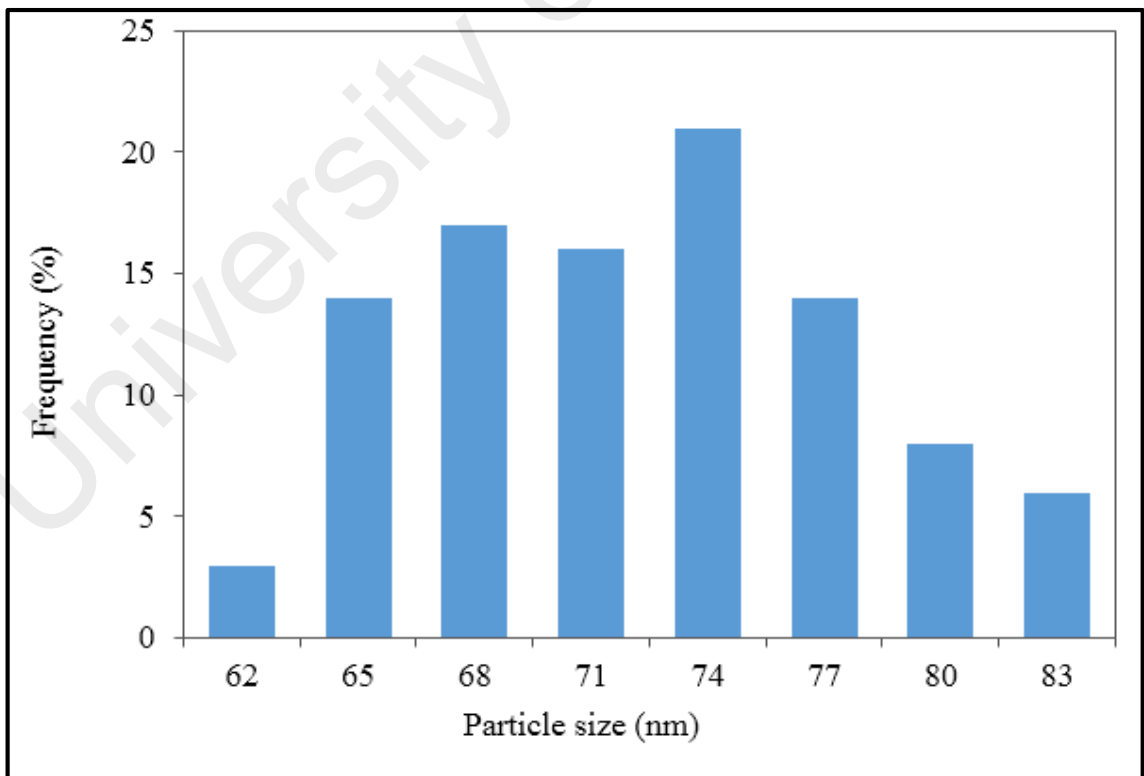


Figure 4.9: Particle size distribution of Au-Ag NPs with 2.0 ml Au seeds volume

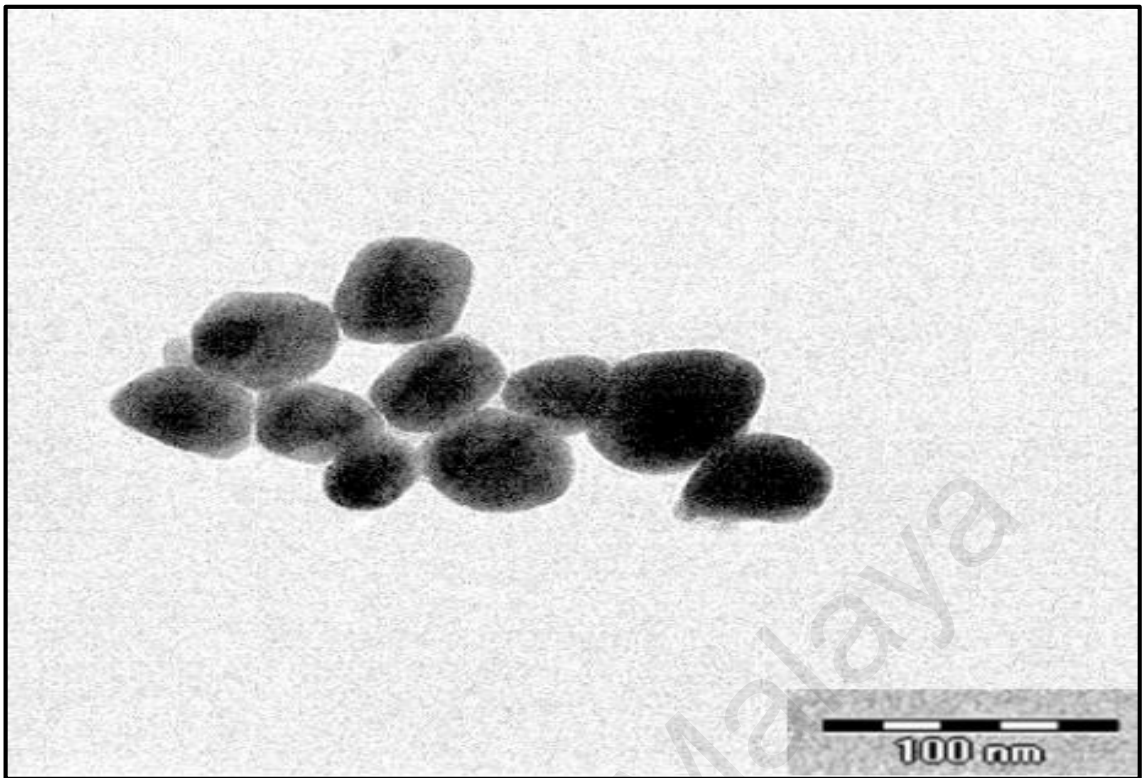


Figure 4.10: TEM image of Au-Ag NPs with 5.0 ml Au seeds volume

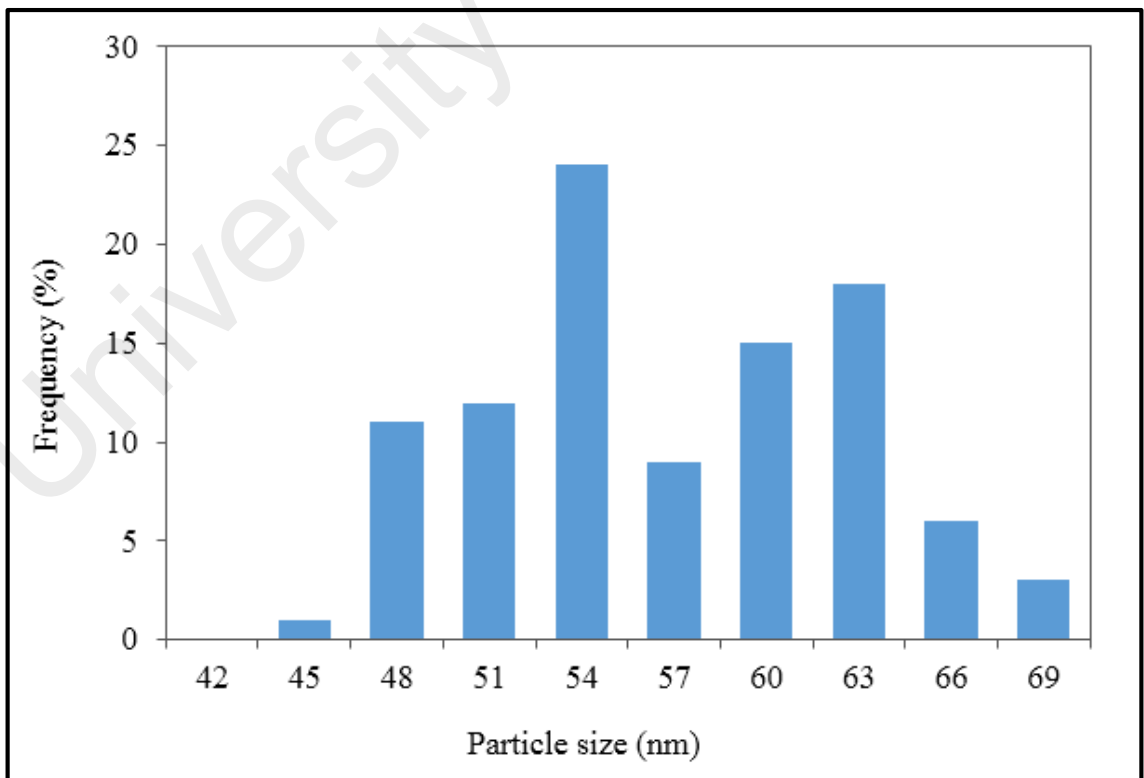


Figure 4.11: Particle size distribution of Au-Ag NPs with 5.0 ml Au seeds volume

4.3.2 Electron Dispersive X-ray Spectroscopy (EDS) Analysis

The EDS spectra of Au, Ag and bimetallic Au-Ag NPs were shown in Figures 4.12-4.15. The EDS of nanoparticles are from bright field-scanning transmission electron microscopy (BF-STEM) images. From the images, the nanoparticles are spherical in shape. The EDS was done to confirm the presence of Au and Ag element at selected points in the solution. The sample testing were performed by drop-casting onto the copper grids and dried a vacuum desiccator.

Figure 4.12 confirms the presence of Au together with the trace peaks for C and Cu in the solution. The peak of Au element occurs at 0.4, 2.1 and 8.5 keV. The signals of C and Cu from the copper grid.

Figure 4.13 depicts the elements present in the Ag nanoparticles. The Ag element present in the Ag nanoparticles. The peak of Ag occurs at 0.3 and 3.0 keV. The signals of C and Cu could have arisen from the copper grid.

The EDS spectra of Au-Ag nanoparticles with different volume of Au seeds are depicted in Figures 4.14-4.15 show the presence of Au, Ag, C and Cu elements. The spectrum of 2.0 ml Au seeds shows peaks corresponding to Au at 2.0, 9.5 and 11.5 keV while the peak at 3.2 keV was attributed to Ag. Meanwhile, 5.0 ml of Au NPs seed spectrum shows Au and Ag peaks at 2.0 and 3.0 keV, respectively. The EDS results confirmed the presence of Au and Ag elements in the bimetallic NPs. The presence of carbon and copper peaks in the spectrum was due to the copper grid used. The intensity of peaks of Au and Ag elements in the Au-Ag nanoparticles depend on the selected points during the EDS measurements. This was the indication of the quality of the bimetallic nanoparticles in terms of their homogeneity.

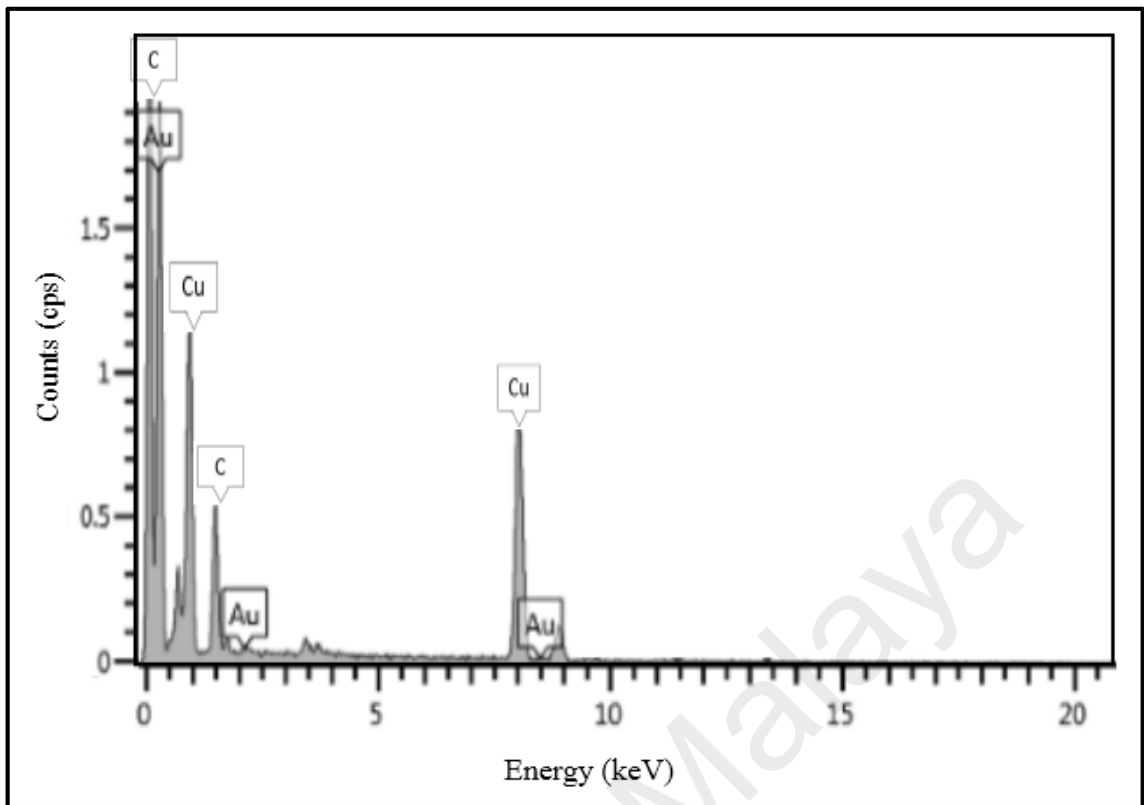


Figure 4.12: EDS spectra of Au NPs

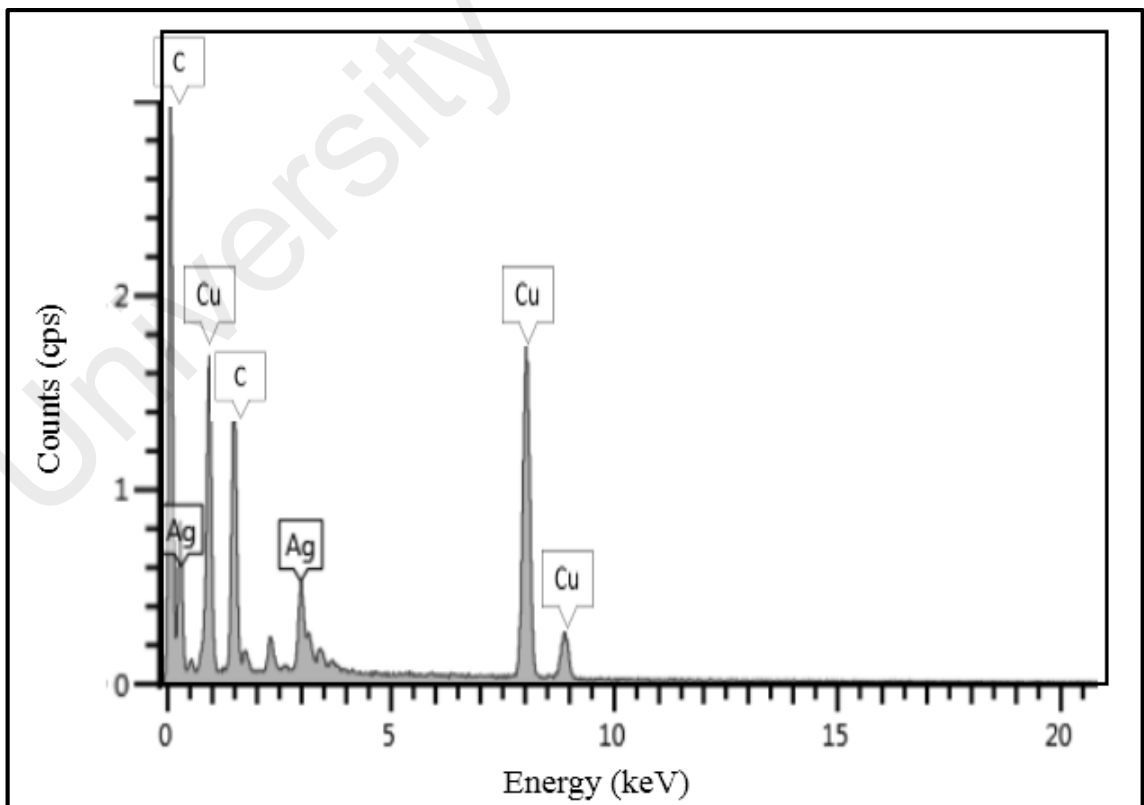


Figure 4.13: EDS spectra of Ag NPs

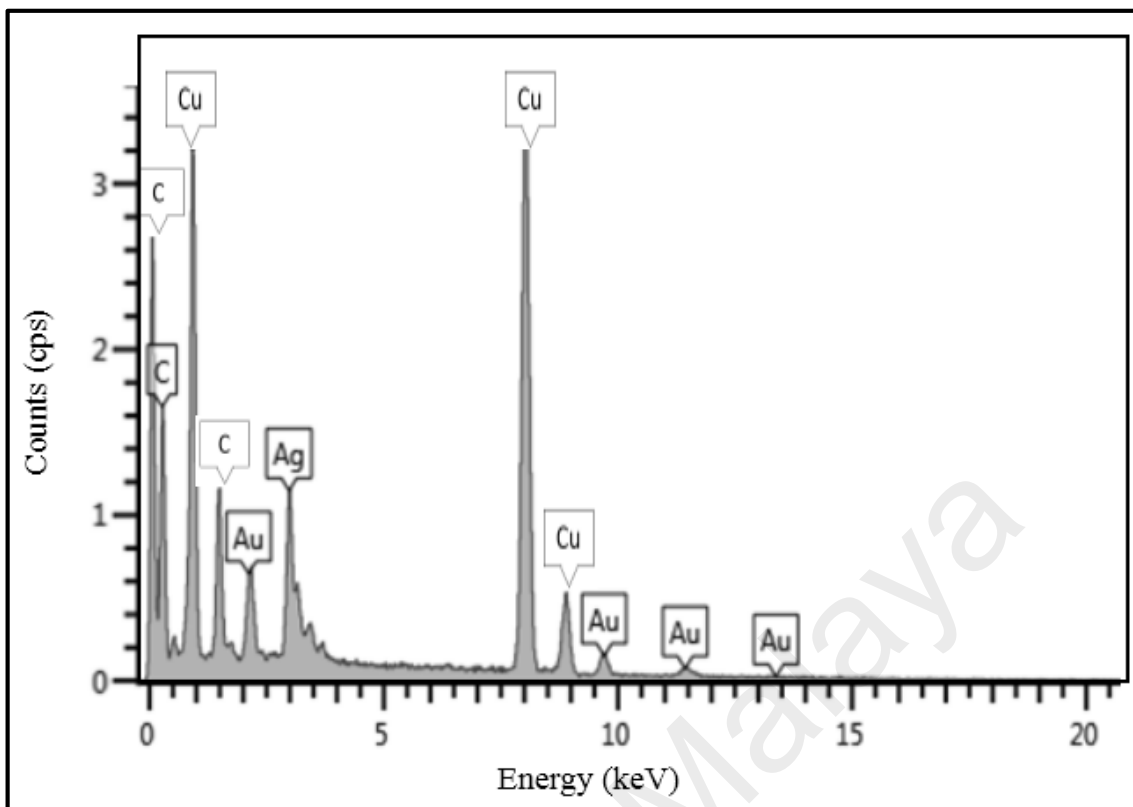


Figure 4.14: EDS spectra of Au-Ag NPs at 2.0 ml Au seeds volume

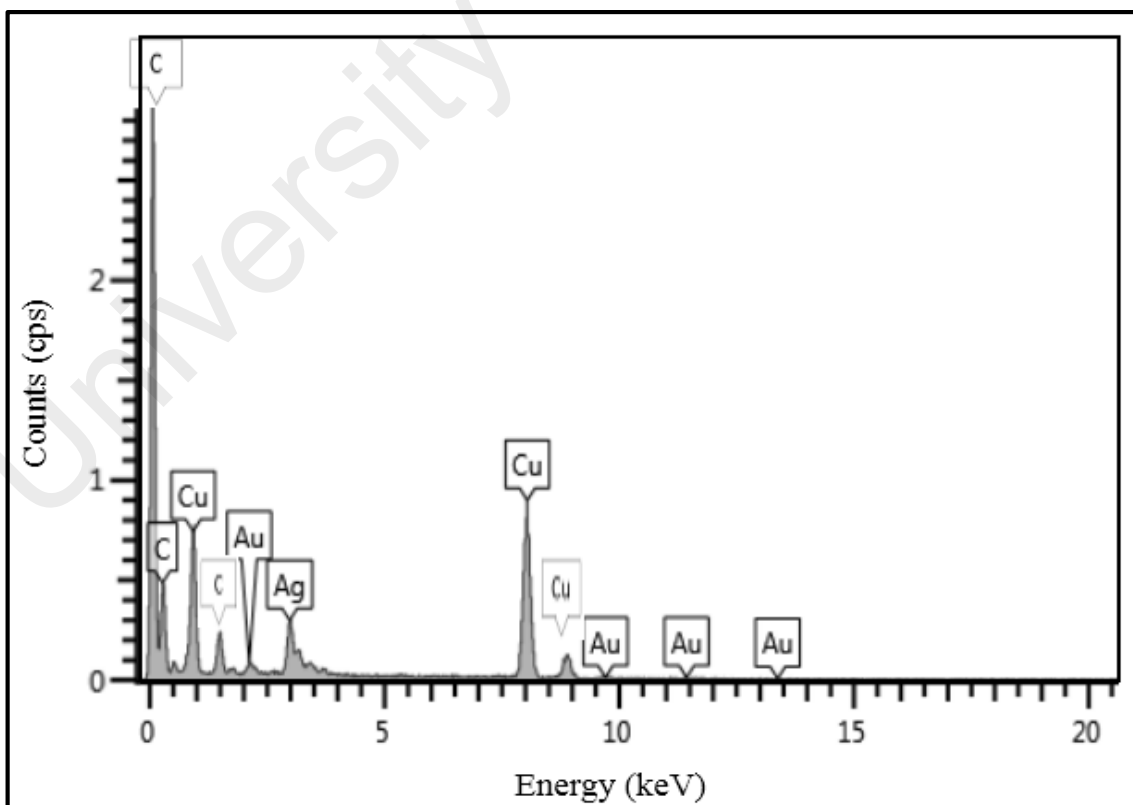


Figure 4.15: EDS spectra of Au-Ag NPs at 5.0 ml Au seeds volume

4.3.3 Zeta Potential Analysis

The zeta potential values of Au, Ag and bimetallic Au-Ag nanoparticles of different volume of Au seed are represented in Table 4.1. While, the electro-kinetic parameters of Au, Ag and Au-Ag NPs are shown in Figure 4.16. The zeta potential for nanoparticles have negative values. The negative zeta potential value revealed that the Au NPs and bimetallic Au-Ag NPs possess moderate stability (Jana et al., 2001). The zeta potential of gold and silver nanoparticles relies on the surface modification. The Au and Ag NPs were prepared by sodium citrate and has a negative value of -39.2 mV and -50.4 mV, respectively. This is due to the charge stabilization through the electrostatic interaction between the Au and Ag NPs with citrate ions (Banerjee et al., 2011; Guarnizo et al., 2015). The negative value is also due to the presence of surface adsorbed and free citrate ions in their aqueous suspension. Meanwhile, the zeta potentials of the bimetallic Au-Ag NPs were -31.5 mV and -20.9 mV for 2.0 ml and 5.0 ml Au seed, respectively. These values are associated with the stability of the nanoparticles; which could be related to the agglomeration phenomenon. In addition, there is less agglomeration at higher zeta potential values which causes the nanoparticles to grow larger (Valdez & Gómez, 2016). The aggregation in aqueous solution is due to the surface hydrophobicity which causes eventual loss of catalytic activity (Yang et al., 2006). In this case, sodium citrate was used to prevent the particle aggregation during the synthesis process of nanoparticles.

The citrate-capped Au NPs and Ag NPs are probably stabilized by the steric repulsions due to the presence of coordinated or adsorbed citrates along with the dangling citrate species, which are not in direct contact with the metal surfaces of Au and Ag NPs. Then, the intermolecular interactions occur between the absorbed citrate and dangling citrate anions through the COOH hydrogen bonds and citrate multilayers are formed on the nanoparticles surface. As a result, the steric repulsion between the citrate layers is

present on the adjacent nanoparticles, and helps to stabilize the nanoparticle dispersion in solution (Monga & Pal, 2015).

Table 4.1: Particle size and zeta potential for Au NPs, Ag NPs and bimetallic Au-Ag NPs

Sample	Particle Size (nm)	Zeta Potential (mV)
Au NPs	24.1 ± 2.7	-39.2
Ag NPs	27.5 ± 4.0	-50.4
Au-Ag NPs (2.0 ml Au seed)	75.2 ± 5.3	-31.5
Au-Ag NPs (5.0 ml Au seed)	55.2 ± 6.0	-20.9

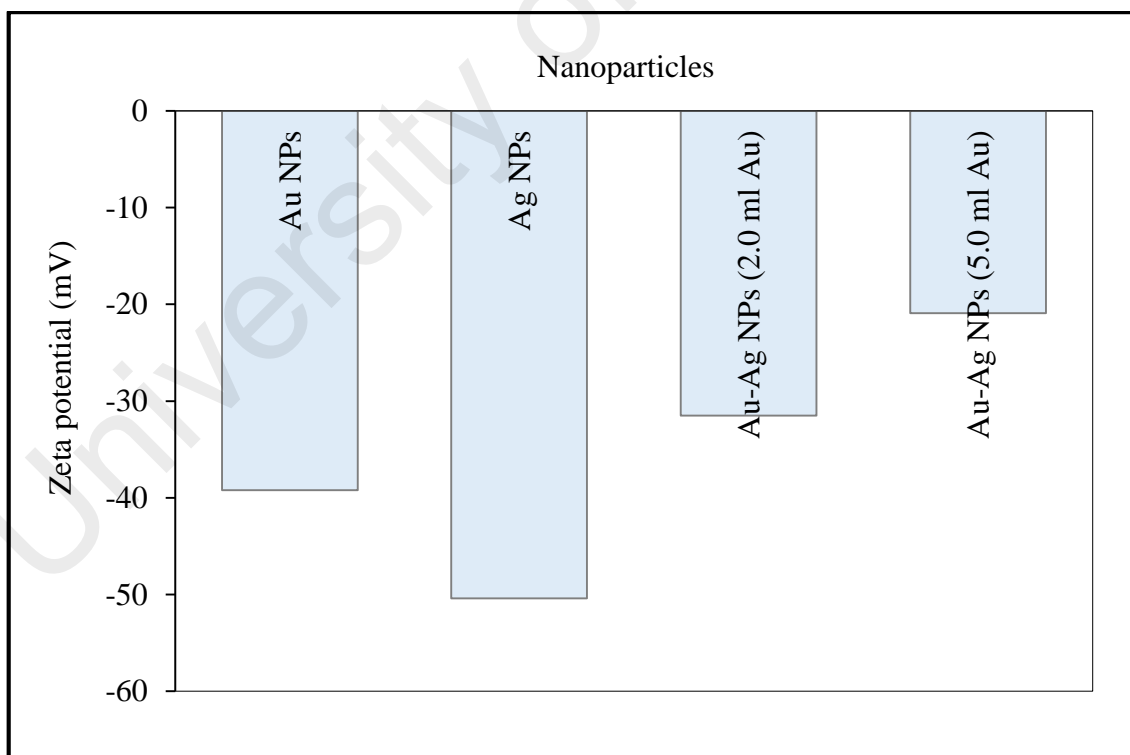


Figure 4.16: Electro-kinetic parameters of Au, Ag and Au-Ag nanoparticles

4.3.4 High Resolution Transmission Electron Microscopy (HRTEM) Analysis

Figures 4.17 (a, b) and 4.14 illustrate the HRTEM images of the Au-Ag bimetallic NPs. A significant change in the contrast between the dark and lighter region indicated the formation of the bimetallic Au-Ag NPs. Figure 4.18 shows a 0.20 nm lattice spacing which was indexed to the (200) plane of face-centered cubic (FCC) of silver (Krishnamurthy et al., 2014), whereas the measured lattice spacing of 0.23 nm matching well with the (111) planes of FCC gold (Banerjee et al., 2011; Monga & Pal, 2015).

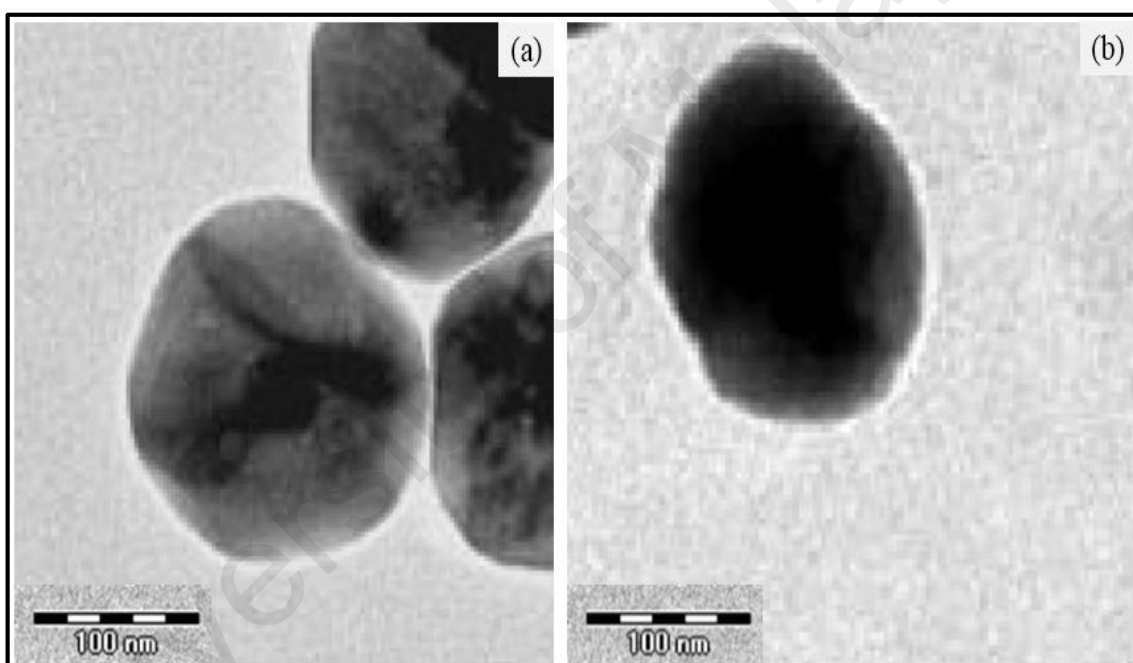


Figure 4.17: HRTEM images of Au-Ag bimetallic NPs for different volume of Au seed

(a) 2.0 ml, (b) 5.0 ml

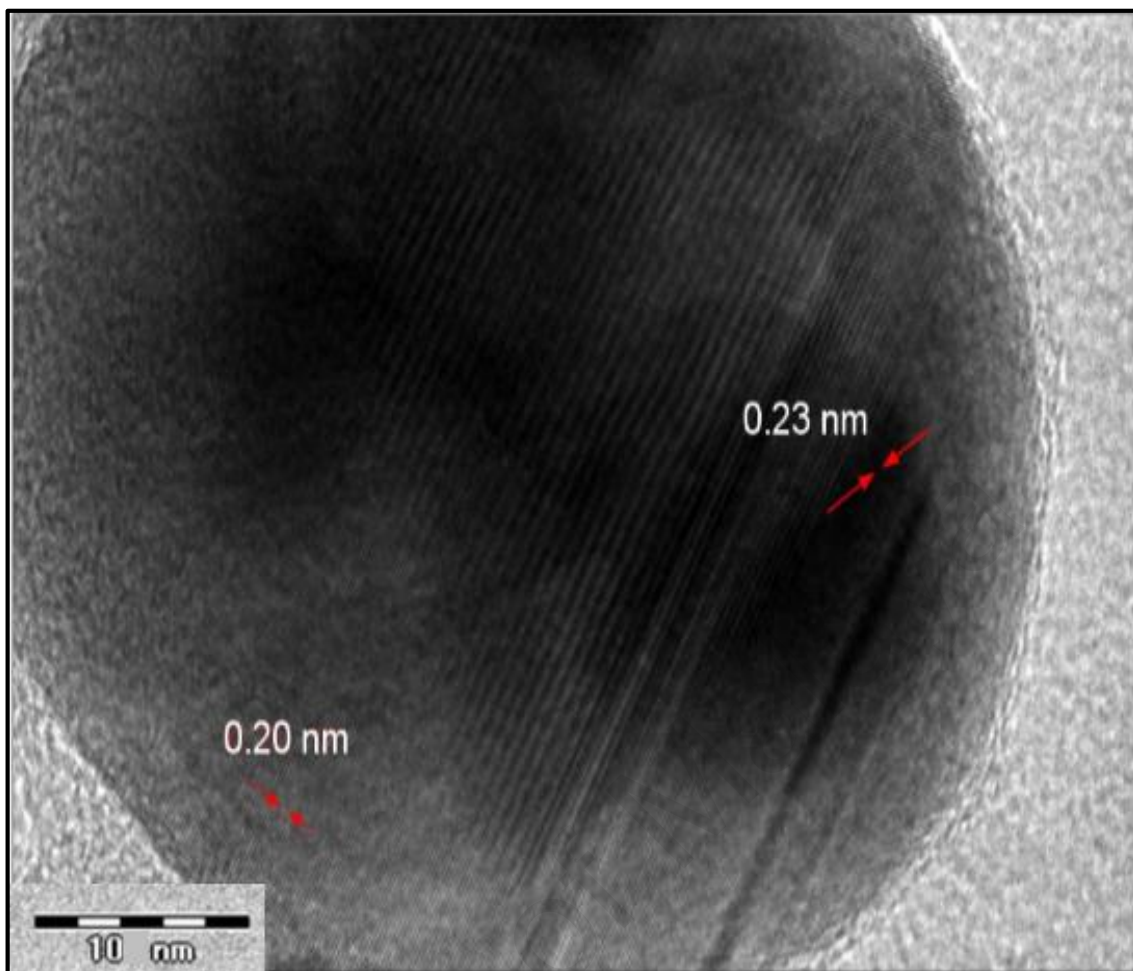


Figure 4.18: HRTEM images of lattice spacing of Au-Ag NPs

4.3.5 High Angle Annular Dark Field Scanning Transmission Electron Microscopy (HAADF-STEM) Analysis

The HAADF-STEM images of the bimetallic Au-Ag NPs at magnification 100 and 200 nm were obtained in Figures 4.19-4.20 and 4.22-4.23 showing a contrast between Au and Ag elements, which dominated by Rutherford scattering (Esparza et al., 2017). Since the signal in HAADF-STEM mode depends on the atomic number of the elements, the strong brightness corresponding to the Au (heavy element) and the low brightness refer to the Ag (lighter element). Difference caused by the atomic number (Z) of gold and silver (79 for Au; 47 for Ag) (Zhang et al., 2011). The image in Figures 4.21 and 4.24 clearly

shows the elemental distribution of the Au and Ag in the bimetallic nanoparticles. According to the EDS mapping as shown in Figures 4.21 (a, b) and 4.24 (a, b), the presence of Au signal (yellow) and Ag signal (turquoise) in the bimetallic Au-Ag NPs were indicated.

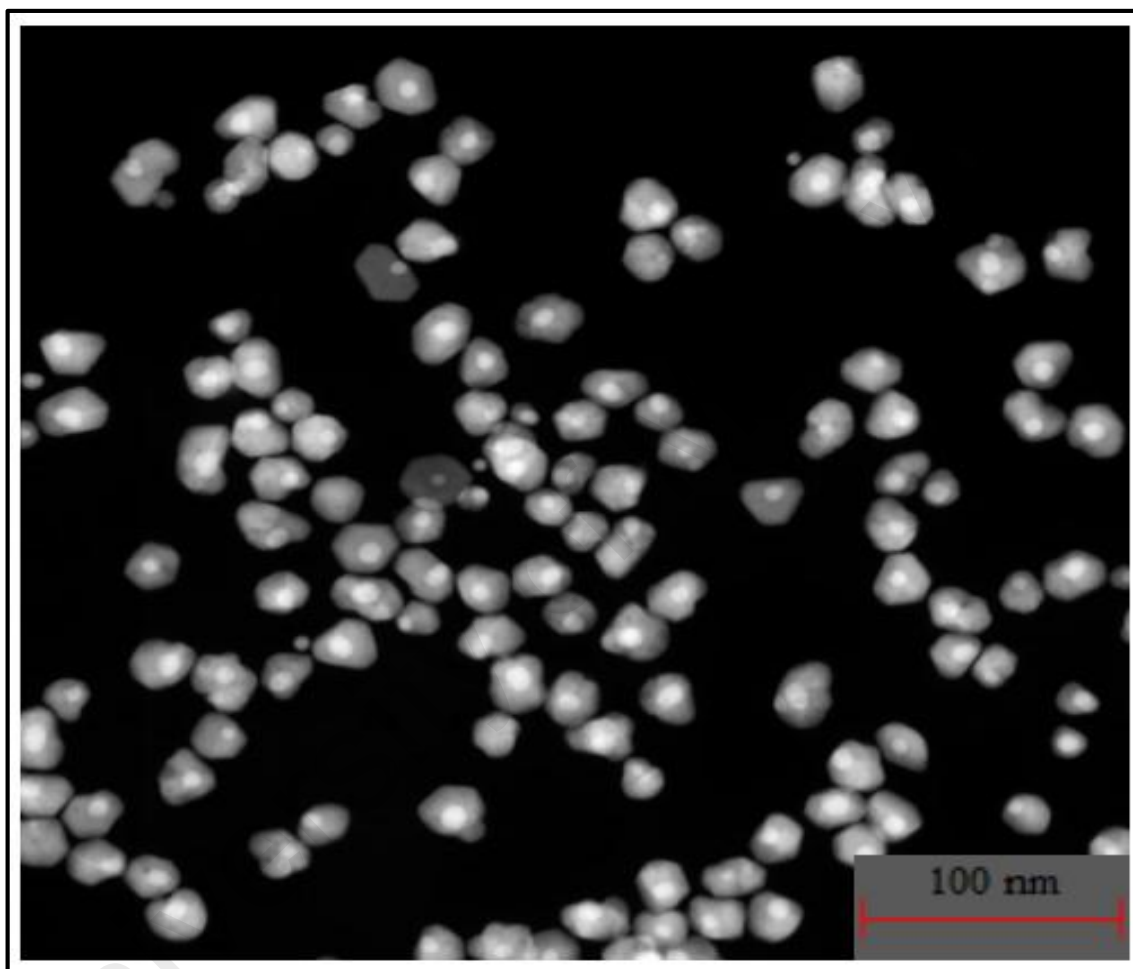


Figure 4.19: HAADF-STEM image of 2.0 ml Au seeds of Au-Ag NPs at magnification

100 nm

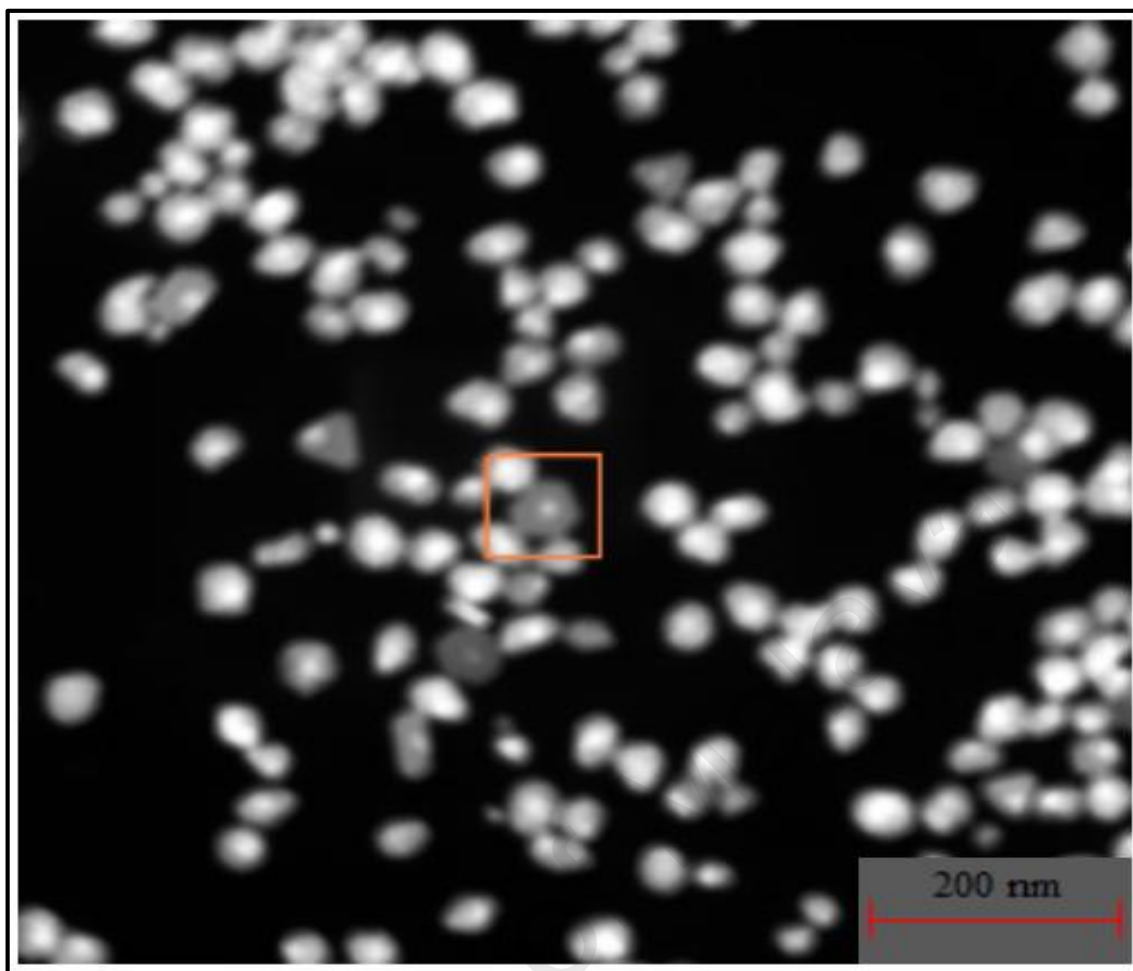


Figure 4.20: HAADF-STEM image of 2.0 ml Au seeds of Au-Ag NPs at magnification 200 nm

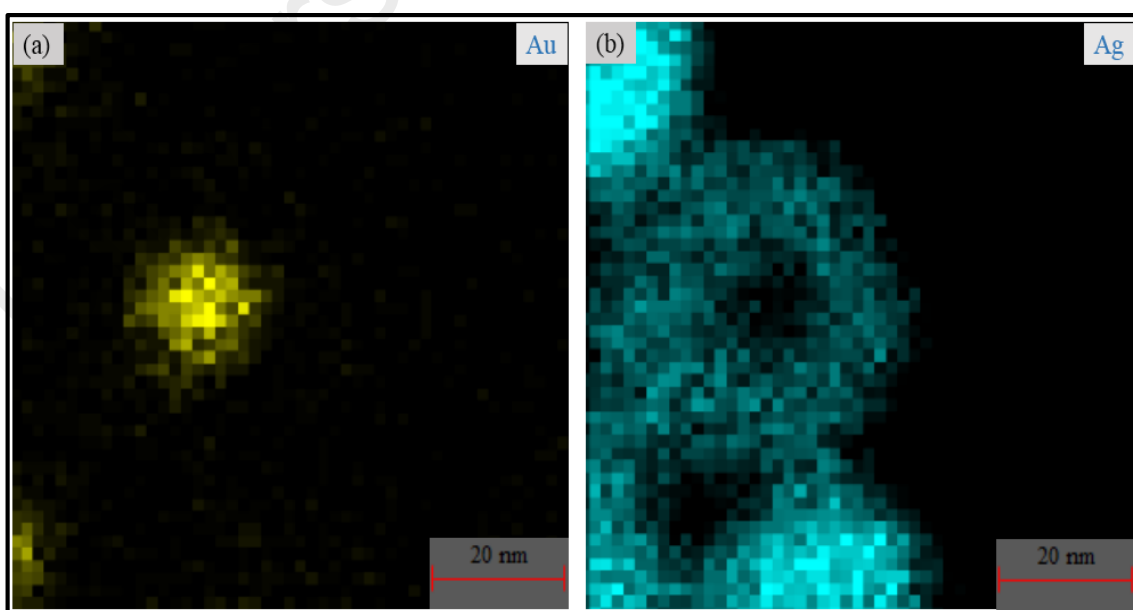


Figure 4.21: Elementals mapping (a) Au and (b) Ag in the 2.0 ml Au seeds of Au-Ag NPs

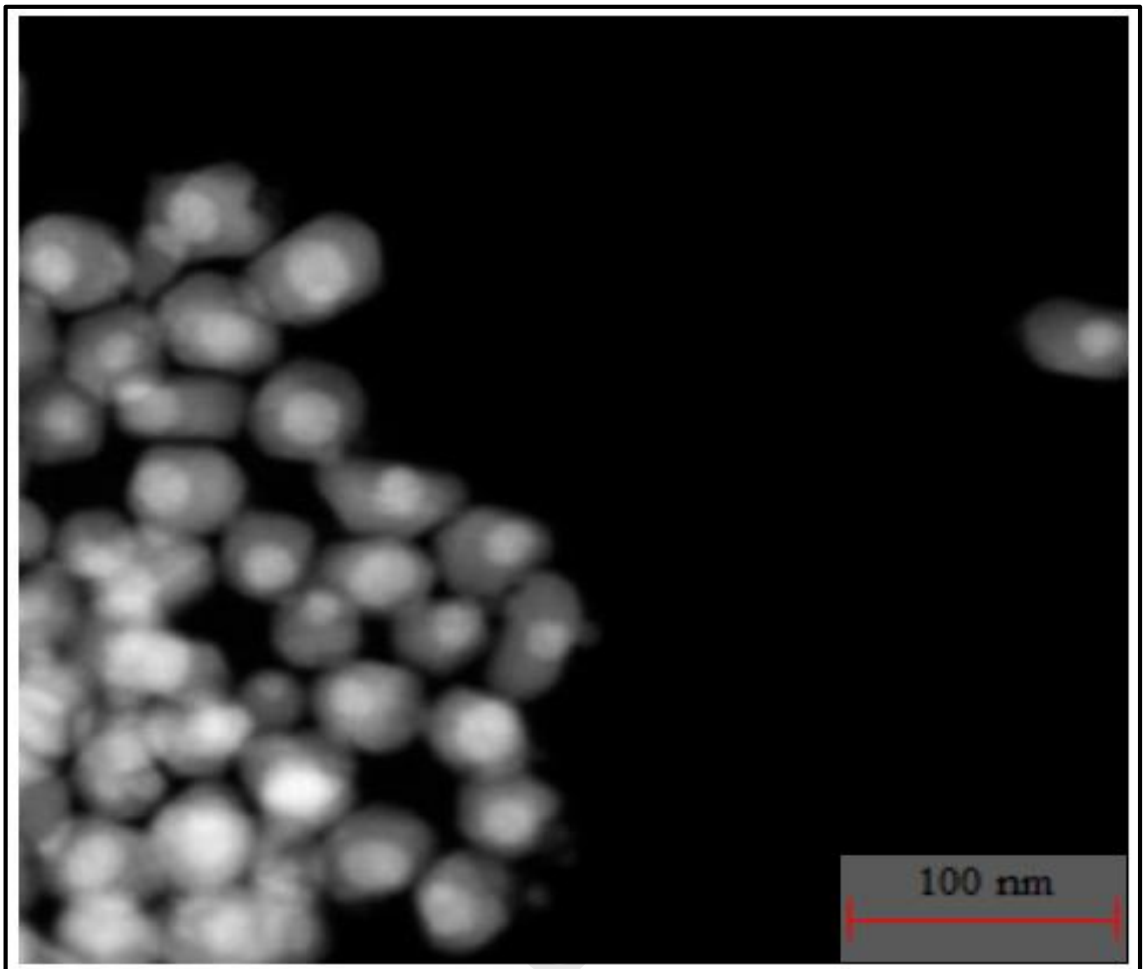


Figure 4.22: HAADF-STEM images of 5.0 ml Au seeds of Au-Ag NPs at magnification 100 nm

University

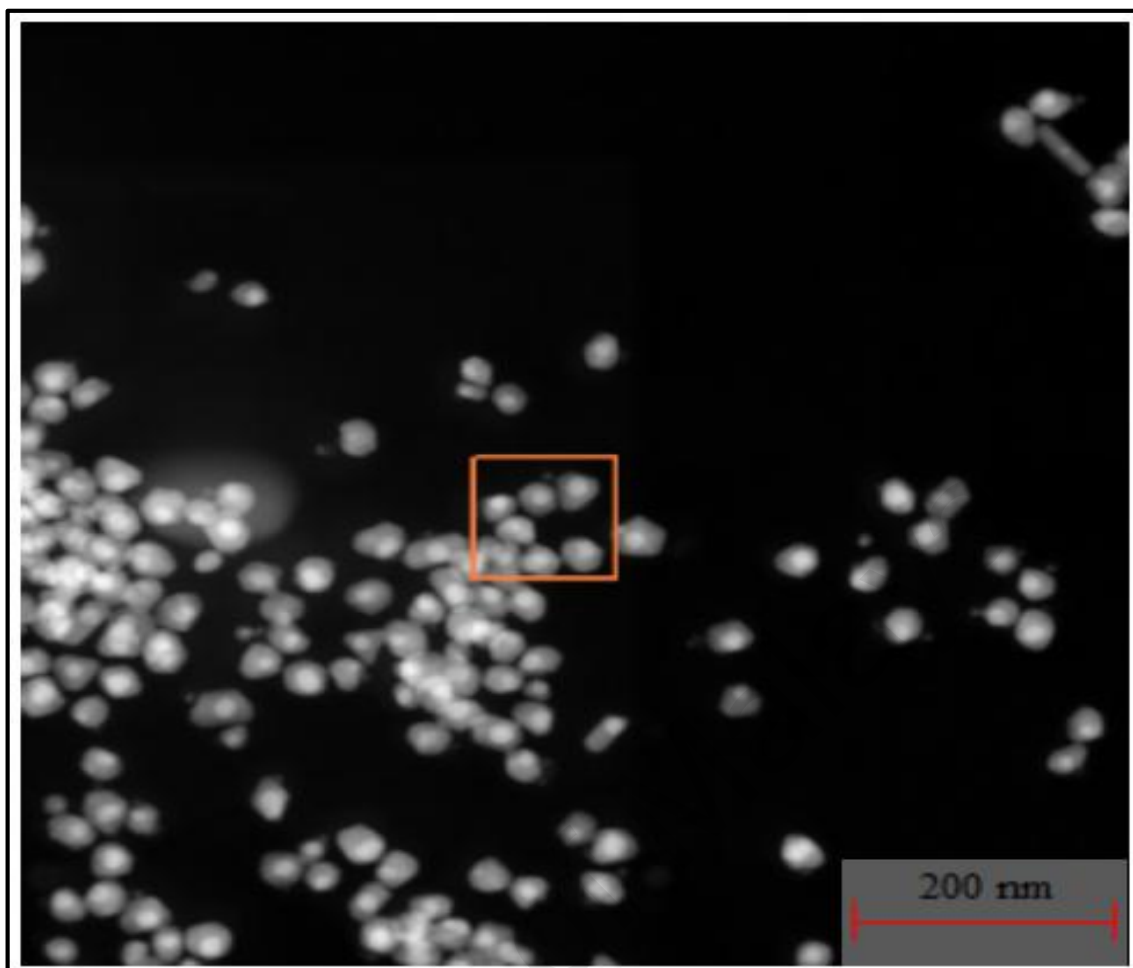


Figure 4.23: HAADF-STEM images of 5.0 ml Au seeds of Au-Ag NPs at magnification 200 nm

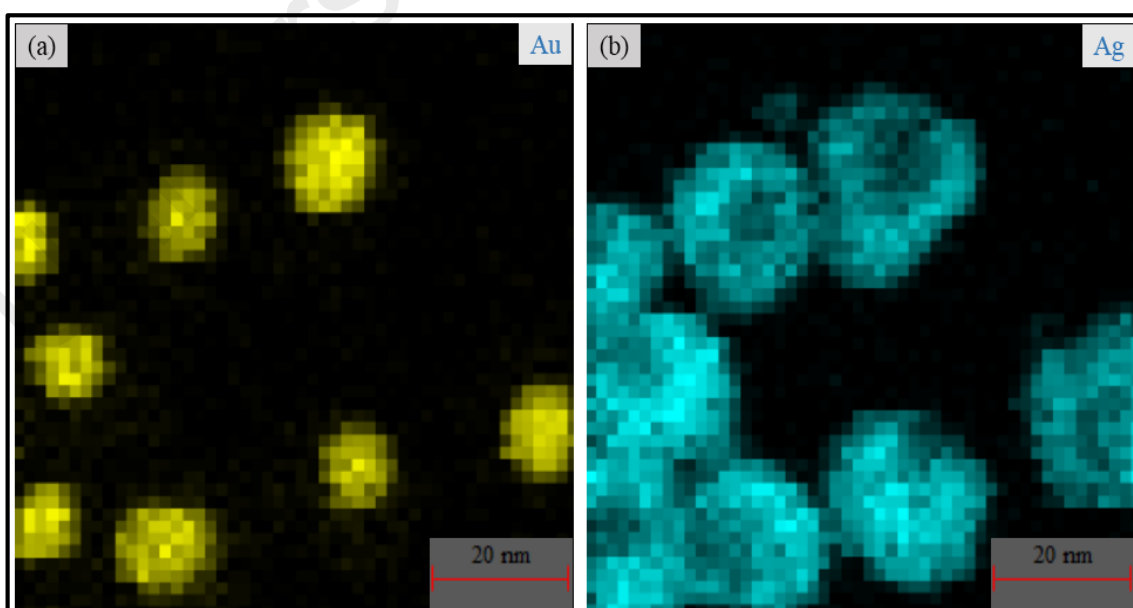


Figure 4.24: Elementals mapping (a) Au and (b) Ag in the 2.0 ml Au seeds of Au-Ag NPs

4.4 Structural Studies

4.4.1 X-Ray Diffraction (XRD) Analysis

Figure 4.25 demonstrates the XRD patterns of Au, Ag and bimetallic Au-Ag NPs at different volume of Au seeds. The synthesized Au nanoparticles show four diffraction peaks (Figure 4.25 (a)) at 2θ values of 38.13° , 44.54° , 64.67° and 77.69° which corresponds to the (111), (200), (220) and (311) planes of a face centered cubic (FCC) gold lattice (JCPDS File No. 03-065-8601) (Ahmad et al., 2015; Krishnamurthy et al., 2014). The XRD pattern of Ag nanoparticles shows peaks (Figure 4.25 (b)) at (111), (200), (220), and (311) planes with the Bragg's reflection at $2\theta = 37.95^\circ$, 44.39° , 64.37° and 77.48° respectively. The maximum peak of Ag nanoparticles is centered at $2\theta = 37.95^\circ$, which represented from face centered cubic (FCC) silver (JCPDS File No. 00-001-1167) (Ahmad et al., 2015).

Meanwhile, Figure 4.25 (c, d) show the XRD pattern of bimetallic Au-Ag NPs for 2.0 ml Au seed shows peaks at (111), (200), (220), and (311) planes for $2\theta = 38.05^\circ$, 44.30° , 64.50° and 77.34° , respectively. Also, the XRD pattern of Au-Ag NPs for 5.0 ml Au seed shows intense peaks at angle of 38.12° , 44.40° , 64.17° and 77.38° corresponding to (111), (200), (220) and (311) planes, respectively (JCPDS File No. 03-065-8424) (Liu et al., 2015). The monometallic Au NPs and bimetallic Au-Ag NPs have the same XRD patterns because gold and silver have almost similar lattice constant (Monga & Pal 2015; Rodríguez-González et al., 2005; Zeng et al., 2015).

Based on Figure 4.25, the broadness of XRD peaks of Au nanoparticles are much broader as compared to Ag nanoparticles. It was suggesting a smaller size distribution for Au nanoparticles (Ahmad et al., 2015). While, the bimetallic Au-Ag nanoparticles with 2.0 ml Au seeds volume have narrower peaks ((Figure 4.25 (c)) as compare to 5.0 ml Au seeds volume ((Figure 4.25 (d)), signifying a bigger size distribution for bimetallic Au-Ag nanoparticles with 2.0 ml Au seeds volume relative to 5.0 ml Au seeds volume. This pattern is also supported by the result obtained from TEM as in Figures 4.4-4.11.

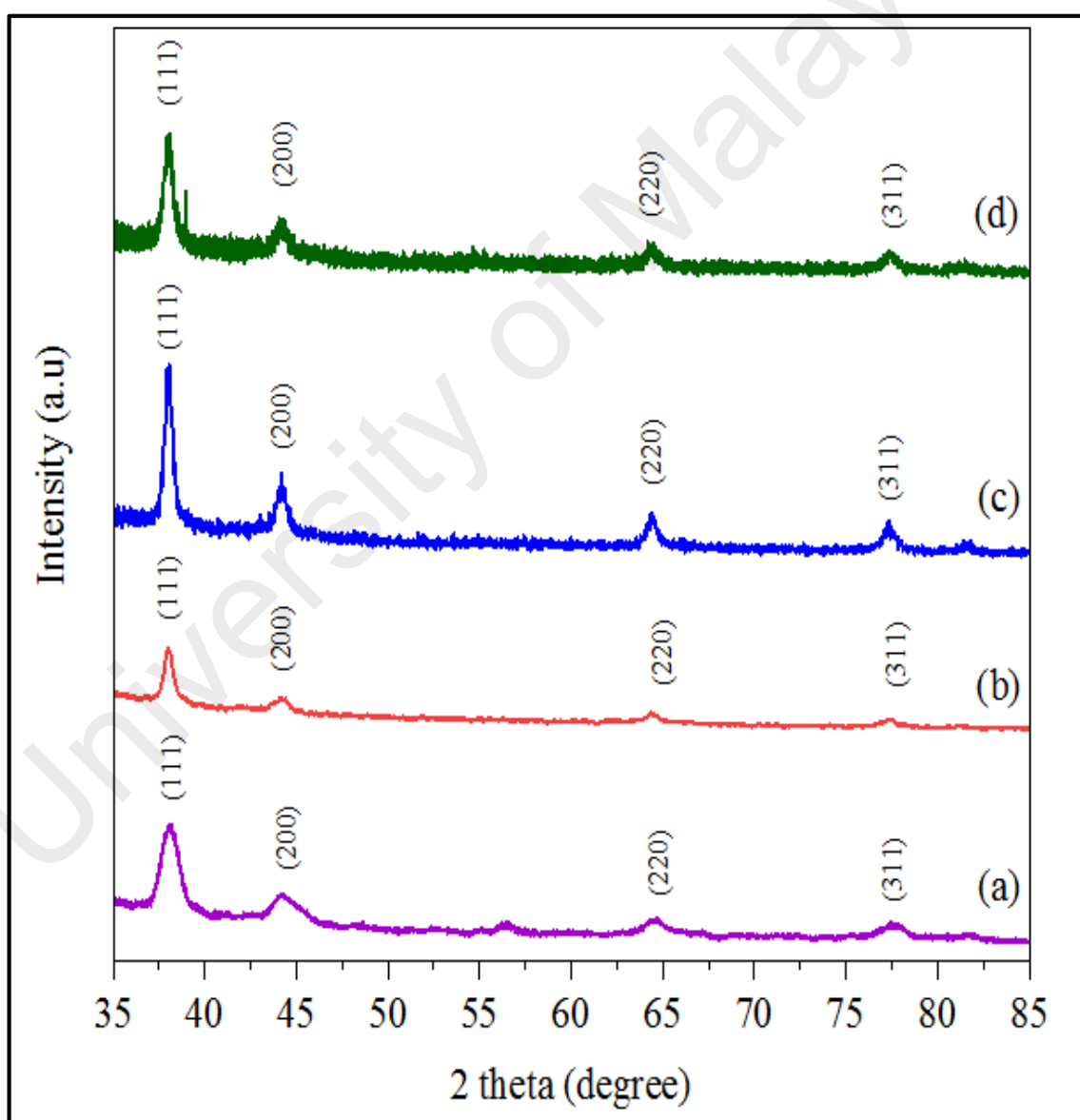


Figure 4.25: XRD patterns of (a) Au NPs, (b) Ag NPs, and Au-Ag NPs with (c) 2.0 ml Au seed, (d) 5.0 ml Au seed

4.5 Catalytic Studies

Figure 4.26 (a) illustrates the catalytic reactions with the 4-NP with the presence of Au NPs. The reaction mechanism can be explained by the inherent hydrogen adsorption by Au NPs which transported the hydrogen between NaBH_4 and 4-NP. The hydrogen comes from the NaBH_4 reduces water. In brief, this behavior could be explained since Au NPs adsorb hydrogen from NaBH_4 and efficiently release it during the reduction reaction. Hence, Au NPs act as a hydrogen carrier in this reduction reaction (Huang et al., 2007).

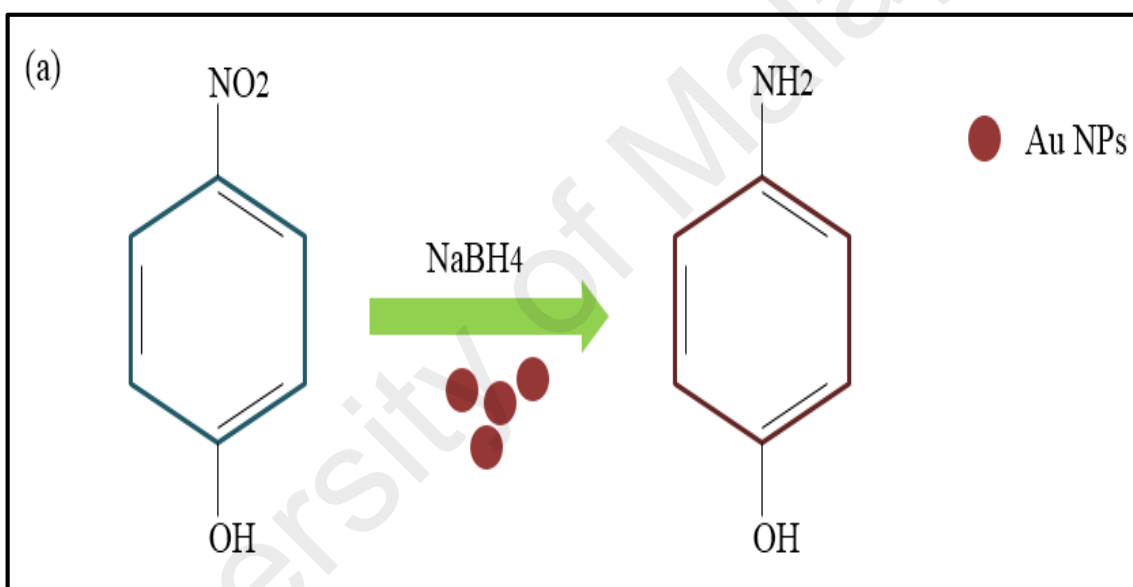


Figure 4.26: Schematic illustration of the catalytic experiments of 4-NP with (a) Au nanoparticles (Luo et al., 2014)

Figure 4.26 (b), the schematic illustration of reduction of 4-nitrophenol to 4-aminophenol by NaBH_4 in the presence of Ag NPs. First, borohydride ions are adsorbed on the surface of synthesized Ag NPs and provide them the electrons. Simultaneously, 4-nitrophenol molecules are adsorbed on the surface of Ag NPs and reduced by these electrons. Then, the produced 4-aminophenol is desorbed from Ag NPs. The reduction potential of Ag NPs is lowered and the surface is exposed to the presence of the borohydride ions, which

is strong nucleophile. However, a backward reduction of this oxide layer owing to the NaBH_4 activates the Ag surface. Subsequently, the BH_4^- and 4-nitrophenolate ions co-adsorb on the surface of Ag NPs. Ag NPs relay the electrons from BH_4^- ions (donor) to the 4-nitrophenolate (acceptor) to catalyze the reaction. Thus the oxide layer on the surface gives adverse effect to the catalytic properties of the Ag NPs (Khoshnamvand et al., 2019).

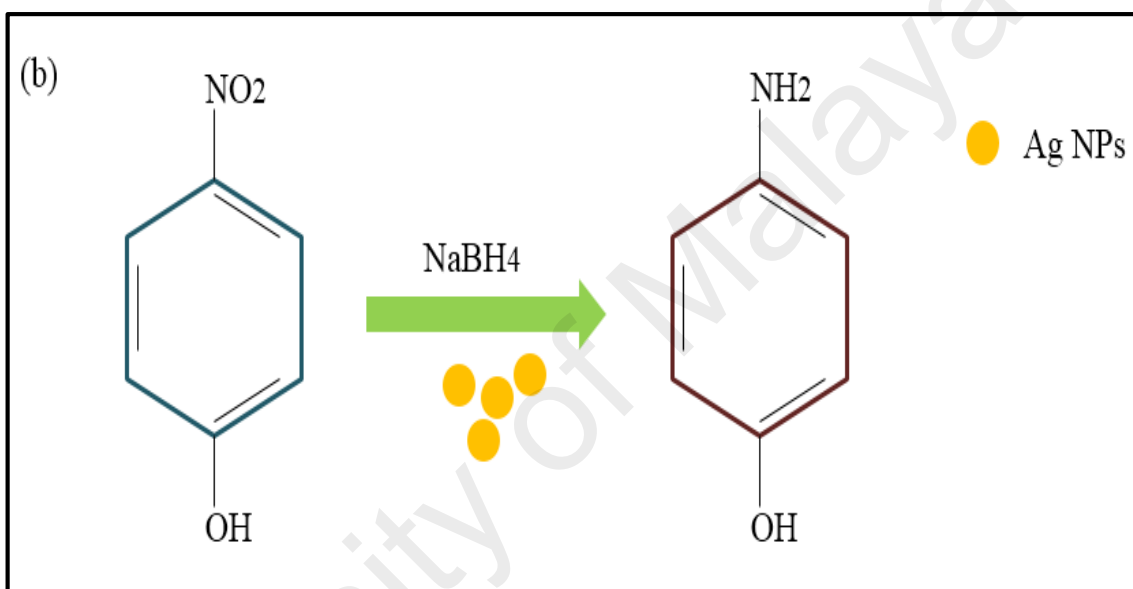


Figure 4.26: Schematic illustration of the catalytic experiments of 4-NP with (b) Ag nanoparticles (Luo et al., 2014)

Based on the Figure 4.26 (c), a possible catalytic mechanism of bimetallic Au-Ag NPs towards the reduction of 4-NP in the presence of NaBH_4 . First, 4-NP in water reacts with NaBH_4 generating an intermediate 4-nitrophenolate ion. Subsequently, the 4-nitrophenolate ions are absorbed by Au-Ag NPs with amino groups. Then, the BH_4^- ions supply electrons to the Au-Ag NPs catalyst and thereby allow the 4-nitrophenolate ions absorbed on the Au-Ag NPs to take electrons at their leisure to generate 4-AP. In the case of the higher catalytic activity exhibited by the Au-Ag NPs, on the one hand, this may be related to the alloy structure of the Au-Ag NPs. Ag has a lower work function than Au.

Therefore, the electrons provided by BH_4^- ions can leave Ag into Au, which ends up with an electron-enriched Au region. The existence of these surplus electrons added inside the Au enables the uptake of electrons by 4-nitrophenolate ions that happen to be close to these regions. On the other hand, the enhanced catalytic reduction of 4-NP by Au-Ag NPs may be due to high adsorption ability towards 4-nitrophenolate ions. Thus increasing the chances for Au-Ag to transfer electrons to 4-nitrophenolate ions and improving the catalytic rate (Fu et al., 2018). During the reduction process, Au-Ag NPs could play two important roles. Au-Ag NPs provided plentiful surface active sites, which promoted NaBH_4 hydrolysis following the generation of a large amount of hydrogen (Equation 4.3). Then, these abundant hydrogen accelerated the rate of 4-NP hydrogenation reaction (Equation 4.4). In addition, the formation of by-products could be prevented because of the strong adsorption of nitro group ($-\text{NO}_2$) to Au-Ag NPs surface (Sun et al., 2018).

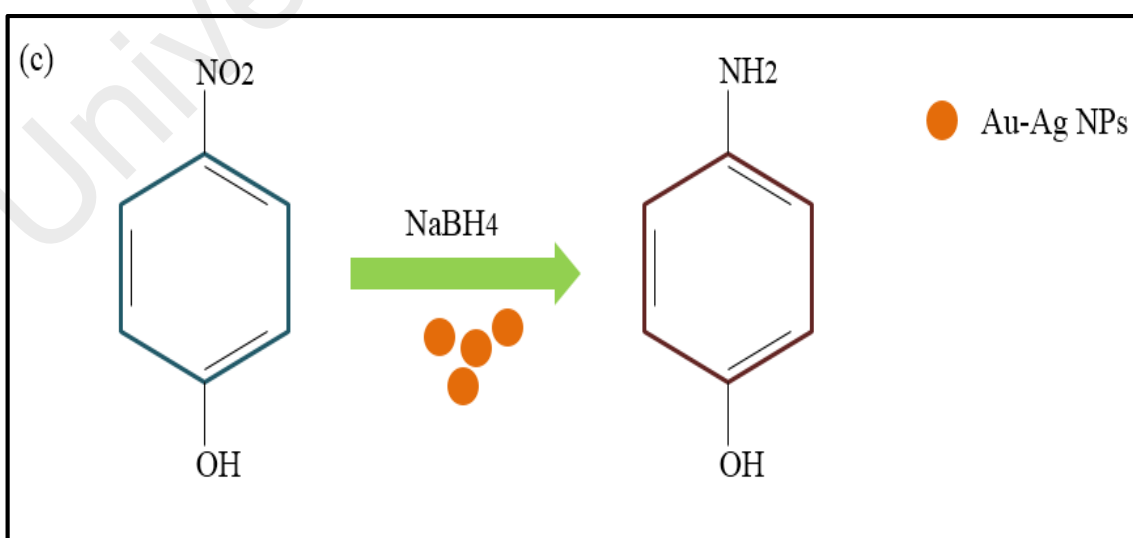
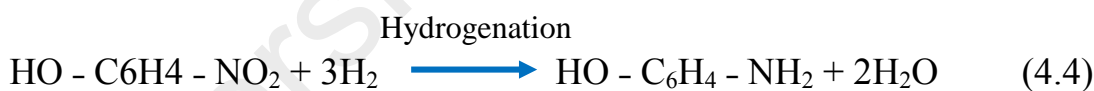
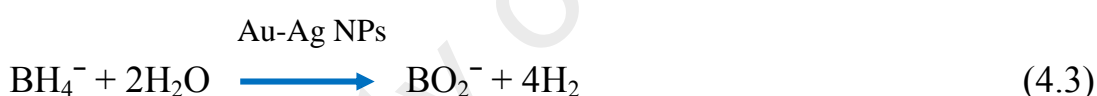


Figure 4.26: Schematic illustration of the catalytic experiments of 4-NP with (c) Au-Ag nanoparticles (Luo et al., 2014)

In a neutral or acidic medium, the 4-NP solution showed a strong absorption peak at 317 nm (Figure 4.27) (Dong et al., 2012; Zelekew & Kuo 2016; Zhang et al., 2007). The addition of NaBH₄ deprotonated the OH group of 4-NP and formed 4-nitrophenolate ion appearing at 400 nm in the UV-vis spectrum (Sharma et al., 2017). The color of the 4-NP solution changed from light yellow to bright yellow immediately due to the 4-nitrophenolate ion formation (Krishnamurthy et al., 2014; Zelekew & Kuo 2016). The reduction of 4-NP does not occur without the presence of a catalyst (Jana et al., 2001; Dong et al., 2012). The thermodynamically favorable reduction of 4-NP to 4-AP ($E_0 = -0.76$ V vs. NHE) and H₃BO₃/BH₄⁻ ($E_0 = -1.33$ V vs. NHE) produced large potential difference with negative free energy (Hong et al., 2016). However, the presence of a large energy between the mutually repelling negative ions of 4-NP and BH₄⁻ was responsible for the slow kinetics of the reaction (Dong et al., 2012; Hong et al., 2016). Alternatively, an introduction to Au-Ag NPs can absorb negative ions and able to act as electronic relay systems to transfer electrons donated by borohydride ions to the nitro groups of 4-NP, which is expected to lower the kinetic barrier and thus catalyze the reduction (Chen et al., 2014).

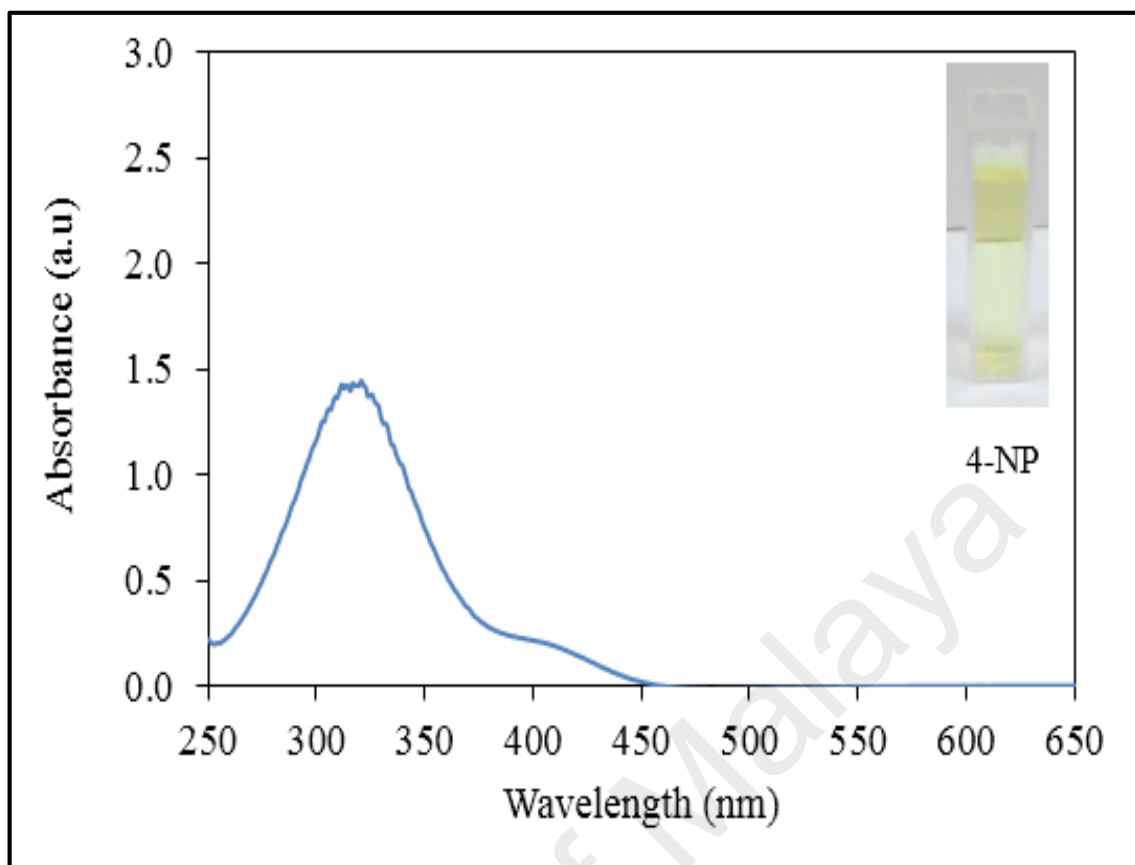


Figure 4.27: Absorption spectra of 4-NP without reducing agent

Metallic nanoparticles are known to catalyze the reduction reaction by facilitating the electron transfer process from the donor BH_4^- to the 4-NP acceptor (Sharma et al., 2017). With the addition of 0.2 ml catalyst to the reaction mixture containing 3.0 ml 4-NP and 0.5 ml NaBH_4 , the absorption peak at 400 nm gradually decreased with time with the simultaneous appearance of a new peak at 300 nm attributed to the 4-AP formation (Dong et al., 2012). The UV-vis spectra also showed an isosbestic point at 317 nm, indicating the reduction of 4-NP to 4-AP without any by-product formation (Huo et al., 2013). The progress of the reduction reactions was monitored by measuring the absorption spectrum of 4-NP and 4-AP as a function of time by applying different catalysts such as Au, Ag and Au-Ag NPs. In the control reduction experiments, only a slight change in the absorption intensity was observed at 400 nm for 4-NP in the absence of a catalyst after 11 minutes, as shown in Figure 4.28 (a). The spectra indicated that the

4-NP was not reduced by the NaBH_4 and the mixture remains yellow (Krishnamurthy et al., 2014). In contrast, when Au, Ag and Au-Ag nanoparticles were used as the catalysts, the absorption intensity at 400 nm decreased and a new peak appeared at 300 nm attributed to the 4-AP formation (Krishnamurthy et al., 2014; Zelekew and Kuo 2016). The reduction reaction was also visible through color change where; bleaching of the yellow color, indicating complete reduction of 4-NP (Huo et al., 2013).

The catalytic activity of the reduction of 4-nitrophenol using Au is faster than the Ag nanoparticles. The catalytic studies were performed using Ag NPs ($k = 0.21 \text{ min}^{-1}$), which exhibited lower catalytic rates relative to Au NPs ($k = 0.36 \text{ min}^{-1}$). Figure 4.28 (b) shows that the total time taken for the Au nanocatalyst to reduce 4-NP to 4-AP is 14 minutes shorter than the Ag NPs. While the Ag NPs takes 16 minutes to complete the reduction reaction as shown in Figure 4.28 (c). This is attributed to the relatively larger nanoparticle size and the possible oxidation of the silver nanoparticles. In addition, the surface area of Au NPs is 1.65 times higher than the Ag NPs. The reduction potential of Ag NPs is lowered and the surface is exposed to the presence of the borohydride ions (BH_4^-), which is strong nucleophile. However, a backward reduction of this oxide layer due to the NaBH_4 activates the Ag surface. Subsequently, the BH_4^- and 4-nitrophenolate ions co-adsorb on the surface of Ag nanoparticles. Silver nanoparticles relay the electrons from BH_4^- ions (donor) to the 4-nitrophenolate (acceptor) to catalyze the reaction. Thus the oxide layer on the surface gives adverse effect to the catalytic properties of the Ag NPs (Gangula et al., 2011).

It was noted that the reduction reaction rate of bimetallic Au-Ag NPs was faster compared to monometallic Au and Ag NPs. Halдар *et al.*, (2014) reported that the catalytic activity of Au-Ag bimetallic NPs is much higher than those associated with the pure Au NPs. These results can be explained by the following factors. First, the improved reduction rates were ascribed to the synergistic effect between the Au and the Ag (Krishnamurthy *et al.*, 2014). The synergistic effect was produced due to strong electronic communication which stimulate the electron transfer from Ag to Au. This happen owing to the difference in electronegativity of Au (2.4 eV) and Ag (1.9 eV) respectively, that make the integration of Au with Ag in bimetallic Au-Ag NPs (Sareen *et al.*, 2018). Electrons could transfer from Ag to Au owing to the synergistic effect that produced, leading to an increase in the electron density on the surface of the bimetallic Au-Ag NPs and then improving the catalytic activity (Xia *et al.*, 2013). Second, the effect from the interactions between the two metals (Xia *et al.*, 2013). The comparison between two types of bimetallic nanoparticles (2.0 and 5.0 ml Au seeds volumes) reduction rates indicated the practical role of the size and composition effect, as it influenced the time needed for the completion of the reduction reaction. Holden *et al.*, (2014) also stated the catalytic properties of bimetallic nanoparticles can be influenced by their size and composition. The present role of the particle size may also due to the change in the surface area of the smaller size NPs as compared to the bulky sized NPs. It is a well-known fact that the surface area increases with a corresponding decrease in the NPs particle sizes (Dong *et al.*, 2012; Kalantari *et al.*, 2017). The increased surface area of the smaller sized NPs contributed to the excellent catalytic activity (Dong *et al.*, 2012; Kalantari *et al.*, 2017). The surface area of 5.0 ml Au seed volume of Au-Ag NPs was 1.3 times higher as compared to the 2.0 ml Au seed volume Au-Ag NPs (Appendix B). The improved surface area was the reason behind the improved catalytic performance of the 5.0 ml Au seed volume of Au-Ag NPs. The reduction reaction completed in 5 minutes and 8 minutes for

the 5.0 ml and 2.0 ml Au seed volumes of the Au-Ag NPs; respectively as shown in Figures 4.28 (d) and (e), respectively.

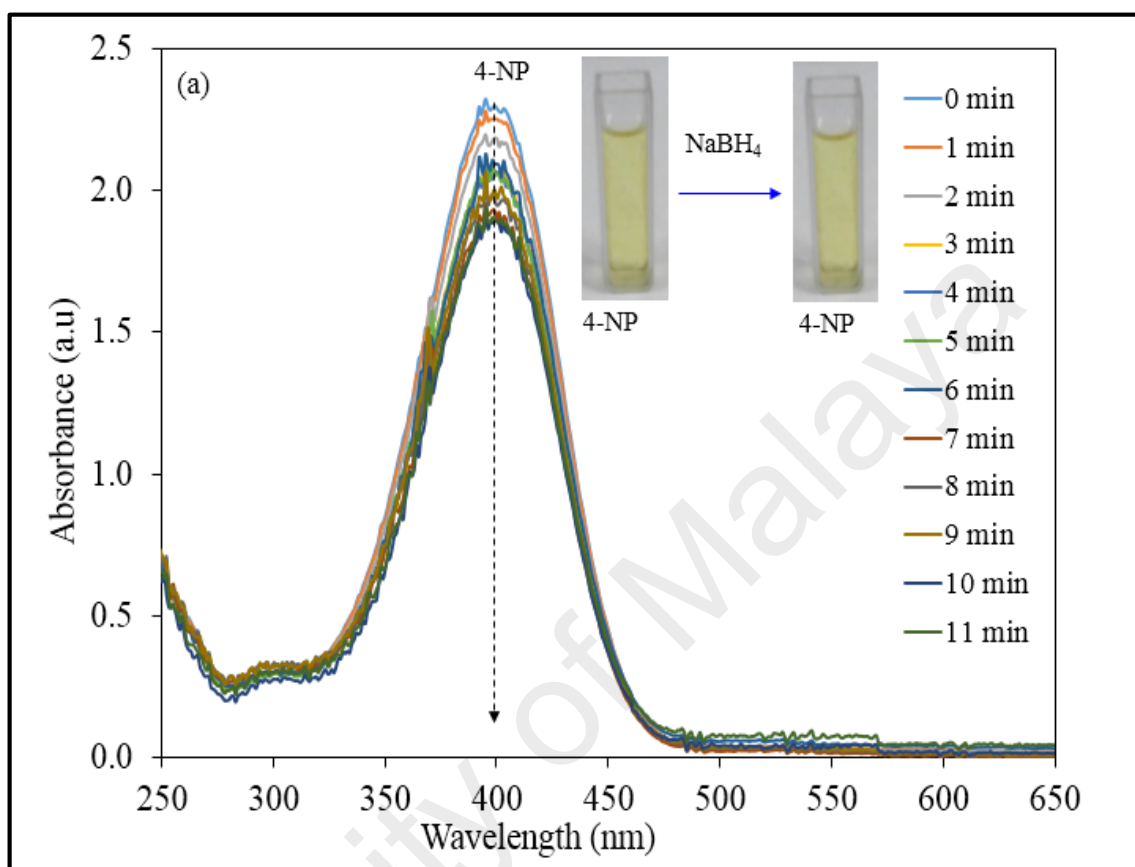


Figure 4.28: Absorption spectra of 4-NP reduced by (a) NaBH₄ only

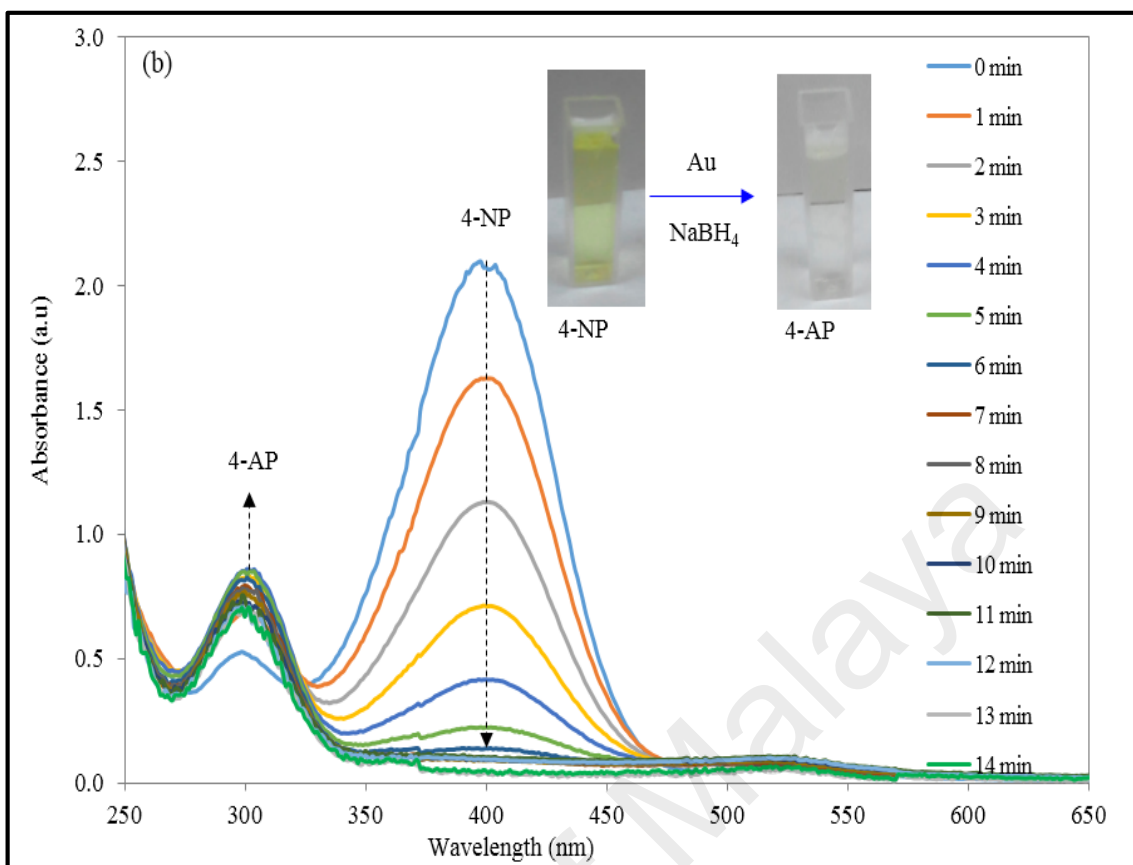


Figure 4.28: Absorption spectra of 4-NP with NaBH_4 in the presence of (b) Au NPs

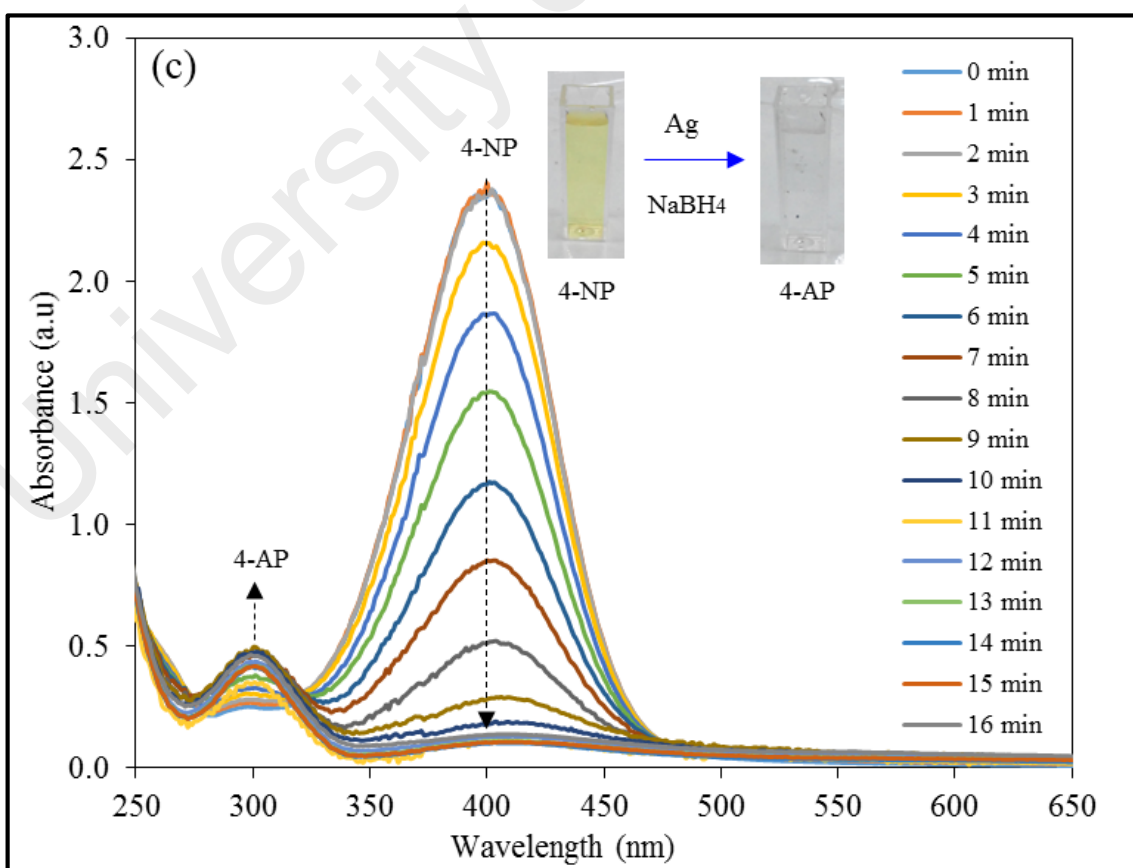


Figure 4.28: Absorption spectra of 4-NP with NaBH_4 in the presence of (c) Ag NPs

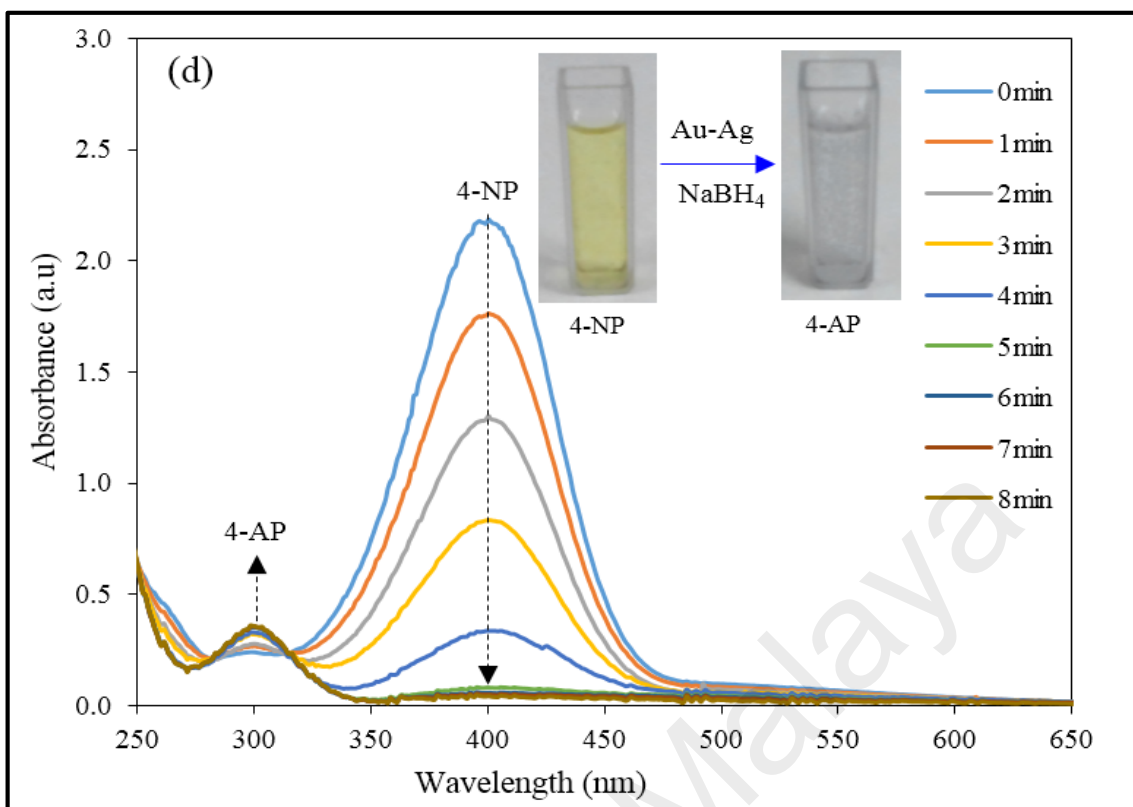


Figure 4.28: Absorption spectra of 4-NP with NaBH₄ in the presence of (d) 2.0 ml Au seeds volume of Au-Ag NPs

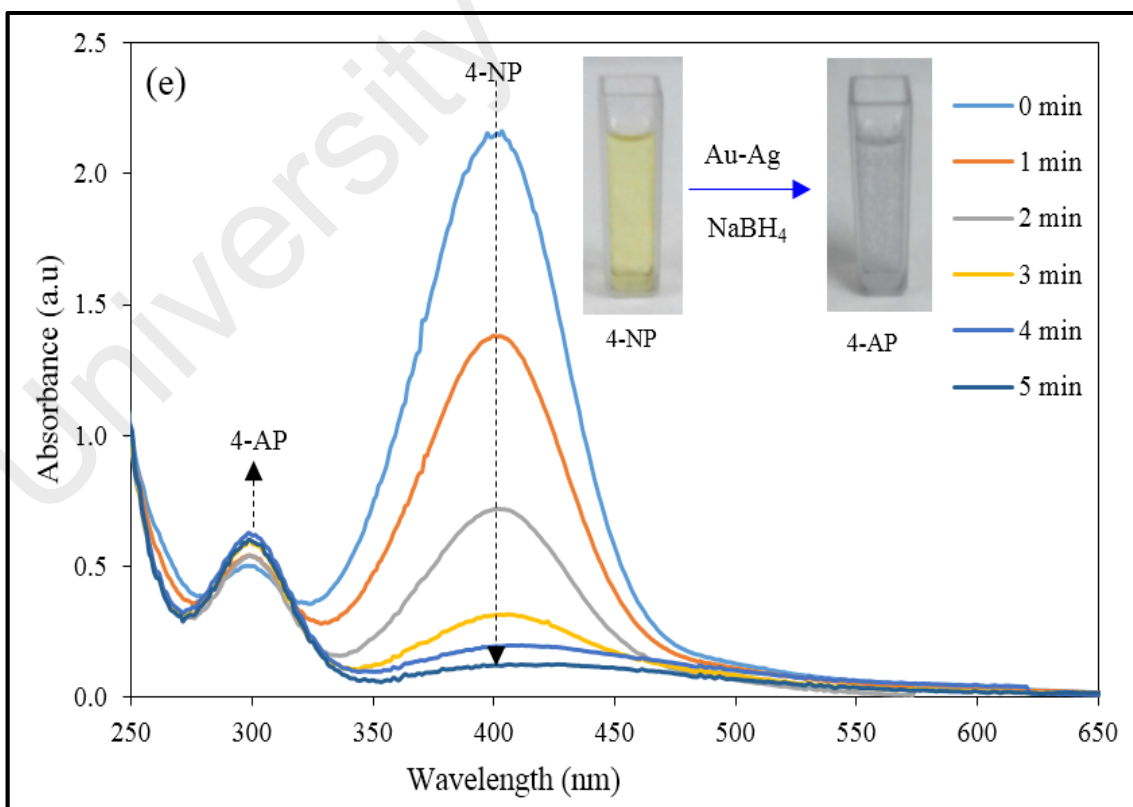


Figure 4.28: Absorption spectra of 4-NP with NaBH₄ in the presence of (e) 5.0 ml Au seeds volume of Au-Ag NPs

The catalytic performance of catalysts highly depends on shape of the catalyst. This is due to the different coordination numbers of atoms on surface. For catalyst with a face-centred cubic (FCC) lattice, the coordination number of atoms on (111), (100) and (110) surfaces is 9, 8 and 7, respectively (Cao et al., 2016; Zhang et al., 2016). There are three main surface structure of a shape controlled nanoparticles for a metal catalyst with a face-centred cubic (FCC) lattice which are (110), (100) and (111). Based on Figure 4.29 (a-c), these three surfaces are differ in terms of electron density, coordination number, distance between adjacent atoms and surface adsorption energy of a molecule. The main difference among them is surface coverage in terms of occupancy by atoms of the topmost layer. Noticeably, the so-called surface occupancy of surface metal atoms for a FCC crystallographic structure conforms to the following order: (111) > (100) > (110) (Figure 4.29 a-c). This may cause large differences in adsorption energy or activation barrier for dissociation of a reactant molecule because the repulsion of adjacent adsorbates (reactant molecules or their dissociated species) strongly depends on coverage of adsorbate and also the coverage of adsorbates mostly relies on surface-dependent occupancy of the metal atom of the topmost layer. As a result, the structural differences among different crystallographic surfaces influence dissociation, adsorption and interaction of intermediate adsorbates in a catalytic activity. As shown XRD result in Figure 4.25, the structure of NPs was FCC structure have intense peak at (111). Since the Au, Ag and Au-Ag NPs have FCC structure with (111) plane which is good surface occupancy of surface metal atoms and suitable for catalytic activity.

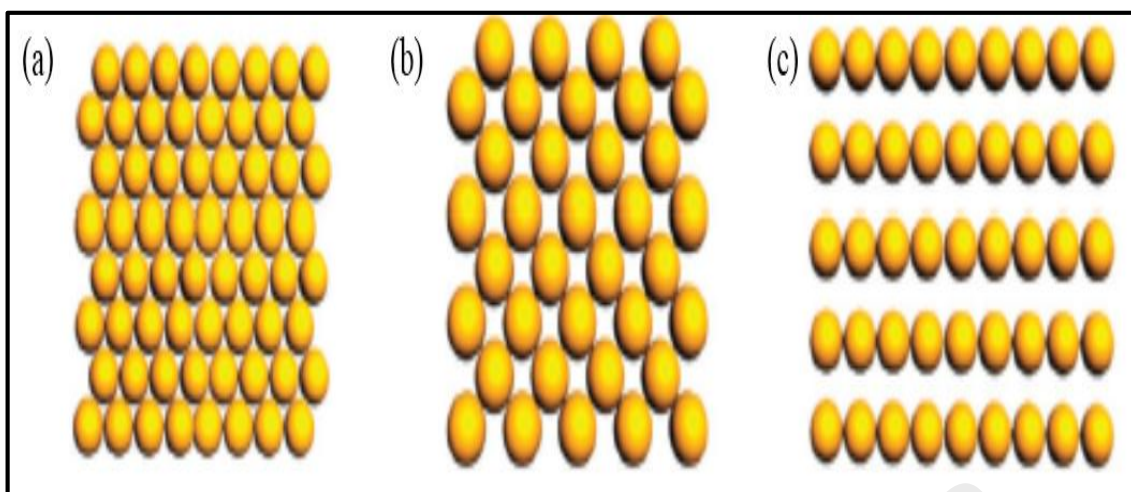


Figure 4.29: Schematic surfaces of a metal in face-centered cubic (FCC) (a) (111), (b) (100) and (c) (110) (Cao et al., 2016).

The concentration of BH_4^- used in the system was much higher than the 4-NP, it was reasonable to assume that the concentration of borohydride ions was constant throughout the reduction reaction. A pseudo first-order kinetics fits the catalytic reduction rate (Dong et al., 2012; Krishnamurthy et al., 2014; Zelekew & Kuo 2016; Zhang et al., 2007). A linear correlation of $\ln(A_0/A_t)$ with time was observed where A_t and A_0 is the absorbance at specific intervals and the initial absorbance of 4-nitrophenolate ion, respectively (Krishnamurthy et al., 2014; Sharma et al., 2017; Zelekew & Kuo 2016; Zhang et al., 2007). The rate constants for each system were measured from the slope of the $\ln(A_0/A_t)$ vs. time graph as shown in Figure 4.30 (a)-(e). The values of the chemical reduction rates were calculated to be 0.02, 0.36, 0.21, 0.52 and 0.62 min^{-1} for NaBH_4 , Au, Ag, 2.0 ml and 5.0 ml Au seed volumes Au-Ag NPs, respectively as summarized in Table 4.2. Among all the catalysts, the 5.0 ml Au seed volume Au-Ag NPs catalyst demonstrated the fastest reduction rate, thus higher catalytic activity for the reduction of 4-NP at room temperature. These experimental phenomena demonstrated that the bimetallic Au-Ag NPs had a better catalytic activity for the reduction of 4-NP.

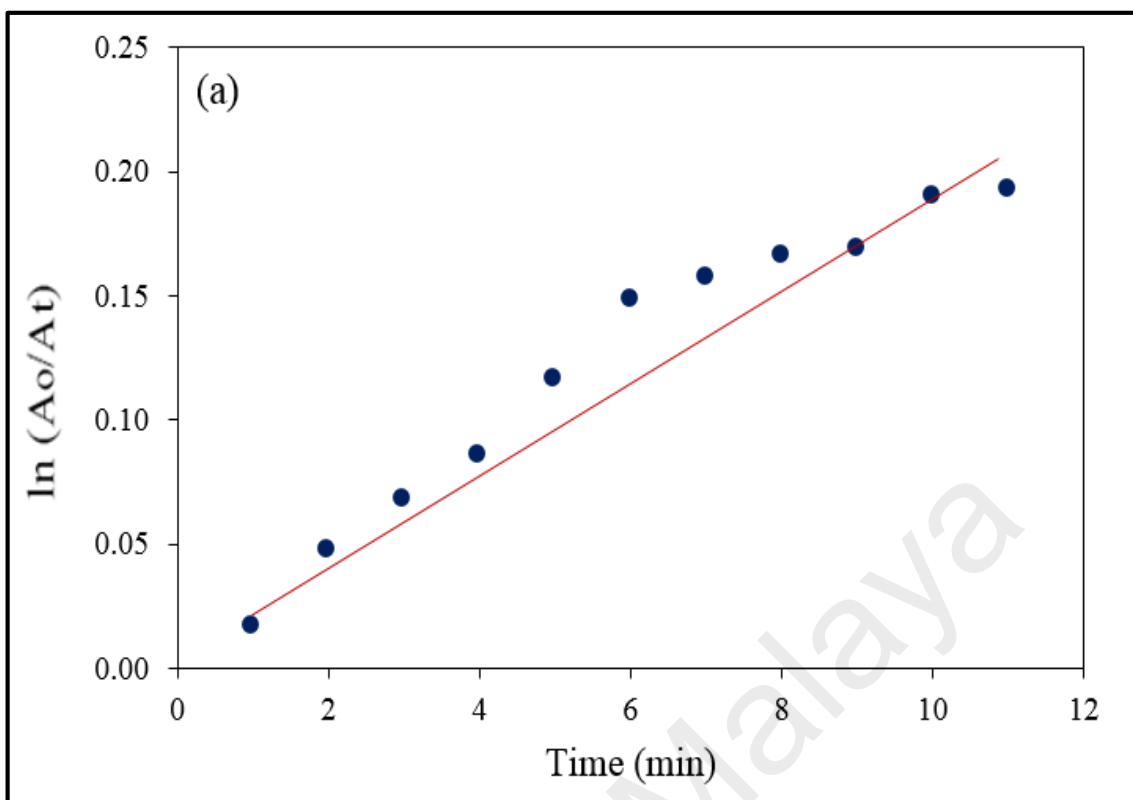


Figure 4.30: Plot of $\ln(A_0/A_t)$ versus time for the determination of rate constants for (a) NaBH_4 only

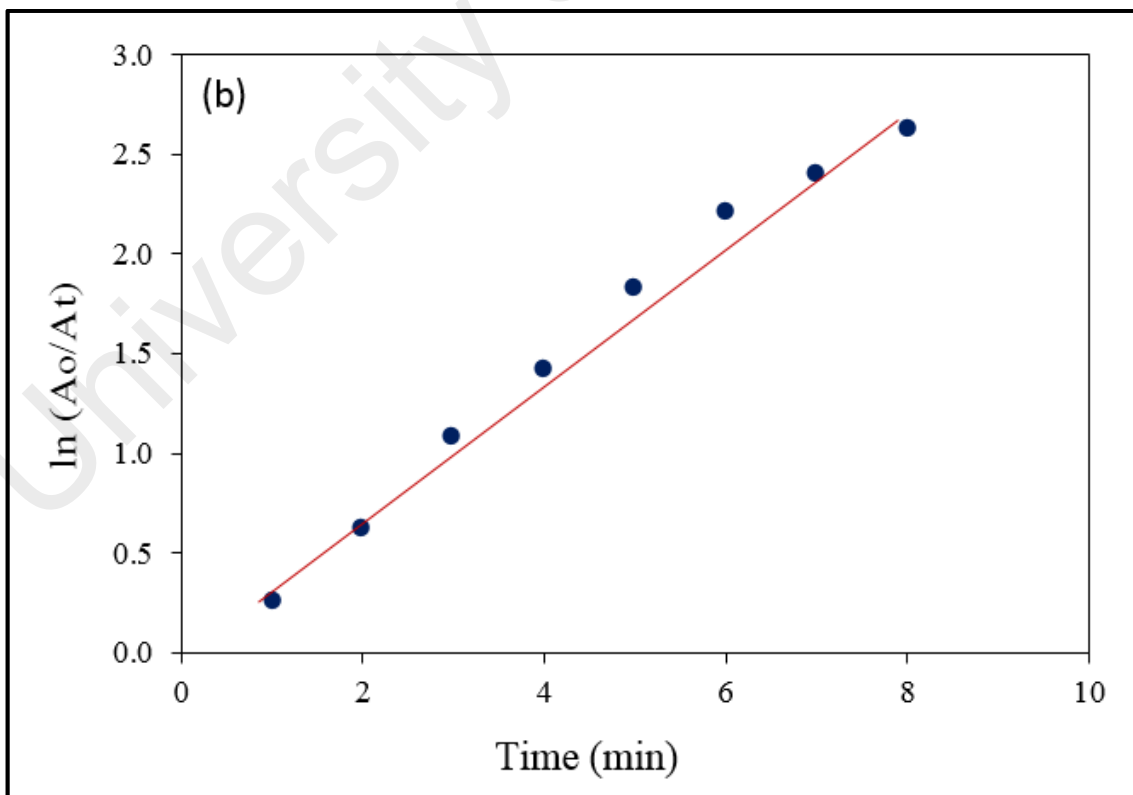


Figure 4.30: Plot of $\ln(A_0/A_t)$ versus time for the determination of rate constants of 4-NP with NaBH_4 in the presence (b) Au NPs

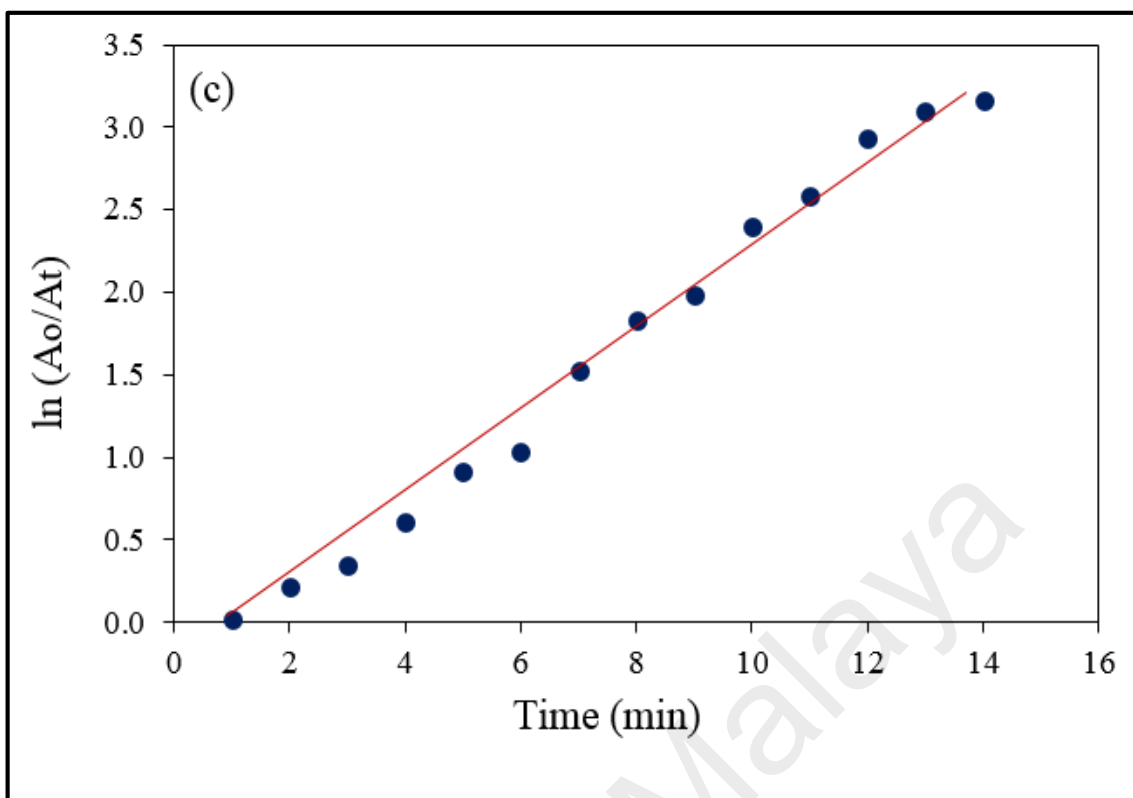


Figure 4.30: Plot of $\ln (A_0/A_t)$ versus time for the determination of rate constants of 4-NP with NaBH_4 in the presence (c) Ag NPs

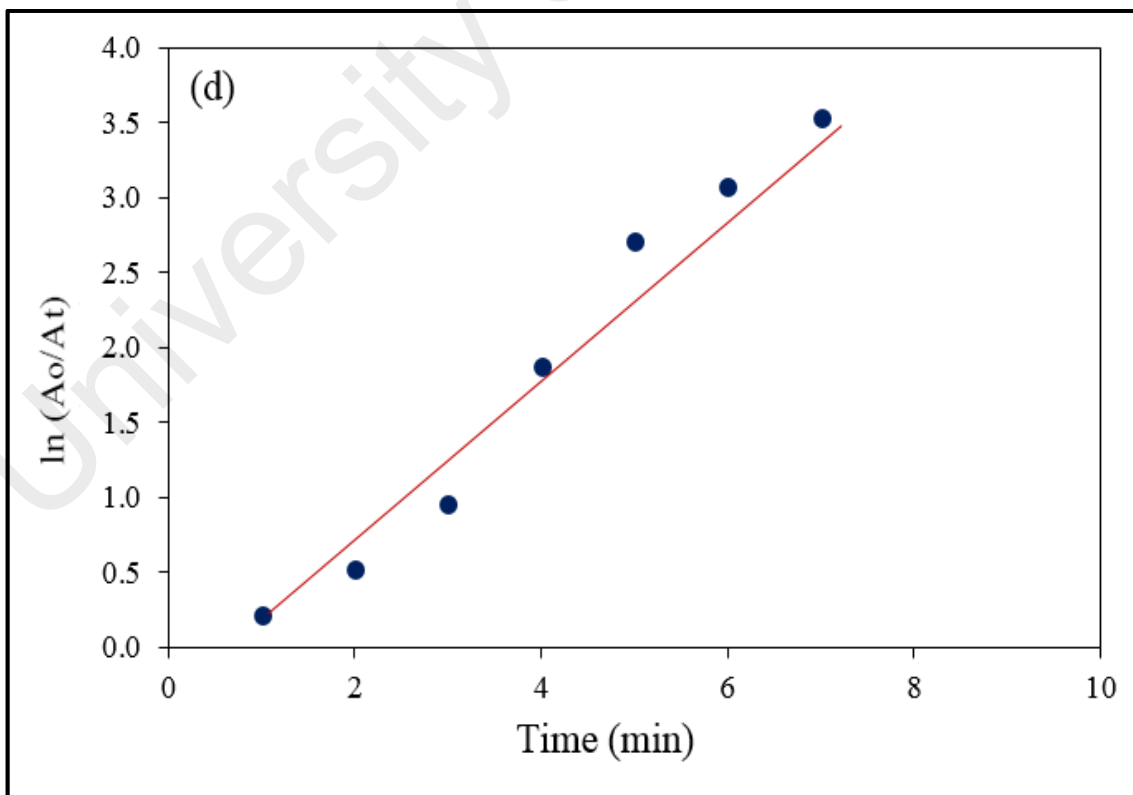


Figure 4.30: Plot of $\ln (A_0/A_t)$ versus time for the determination of rate constants of 4-NP with NaBH_4 in the presence (d) 2.0 ml Au seeds volume of Au-Ag NPs

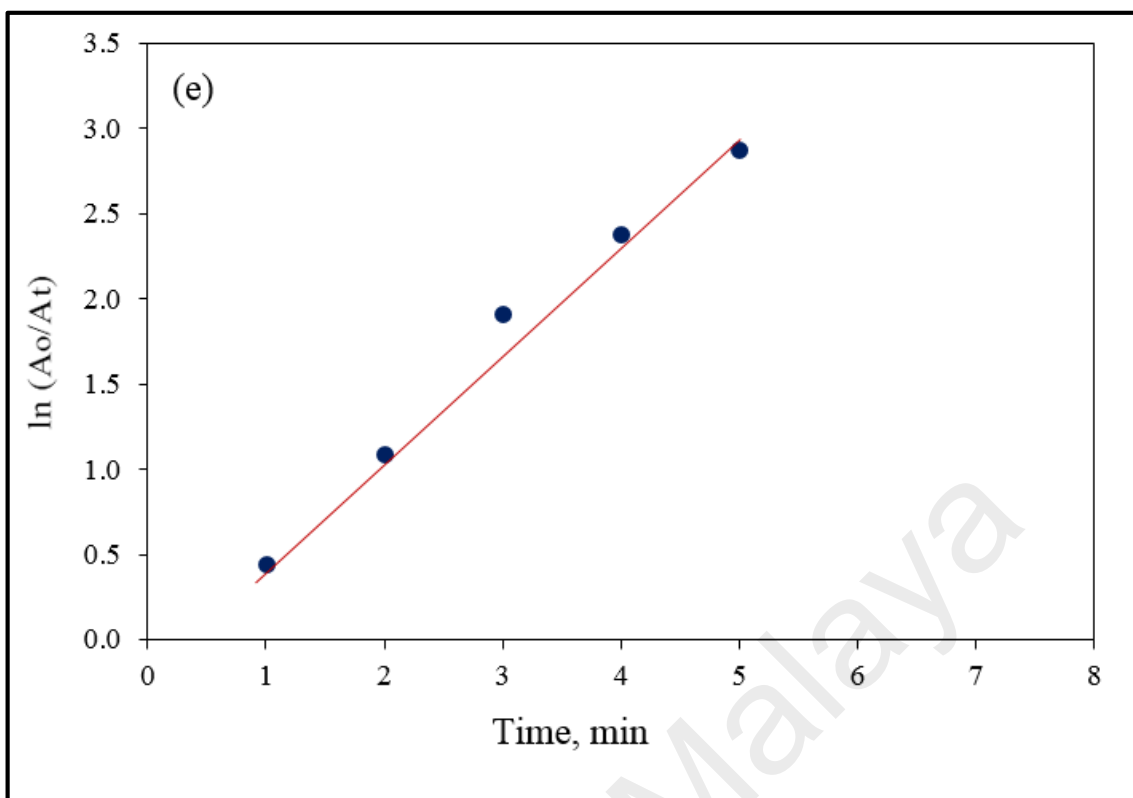


Figure 4.30: Plot of $\ln(A_0/A_t)$ versus time for the determination of rate constants of 4-NP with NaBH_4 in the presence (e) 5.0 ml Au seeds volume of Au-Ag NPs

Table 4.2 shows the summary of the rate constants of the reduction 4-NP using Au, Ag and Au-Ag nanocatalysts, which shown the result of different size and composition. It can see clearly that the reduction of 4-NP can be influenced by the size and composition of nanoparticles.

Table 4.2: Summary of the catalytic reduction of 4-NP by Au, Ag and Au-Ag catalysts

Catalysts	Shape of NPs	Reducing Agents	Rate Constant (min ⁻¹)	Time (min)	Particle Size (nm)
Au NPs	Spherical	NaBH ₄	0.36	14	24.1
Ag NPs	Spherical	NaBH ₄	0.21	16	27.5
Au-Ag NPs (2.0 ml Au seeds)	Spherical	NaBH ₄	0.52	8	75.2
Au-Ag NPs (5.0 ml Au seeds)	Spherical	NaBH ₄	0.62	5	55.2

CHAPTER FIVE

CONCLUSION

5.1 Conclusion

The Au and Ag NPs were synthesized using the citrate thermal reduction method. The bimetallic Au-Ag NPs was successfully prepared by a seeding colloid technique with different diameter. The Au, Ag and Au-Ag NPs gives different sizes from TEM analysis, which are 24.1 ± 2.7 , 27.5 ± 4.0 nm , 75.2 ± 5.3 (2.0 ml Au seeds) and 55.2 ± 6.0 nm (5.0 ml Au seeds), respectively. The bimetallic NPs have better catalytic activity for the reduction of 4-NP as compared to monometallic NPs. This is due to synergistic effect between different elements. The bimetallic NPs with smaller diameter has higher reduction rate than the largest diameter Au-Ag NPs due to the larger surface area. From the UV-vis absorbance spectra, it could be observed that the SPR band is gradually red-shifted as the seed volume is decreased, suggesting the formation of Au-Ag nanoparticles with large diameter. The UV-vis result also proves that the size of the Au-Ag NPs increases as the volume of the Au seed decreases. The monometallic Au NPs need shorter time to reduce the 4-nitrophenols compared to the Ag NPs due to the possible oxidation of Ag NPs.

In conclusion, the study revealed that the catalytic performance of the reduction 4-NP to 4-AP was remarkably improved by controlling the composition of the bimetallic Au-Ag NPs.

5.2 Future Recommendations

The reduction of nitrophenols using bimetallic Au-Ag nanoparticles with different diameter exhibits different catalytic rates of reduction which could be further investigated by using diameter less than 55.2 nm. Since, the 5.0 ml Au seeds with diameter 55.2 nm exhibit the highest catalytic activity. Thus, the diameter of the bimetallic nanoparticles could be less than 55.2 nm to get optimum reduction rate of 4-NP to 4-AP.

The effect of the composition of bimetallic Au-Ag nanoparticles on the reduction rate of 4-NP may be further investigated via seed colloid technique. The bimetallic Au-Ag nanoparticles with 5.0 ml Au seed shows the highest rate of reduction through this work. As suggestion, the synthesized Au-Ag nanoparticles could be more than 5.0 ml Au seeds volume. For instance, the volume of the Au seeds could be 6.0 ml or more, in order to obtain the optimum result for the reduction of 4-NP to 4-AP.

REFERENCES

- Abdelhalim, M. A. K., Mady, M. M., & Ghannam, M. M. (2012). Physical properties of different gold nanoparticles: Ultraviolet-Visible and Fluorescence measurements. *Journal Nanomedicine and Nanotechnology*, 3, 133.
- Abood, M. M., Moheel, M. H., & Omran, A. H. (2018). Antibacterial Activity of Mono and Bimetallic Au: Ag Colloidal Nanoparticles Prepared by Pulse Laser ablation PLA. *Journal of Kufa-physics*, 10, 8-19.
- Admala, S. K. (2017). Synthesis of Au/Ag, Pd/Ag and Pt/Ag Nanoparticles by Galvanic Replacement Reaction.
- Ahmad, A., Syed, F., Shah, A., Khan, Z., Tahir, K., Khan, A. U., & Yuan, Q. (2015). Silver and gold nanoparticles from Sargentodoxacuneata: synthesis, characterization and antileishmanial activity. *RSC Advances*, 5, 73793-73806.
- Ahmad, A., Mukherjee, P., Senapati, S., Mandal, D., Khan, M. I., Kumar, R., & Sastry, M. (2003). Extracellular biosynthesis of silver nanoparticles using the fungus *Fusarium oxysporum*. *Colloids and Surfaces B: Biointerfaces*, 28, 313-318.
- Ajitha, B., Reddy, Y. A. K., Reddy, P. S., Suneetha, Y., Jeon, H. J., & Ahn, C. W. (2016). Instant biosynthesis of silver nanoparticles using *Lawsonia inermis* leaf extract: Innate catalytic, antimicrobial and antioxidant activities. *Journal of molecular liquids*, 219, 474-481.
- Akbari, B., Tavandashti, M. P., & Zandrahimi, M. (2011). Particle Size Characterization of Nanoparticles-A Practical approach. *Iranian Journal of Materials Science and Engineering*, 8, 48-56.
- Akita, T., Hiroki, T., Tanaka, S., Kojima, T., Kohyama, M., Iwase, A., & Hori, F. (2008). Analytical TEM observation of Au-Pd nanoparticles prepared by sonochemical method. *Catalysis Today*, 131, 90-97.
- Albonetti, S., Blosi, M., Gatti, F., Migliori, A., Ortolani, L., Morandi, V., Baldi, G., Barzanti, A., & Dondi, M. (2010). Microwave-assisted synthesis of Au, Ag and Au-Ag nanoparticles and their catalytic activities for the reduction of nitrophenol. *Studies in Surface Science and Catalysis*, 175, 621-624.
- Alshammari, A., Kalevaru, V. N., & Martin, A. (2016). Bimetallic catalysts containing gold and palladium for environmentally important reactions. *Catalysts*, 6, 97.

- Alzoubi, F. Y., Alzouby, J. Y., Alqadi, M. K., Alshboul, H. A., & Aljarrah, K. M. (2015). Synthesis and Characterization of Colloidal Gold Nanoparticles Controlled by the pH and Ionic Strength. *Chinese Journal of Physics*, 53, 100801-1.
- Arora, N., Mehta, A., Mishra, A., & Basu, S. (2018). 4-Nitrophenol reduction catalysed by Au-Ag bimetallic nanoparticles supported on LDH: Homogeneous vs. heterogeneous catalysis. *Applied Clay Science*, 151, 1-9.
- Baba, A., Imazu, K., Yoshida, A., Tanaka, D., & Tamada, K. (2014). Surface plasmon resonance properties of silver nanoparticle 2D sheets on metal gratings. *Springer Plus*, 3, 284.
- Babick, F. (2016). Suspensions of colloidal particles and aggregates (Vol. 20). Cham, Switzerland: Springer.
- Bai, T., Tan, Y., Zou, J., Nie, M., Guo, Z., Lu, X., & Gu, N. (2015). AuBr₂⁻ engaged galvanic replacement for citrate-capped Au-Ag alloy nanostructures and their solution-based surface-enhanced Raman scattering activity. *The Journal of Physical Chemistry C*, 119, 28597-28604.
- Balch, W.E., Fox, G.E., Magrum, L. J., Woese, C.R., & Wolfe, R.S. (1979). Methanogens: reevaluation of a unique biological group. *Microbiological reviews*, 43, 260.
- Blackborrow, J. R., & Young, D. (1979). Metal vapor synthesis. Springer-Verlag, New York.
- Banerjee, M., Sharma, S., Chattopadhyay, A., & Ghosh, S. S. (2011). Enhanced antibacterial activity of bimetallic gold-silver core-shell nanoparticles at low silver concentration. *Nanoscale*, 3, 5120-5125.
- Barroso-Martín, I., Moretti, E., Talon, A., Storaro, L., Rodríguez-Castellón, E., & Infantes-Molina, A. (2018). Au and AuCu nanoparticles supported on SBA-15 ordered mesoporous titania-silica as catalysts for methylene blue photodegradation. *Materials*, 11, 890.
- Bhatia, P., Verma, S. S., & Sinha, M. M. (2018). Size-dependent optical response of magneto-plasmonic core-shell nanoparticles. *Advanced Nano Research*, 1, 1-13.
- Biggs, S., Mulvaney, P., Zukoski, C. F., & Grieser, F. J. (1994). *Journal of American Chemical Society*, 116, 9150-9157.

- Bijanzadeh, A. R., Vakili, M. R., & Khordad, R. (2012). A study of the surface plasmon absorption band for nanoparticles. *International Journal of Physical Sciences*, 7, 1943-1948.
- Bradley, J. S. (1994). *Clusters and Colloids* (G. Schmid, Ed.). VCH, Weinheim, 477.
- Burda, C., Chen, X., Narayanan, R., & El-Sayed, M. A. (2005). Chemistry and properties of nanocrystals of different shapes. *Chemical reviews*, 105, 1025-1102.
- Calagua, A., Alarcon, H., Paraguay, F., & Rodriguez, J. (2015). Synthesis and Characterization of Bimetallic Gold-Silver Core-Shell Nanoparticles: A Green Approach. *Advances in Nanoparticles*, 4, 116.
- Campbell, C. T., Parker, S. C., & Starr, D. E. (2002). The effect of size-dependent nanoparticle energetics on catalyst sintering. *Science*, 298, 811-814.
- Cao, G. Z. (2004). *Nanostructures and Nanomaterials, Synthesis, Properties and Applications*. Imperial College Press, London, UK.
- Cao, S., Jiang, J., Zhu, B., & Yu, J. (2016). Shape-dependent photocatalytic hydrogen evolution activity over a Pt nanoparticle coupled g-C₃N₄ photocatalyst. *Physical Chemistry Chemical Physics*, 18, 19457-19463.
- Cao, S., Tao, F., Tang, Y., Li, Y., & Yu, J. (2016). Size- and shape-dependent catalytic performances of oxidation and reduction reactions on nanocatalysts. *Chemical Society Reviews*, 45, 4747-4765.
- Cao, Y., Jin, R., & Mirkin, C. A. (2001). DNA-Modified Core-Shell Ag/Au Nanoparticles. *Journal of the American Chemical Society*, 123, 7961-7962.
- Carrillo-Torres, R. C., García-Soto, M. J., Morales-Chávez, S. D., Garibay-Escobar, A., Hernández-Paredes, J., Guzman, R., Barboza-Flores, M., & Álvarez-Ramos, M. E. (2016). Hollow Au-Ag bimetallic nanoparticles with high photothermal stability. *RSC advances*, 6, 41304-41312.
- Chandran, S. P., Ghatak, J., Satyam, P. V., & Sastry, M. (2007). Interfacial deposition of Ag on Au seeds leading to Au core Ag shell in organic media. *Journal of colloid and interface science*, 312, 498-505.

- Chawla, M., Kumar, R., & Siril, P. F. (2016). High catalytic activities of palladium nanowires synthesized using liquid crystal templating approach. *Journal of Molecular Catalysis A: Chemical*, 423, 126-134.
- Chen, D. H., & Chen, C.J. (2002). Formation and characterization of Au-Ag bimetallic nanoparticles in water-in-oil microemulsions. *Journal Materials Chemistry*, 12, 1557–1562.
- Chen, M., He, Y., & Zhu, J. (2017). Preparation of Au-Ag bimetallic nanoparticles for enhanced solar photothermal conversion. *International Journal of Heat and Mass Transfer*, 114, 1098-1104.
- Chen, X., Cai, Z., Chen, X., & Oyama, M. (2014). AuPd bimetallic nanoparticles decorated on graphene nanosheets: Their green synthesis, growth mechanism and high catalytic ability in 4-nitrophenol reduction. *Journal Materials Chemistry A*, 2, 5668–5674.
- Choi, W. S., Koo, H. Y., & Kim, D. Y. (2008). Facile fabrication of core-in-shell particles by the slow removal of the core and its use in the encapsulation of metal nanoparticles. *Langmuir*, 24, 4633-4636.
- Czaplinska, J., Sobczak, I., & Ziolek, M. (2014). Bimetallic AgCu/SBA-15 system: The effect of metal loading and treatment of catalyst on surface properties. *Journal Physics Chemistry C*, 118, 12796–12810.
- Dai, L., Song, L., Huang, Y., Zhang, L., Lu, X., Zhang, J., & Chen, T. (2017). Bimetallic Au/Ag core-shell superstructures with tunable surface plasmon resonance in the near-infrared region and high performance surface-enhanced Raman scattering. *Langmuir*, 33, 5378-5384.
- Dehghan Banadaki, A., & Kajbafvala, A. (2014). Recent advances in facile synthesis of bimetallic nanostructures: an overview. *Journal of Nanomaterials*, 2014.
- De Leeuw, D. M., Simenon, M. M. J., Brown, A. R., & Einerhand, R. E. F. (1997). Stability of n-type doped conducting polymers and consequences for polymeric microelectronic devices. *Synthetic Metals*, 87, 53-59.
- Dong, F., Guo, W., Park, S. K., & Ha, C. S. (2012). Controlled synthesis of novel cyanopropylpolysilsesquioxane hollow spheres loaded with highly dispersed Au nanoparticles for catalytic applications. *Chemical Communications*, 48, 1108-1110.

- Dougherty, G. M., Rose, K. A., Tok, J. B. H., Pannu, S. S., Chuang, F. Y. S., Sha, M. Y., Chakarova, G., & Penn, S. G. (2007). The zeta potential of surface functionalized metallic nanorod particles in aqueous solution. *Electrophoresis*, 29, 1131-1139.
- Dwivedi, A. D., & Gopal, K. (2010). Biosynthesis of silver and gold nanoparticles using *Chenopodium album* leaf extract. *Colloids and Surfaces A: Physicochemical and Engineering Aspects*, 369, 27-33.
- Eisa, W. H., Al-Ashkar, E., El-Mossalamy, S. M., & Ali, S. S. (2016). PVP induce self-seeding process for growth of Au@Ag core@shell nanocomposites. *Chemical Physics Letters*, 651, 28-33.
- Emam, H. E. (2019). Arabic gum as bio-synthesizer for Ag–Au bimetallic nanocomposite using seed-mediated growth technique and its biological efficacy. *Journal of Polymers and the Environment*, 27, 210-223.
- Emam, H. E., & Abdelhameed, R. M. (2017). Anti-UV radiation textiles designed by embracing with nano-MIL (Ti, In) “Metal organic framework”. *ACS applied materials & interfaces*, 9, 28034-28045.
- Ershov, B. G., Janata, E., Henglein, A., & Fojtik, A. (1993). Silver atoms and clusters in aqueous solution: absorption spectra and the particle growth in the absence of stabilizing Ag⁺ ions. *Journal Physics Chemistry*, 97, 4589-4594.
- Esparza, R., Santoveña, A., Ruíz-Baltazar, A., Angeles-Pascual, A., Bahena, D., Maya-Cornejo, J., Ledesma-García, J., & Pérez, R. (2017). Study of PtPd Bimetallic Nanoparticles for Fuel Cell Applications. *Materials Research*, 20, 1193–1200.
- Fauzia, V., Irmavianti, D., Roza, L., Hafizah, M. A. E., Imawan, C., & Umar, A. A. (2019). Bimetallic AuAg sharp-branch mesoflowers as catalyst for hydrogenation of acetone. *Materials Chemistry and Physics*, 225, 443-450.
- Feng, Y., Chang, Y., Sun, X., Liu, N., Cheng, Y., Feng, Y., Zhang, H., & Li, X. (2017). Understanding the Property–Activity Relationships of Polyhedral Cuprous Oxide Nanocrystals in Terms of Reactive Crystallographic Facets. *Toxicological Sciences*, 156, 480-491.
- Feng, Y., Yin, J., Liu, S., Wang, Y., Li, B., & Jiao, T. (2020). Facile synthesis of Ag/Pd nanoparticle-loaded poly (ethylene imine) composite hydrogels with highly efficient catalytic reduction of 4-nitrophenol. *ACS omega*, 5, 3725-3733.

- Ferrer, D., Torres-Castro, A., Gao, X., Sepulveda-Guzman, S., Ortiz-Mendez, U., & Jose-Yacaman, M. (2007). Three-layer core/shell structure in Au-Pd bimetallic nanoparticles. *Nano letters*, 7, 1701-1705.
- Frederix, F., Friedt, J. M., Choi, K. H., Laureyn, W., Campitelli, A., Mondelaers, D., Maes, G. & Borghs, G. (2003). Biosensing based on light absorption of nanoscaled gold and silver particles. *Analytical Chemistry*, 75, 6894-6900.
- Fu, J., Wang, S., Zhu, J., Wang, K., Gao, M., Wang, X., & Xu, Q. (2018). Au-Ag bimetallic nanoparticles decorated multi-amino cyclophosphazene hybrid microspheres as enhanced activity catalysts for the reduction of 4-nitrophenol. *Materials Chemistry Physics*, 207, 315–324.
- Gaffet, E., Tachikart, M., Kedim, O. E. I., & Rahouadj, R. (1996). Nanostructural materials formation by mechanical alloying: Morphologic analysis based on transmission and scanning electron microscopic observations. *Materials Characterization*, 36, 185.
- Gangula, A., Podila, R., Karanam, L., Janardhana, C., & Rao, A. M. (2011). Catalytic reduction of 4-nitrophenol using biogenic gold and silver nanoparticles derived from *Breyniarhamnoides*. *Langmuir*, 27, 15268-15274.
- Ghorai, T. K. (2015). Synthesis of spherical mesoporous titania modified iron-niobate nanoclusters for photocatalytic reduction of 4-nitrophenol. *Journal of Materials Research and Technology*, 4, 133-143.
- Ghosh Chaudhuri, R., & Paria, S. (2011). Core/shell nanoparticles: classes, properties, synthesis mechanisms, characterization, and applications. *Chemical reviews*, 112, 2373-2433.
- Ghosh, S., Patil, S., Ahire, M., Kitture, R., Gurav, D. D., Jabgunde, A. M., Kale, S., Pardesi, K., Shinde, V., Bellare, J., & Dhavale, D. D. (2012). *Gnidiaglauca* flower extract mediated synthesis of gold nanoparticles and evaluation of its chemocatalytic potential. *Journal of Nanobiotechnology*, 10, 17.
- Gopalakrishnan, R., Loganathan, B., & Raghu, K. (2015). Green synthesis of Au–Ag bimetallic nanocomposites using *Silybummarianum* seed extract and their application as a catalyst. *RSC Advances*, 5, 31691-31699.
- Gu, Y., Jiao, Y., Zhou, X., Wu, A., Buhe, B., & Fu, H. (2018). Strongly coupled Ag/TiO₂ heterojunctions for effective and stable photothermal catalytic reduction of 4-nitrophenol. *Nano Research*, 11, 126-141.

- Guarnizo, A., Angurell, I., Rossell, M. D., Llorca, J., Muller, G., Seco, M., & Rossell, O. (2015). 4-Mercaptophenyldiphenylphosphine as linker to immobilize Pd onto the surface of magnetite nanoparticles. Excellent catalytic efficiency of the system after partial linker removal. *RSC Advances*, 5, 91340-91348.
- Guha, S., Roy, S., & Banerjee, A. (2011). Fluorescent Au@Ag core-shell nanoparticles with controlled shell thickness and HgII sensing. *Langmuir*, 27, 13198-13205.
- Gupta, S. S. R., Kantam, M. L., & Bhanage, B. M. (2018). Shape-selective synthesis of gold nanoparticles and their catalytic activity towards reduction of p-nitroaniline. *Nano-Structure Nano-Objects*, 14, 125-130.
- Güzel, R., Üstündağ, Z., Ekşi, H., Keskin, S., Taner, B., Durgun, Z. G., Turan, A. A. İ. & Solak, A. O. (2010). Effect of Au and Au@Ag core-shell nanoparticles on the SERS of bridging organic molecules. *Journal of colloid and interface science*, 351, 35-42.
- Haldar, K. K., Kundu, S., & Patra, A. (2014). Core-size-dependent catalytic properties of bimetallic Au/Ag core-shell nanoparticles. *ACS applied materials & interfaces*, 6, 21946-21953.
- Han, J., Wang, M., Chen, R., Han, N., & Guo, R. (2014). Beyond yolk-shell nanostructure: a single Au nanoparticle encapsulated in the porous shell of polymer hollow spheres with remarkably improved catalytic efficiency and recyclability. *Chemical Communications*, 50, 8295-8298.
- Hareesh, K., Sunitha, D. V., Dhole, S. D., Bhoraskar, V. N., Phase, D. M., & Williams, J. (2019). One-step gamma radiation aided diffusion of Ag-Au alloy nanoparticles into polycarbonate and its application towards the reduction of 4-Nitrophenol. *Radiation Physics and Chemistry*, 162, 126-130.
- Henglein, A. (1989). Small-particle research: physicochemical properties of extremely small colloidal metal and semiconductor particles. *Chemical Reviews*, 89, 1861-1864.
- Henglein, A. (1998). Colloidal silver nanoparticles: photochemical preparation and interaction with O₂, CCl₄, and some metal ions. *Chemistry of Materials*, 10, 444-450.
- Heshmatpour, F., Abazari, R., & Balalaie, S. (2012). Preparation of monometallic (Pd, Ag) and bimetallic (Pd/Ag, Pd/Ni, Pd/Cu) nanoparticles via reversed micelles and their use in the Heck reaction. *Tetrahedron*, 68, 3001-3011.

- Hirakawa, T., & Kamat, P. V. (2005). Charge separation and catalytic activity of Ag@TiO₂ core-shell composite clusters under UV-irradiation. *Journal of the American Chemical Society*, 127, 3928-3934.
- Holden, M. S., Nick, K. E., Hall, M., Milligan, J. R., Chen, Q., & Perry, C. C. (2014). Synthesis and catalytic activity of pluronic stabilized silver-gold bimetallic nanoparticles. *RSC Advanced*, 4, 52279–52288.
- Hong, M., Xu, L., Wang, F., Xu, S., Li, H., Li, C. Z., & Liu, J. (2016). In situ synthesized Au–Ag nanocages on graphene oxide nanosheets: a highly active and recyclable catalyst for the reduction of 4-nitrophenol. *New Journal of Chemistry*, 40, 1685-1692.
- Hsia, C. F., Madasu, M., & Huang, M. H. (2016). Aqueous phase synthesis of Au-Cu core-shell nanocubes and octahedra with tunable sizes and noncentrally located cores. *Chemistry of Materials*, 28, 3073-3079.
- Hu, J.-W., Zhang, Y., Li, J.-F., Liu, Z., Ren, B., Sun, S.-G., Tian, Z.-Q., & Lian, T. (2005). Synthesis of Au@Pd core-shell nanoparticles with controllable size and their application in surface-enhanced Raman spectroscopy. *Chemistry Physics Letter*, 408, 354-359.
- Huang, C. J., Chiu, P. H., Wang, Y. H., Chen, K. L., Linn, J. J., & Yang, C. F. (2006). Electrochemically controlling the size of gold nanoparticles. *Journal of the Electrochemical Society*, 153, D193-D198.
- Huang, H. H., Ni, X. P., Loy, G. L., Chew, C. H., Tan, K. L., Loh, F. C., Deng, J. F., & Xu, G. Q. (1996). Photochemical formation of silver nanoparticles in poly (N-vinylpyrrolidone). *Langmuir*, 12, 909-912.
- Huang, J., Li, Q., Sun, D., Lu, Y., Su, Y., Yang, X., Wang, H., Wang, Y., Shao, W., & He, N. (2007). Biosynthesis of silver and gold nanoparticles by novel sun dried *Cinnamomum camphora* leaf. *Nanotechnology*, 18, 105104.
- Huang, J., Vongehr, S., Tang, S., Lu, H., Shen, J., & Meng, X. (2009). Ag dendrite-based Au/Ag bimetallic nanostructures with strongly enhanced catalytic activity. *Langmuir*, 25, 11890-11896.
- Huo, S., Ma, H., Huang, K., Liu, J., Wei, T., Jin, S., Zhang, J., He, S. & Liang, X. J. (2013). Superior penetration and retention behavior of 50 nm gold nanoparticles in tumors. *Cancer research*, 73, 319-330.

- Iqbal, M., Chung, Y. I., & Tae, G. (2007). An enhanced synthesis of gold nanorods by the addition of Pluronic (F-127) via a seed mediated growth process. *Journal of Materials Chemistry*, 17, 335-342.
- Jana, N. R., Gearheart, L., & Murphy, C. J. (2001). Evidence for seed-mediated nucleation in the chemical reduction of gold salts to gold nanoparticles. *Chemistry of Materials*, 13, 2313-2322.
- Jana, N. R., Gearheart, L., & Murphy, C. J. (2001). Seed-mediated growth approach for shape-controlled synthesis of spheroidal and rod-like gold nanoparticles using a surfactant template. *Advanced Materials*, 13, 1389.
- Jayalakshmi, K., Ibrahim, M., & Rao, K. V. (2014). Effect of pH on the size of gold nanoparticles. *International Journal of Electronic and Electrical Engineering* 7, 159-64.
- Jeevanandam, J., Barhoum, A., Chan, Y. S., Dufresne, A., & Danquah, M. K. (2018). Review on nanoparticles and nanostructured materials: history, sources, toxicity and regulations. *Beilstein journal of nanotechnology*, 9, 1050-1074.
- Ji, X., Song, X., Li, J., Bai, Y., Yang, W., & Peng, X. (2007). Size control of gold nanocrystals in citrate reduction: the third role of citrate. *Journal of American Chemical Society*, 129, 13939-13948.
- Jin, R. C., Cao, Y. W., Mirkin, C. A., Kelly, K. L., Schatz, G. C., & Zheng, J. G. (2001). Photoinduced conversion of silver nanospheres to nanoprisms. *Sciences*, 294, 1901-1903.
- Kahraman, M., Aydın, Ö., & Çulha, M. (2009). Oligonucleotide-mediated Au–Ag core–shell nanoparticles. *Plasmonics*, 4, 293.
- Kalantari, K., Afifi, A. B. M., Bayat, S., Shameli, K., Yousefi, S., Mokhtar, N., & Kalantari, A. (2017). Heterogeneous catalysis in 4-nitrophenol degradation and antioxidant activities of silver nanoparticles embedded in Tapioca starch. *Arabian Journal of Chemistry*.
- Kamat, P. V., Flumiani, M., & Hartland, G. V. (1998). Picosecond dynamics of silver nanoclusters. *Journal of Physical Chemistry B*, 106, 7729.
- Kamat, P. V. (2002). Photophysical, photochemical and photocatalytic aspects of metal nanoparticles. *The Journal of Physical Chemistry B*, 106, 7729-7744.

- Kanatzidis, M. G. (1990). Polymeric electrical conductors. *Chemical and Engineering News*, 36.
- Karthik, R., Hou, Y. S., Chen, S. M., Elangovan, A., Ganesan, M., & Muthukrishnan, P. (2016). Eco-friendly synthesis of Ag-NPs using *Cerasus serrulata* plant extract-Its catalytic, electrochemical reduction of 4-NPh and antibacterial activity. *Journal of Industrial and Engineering Chemistry*, 37, 330-339.
- Khadzhiev, S. N. (2016). Nanoheterogeneous catalysis: Definition, state, and research prospects. *Petroleum Chemistry*, 56, 465-479.
- Khan, I., Saeed, K., & Khan, I. (2019). Nanoparticles: Properties, applications and toxicities. *Arabian journal of chemistry*, 12, 908-931.
- Khoshnamvand, M., Huo, C., & Liu, J. (2019). Silver nanoparticles synthesized using *Allium ampeloprasum* L. leaf extract: characterization and performance in catalytic reduction of 4-nitrophenol and antioxidant activity. *Journal of Molecular Structure*, 1175, 90-96.
- Kim, Y. H., Lee, D. K., & Kang, Y. S. (2005). Synthesis and characterization of Ag and Ag-SiO₂ nanoparticles. *Colloids and Surfaces A: Physicochemical and Engineering Aspects*, 257, 273-276.
- Kirubha, E., & Palanisamy, P. K. (2014). Green synthesis, characterization of Au-Ag core-shell nanoparticles using gripe water and their applications in nonlinear optics and surface enhanced Raman studies. *Advances in Natural Sciences: Nanoscience and Nanotechnology*, 5, 045006.
- Klabunde, K. J., Li, Y. X., & Tan, B. J. (1991). Solvated metal atom dispersed catalysts. *Chemistry of materials*, 3, 30-39.
- Knauer, A., Eisenhardt, A., Krischok, S., & Koehler, J. M. (2014). Nanometer precise adjustment of the silver shell thickness during automated Au-Ag core-shell nanoparticle synthesis in micro fluid segment sequences. *Nanoscale*, 6, 5230-5238.
- Ko, F. H., & Chang, Y. C. (2014). Aptamer based surface enhanced Raman scattering detection of adenosine using various core sizes of Au-Ag core-shell nanoparticles. *RSC Advances*, 4, 26251-26257.

- Konar, S., Kalita, H., Puvvada, N., Tantubay, S., Mahto, M. K., Biswas, S., & Pathak, A. (2016). Shape-dependent catalytic activity of CuO nanostructures. *Journal of catalysis*, 336, 11-22.
- Kong, X., Zhu, H., Chen, C., Huang, G., & Chen, Q. (2017). Insights into the reduction of 4-nitrophenol to 4-aminophenol on catalysts. *Chemical Physics Letters*, 684, 148-152.
- Krishnamurthy, S., Esterle, A., Sharma, N. C., Sahi., & S.V. (2014). Yucca-derived synthesis of gold nanomaterial and their catalytic potential. *Nanoscale Research Letter*, 9, 627.
- Kumar, S., Upadhyay, S. N., & Upadhya, Y.D. (1987). Removal of phenols by adsorption on fly ash. *Journal of Chemical Technology and Biotechnology*, 37, 281-290.
- Kumar, V., & Yadav, S. K. (2009). Plant-mediated synthesis of silver and gold nanoparticles and their applications. *Journal of chemical Technology and Biotechnology*, 84, 151-157.
- Kumari, M. M., Jacob, J., & Philip, D. (2015). Green synthesis and applications of Au–Ag bimetallic nanoparticles. *SpectrochimicaActa Part A: Molecular and Biomolecular Spectroscopy*, 137, 185-192.
- Kumari, M., Mishra, A., Pandey, S., Singh, S. P., Chaudhry, V., Mudiam, M. K. R., Shukla, S., Kakkar, P., & Nautiyal, C. S. (2016). Physico-chemical condition optimization during biosynthesis lead to development of improved and catalytically efficient gold nanoparticles. *Scientific reports*, 6.
- Kurihara, L. K., Chow, G. M., & Schoen, P. E. (1995). Nanocrystalline metallic powders and films produced by the polyol method. *Nanostructured Materials*, 5, 607-613.
- Lee, P. C., & Meisel, D. (1982). Adsorption and Surface Enhanced Raman of Dyes on Silver and Gold Sols. *Journal Physics Chemistry*, 86, 3391.
- Li, C. F., Li, D. X., Wan, G. Q., Xu, J. & Hou, W. G. (2011). Facile synthesis of concentrated gold nanoparticles with low size-distribution in water: temperature and pH controls. *Nanoscale Research Letters*, 6, 1440.
- Li, Y., Tang, Z., Prasad, P. N., Knecht, M. R., & Swihart, M. T. (2014). Peptide-mediated synthesis of gold nanoparticles: effects of peptide sequence and nature of binding on physicochemical properties. *Nanoscale*, 6, 3165-3172.

- Li, Y., Wang, Q., Zhou, X., Wen, C. Y., Yu, J., Han, X., Li, X., Yan, Z.F., & Zeng, J. (2016). A convenient colorimetric method for sensitive and specific detection of cyanide using Ag@Au core-shell nanoparticles. *Sensors and Actuators B: Chemical*, 228, 366-372.
- Liang, M., Wang, L., Su, R., Qi, W., Wang, M., Yu, Y., & He, Z. (2013). Synthesis of silver nanoparticles within cross-linked lysozyme crystals as recyclable catalysts for 4-nitrophenol reduction. *Catalysis Science & Technology*, 3, 1910-1914.
- Lin, F. H., & Doong, R. A. (2014). Highly efficient reduction of 4-nitrophenol by heterostructured gold-magnetite nanocatalysts. *Applied Catalysis A: General* 486, 486, 32-41.
- Liu, R., Guo, J., Ma, G., Jiang, P., Zhang, D., Li, D., Chen, L., Guo, Y., & Ge, G. (2016). Alloyed crystalline Au-Ag hollow nanostructures with high chemical stability and catalytic performance. *ACS applied materials & interfaces*, 8, 16833-16844.
- Liu, Y., Zhou, J., Wang, B., Jiang, T., Ho, H. P., Petti, L., & Mormile, P. (2015). Au@Ag core-shell nanocubes: epitaxial growth synthesis and surface-enhanced Raman scattering performance. *Physical Chemistry Chemical Physics*, 17, 6819-6826.
- Lou, X. W. D., Archer, L. A., & Yang, Z. (2008). Hollow micro-nanostructures: Synthesis and applications. *Advanced Materials*, 20, 3987-4019.
- Lu, L., Burkey, G., Halaciuga, I., & Goia, D. V. (2013). Core-shell gold/silver nanoparticles: Synthesis and optical properties. *Journal of colloid and interface science*, 392, 90-95.
- Luo, J., Zhang, N., Liu, R., & Liu, X. (2014). In situ green synthesis of Au nanoparticles onto polydopamine-functionalized graphene for catalytic reduction of nitrophenol. *RSC Advances*, 4, 64816-64824.
- Mahmud, S., Satter, S. S., Singh, A. K., Rahman, M. M., Mollah, M. Y. A., & Susan, M. A. B. H. (2019). Tailored Engineering of Bimetallic Plasmonic Au@Ag Core@Shell Nanoparticles. *ACS omega*, 4, 18061-18075.
- Maillard, M., Giorgio, S., & Pileni, M. P. (2002). Silver Nanodisks. *Advance Materials*, 14, 1084-1086.
- McGilvray, K. L., Fasciani, C., Bueno-Alejo, C. J., Schwartz-Narbonne, R., Scaiano, J. C. (2012). Photochemical strategies for the seed-mediated growth of gold and gold-silver nanoparticles. *Langmuir*, 28, 16148-16155.

- Mechler, A., Torriero, A. A., Nafady, A., Lee, C. Y., Bond, A. M., O'Mullane, A. P., & Bhargava, S. K. (2010). The formation of gold nanoparticles using hydroquinone as a reducing agent through a localized pH change upon addition of NaOH to a solution of H₂AuCl₄. *Colloids and Surfaces A: Physicochemical and Engineering Aspects*, 370, 35-41.
- Mohamed, M. B., Wang, Z. L., & El-Sayed, M. A. (1999). Temperature-dependent size-controlled nucleation and growth of gold nanoclusters. *The Journal of Physical Chemistry A*, 103, 10255-10259.
- Monga, A., & Pal, B. (2015). Improved catalytic activity and surface electro-kinetics of bimetallic Au-Ag core-shell nanocomposites. *New Journal of Chemistry*, 39, 304-313.
- Mott, D., Thuy, N. T., Aoki, Y., & Maenosono, S. (2010). Aqueous synthesis and characterization of Ag and Ag–Au nanoparticles: addressing challenges in size, monodispersity and structure. *Philosophical Transactions of the Royal Society of London A: Mathematical, Physical and Engineering Sciences*, 368, 4275-4292.
- Nabid, M. R., Bide, Y., Shojaipour, M., & Dastar, F. (2016). Yolk/Shell AuNPs@ Polyethyleneimine-Derived Carbon Nanoparticles as Nanoreactor for Catalytic Nitroarenes Reduction. *Catalysis Letters*, 146, 229-237.
- Nasrollahzadeh, M., Sajadi, S. M., Rostami-Vartooni, A., & Hussin, S. M. (2016). Green synthesis of CuO nanoparticles using aqueous extract of *Thymus vulgaris* L. leaves and their catalytic performance for N-arylation of indoles and amines. *Journal of colloid and interface science*, 466, 113-119.
- Nikoobakht, B., & El-Sayed, M. A. (2003). Preparation and growth mechanism of gold nanorods (NRs) using seed-mediated growth method. *Chemistry of Materials*, 15, 1957-1962.
- Noruzi, M., Zare, D., & Davoodi, D. (2012). A rapid biosynthesis route for the preparation of gold nanoparticles by aqueous extract of cypress leaves at room temperature. *SpectrochimicaActa Part A: Molecular and Biomolecular Spectroscopy*, 94, 84-88.
- Paik, P. (2013). Recent advancement in functional core-shell nanoparticles of polymers: synthesis, physical properties, and applications in medical biotechnology. *Journal of Nanoparticles*, 2013.

- Pande, S., Ghosh, S. K., Praharaj, S., Panigrahi, S., Basu, S., Jana, S., Pal, A., Tsukuda, T., & Pal, T. (2007). Synthesis of normal and inverted gold-silver core-shell architectures in β -cyclodextrin and their applications in SERS. *The Journal of Physical Chemistry C*, 111, 10806-10813.
- Park, G., Seo, D., Jung, J., Ryu, S., & Song, H. (2011). Shape evolution and gram-scale synthesis of Gold@Silver Core-shell Nanopolyhedrons. *Journal Physics Chemistry C*, 115, 9417-9423.
- Patra, J. K., & Baek, K. H. (2015). Novel green synthesis of gold nanoparticles using *Citrullus lanatus* rind and investigation of proteasome inhibitory activity, antibacterial, and antioxidant potential. *International journal of Nanomedicine*, 10, 7253.
- Pérez-Juste, J., Pastoriza-Santos, I., Liz-Marzán, L. M., & Mulvaney, P. (2005). Gold nanorods: synthesis, characterization and applications. *Coordination Chemistry Reviews*, 249, 1870-1901.
- Pittaway, F., Paz-Borbón, L. O., Johnston, R. L., Arslan, H., Ferrando, R., Mottet, C., Barcaro, G., & Fortunelli, A. (2009). Theoretical studies of palladium-gold nanoclusters: Pd-Au clusters with up to 50 atoms. *The Journal of Physical Chemistry C*, 113, 9141-9152.
- Polte, J. (2015). Fundamental growth principles of colloidal metal nanoparticles—a new perspective. *CrystEngComm*, 17, 6809-6830.
- Praharaj, S., Nath, S., Ghosh, S. K., Kundu, S., & Pal, T. (2004). Immobilization and recovery of Au nanoparticles from anion exchange resin: resin-bound nanoparticle matrix as a catalyst for the reduction of 4-nitrophenol. *Langmuir*, 20, 9889-9892.
- Premkumar, T., Lee, K., & Geckeler, K. E. (2011). Shape-tailoring and catalytic function of anisotropic gold nanostructures. *Nanoscale Research Letters*, 6, 547.
- Ranoszek-Soliwoda, K., Tomaszewska, E., Socha, E., Krzyczmonik, P., Ignaczak, A., Orłowski, P., Krzyzowska, M., Celichowski, G., & Grobelny, J. (2017). The role of tannic acid and sodium citrate in the synthesis of silver nanoparticles. *Journal of Nanoparticle Research*, 19, 273.
- Rashid, M. U., Bhuiyan, M. K. H., & Quayum, M. E. (2013). Synthesis of silver nanoparticles (Ag-NPs) and their uses for quantitative analysis of vitamin C tablets. *Dhaka University Journal of Pharmaceutical Sciences*, 12, 29-33.

- Rath, P. C., Saikia, D., Mishra, M., & Kao, H. M. (2018). Exceptional catalytic performance of ultrafine Cu₂O nanoparticles confined in cubic mesoporous carbon for 4-nitrophenol reduction. *Applied Surface Science*, 427, 1217-1226.
- Rather, J. A., Khudaish, E. A., Munam, A., Qurashi, A., & Kannan, P. (2016). Electrochemically reduced fullerene–graphene oxide interface for swift detection of Parkinsons disease biomarkers. *Sensor Actuators B*, 237, 672–684.
- Raza, M. A., Kanwal, Z., Rauf, A., Sabri, A. N., Riaz, S., & Naseem, S. (2016). Size- and shape-dependent antibacterial studies of silver nanoparticles synthesized by wet chemical routes. *Nanomaterials*, 6, 74.
- Revathy, T. A., Dhanavel, S., Sivaranjani, T., Narayanan, V., Maiyalagan, T., & Stephen, A. (2018). Highly active graphene-supported palladium-nickel alloy nanoparticles for catalytic reduction of 4-nitrophenol. *Applied Surface Science*, 449, 764-771.
- Rodríguez-González, B., Burrows, A., Watanabe, M., Kiely, C. J., & Marzán, L. M. L. (2005). Multishell bimetallic AuAg nanoparticles: synthesis, structure and optical properties. *Journal of Materials Chemistry*, 15, 1755-1759.
- Rosi, N. L., & Mirkin, C. A. (2005). Nanostructures in Biodiagnostics. *Chemical Review*, 105, 1547.
- Rossi, G., Rapallo, A., Mottet, C., Fortunelli, A., Baletto, F., & Ferrando, R. (2004). Magic polyicosahedral core-shell clusters. *Physical Review Letters*, 93, 105503.
- Saha, S., Pal, A., Kundu, S., Basu, S., & Pal, T. (2009). Photochemical green synthesis of calcium-alginate-stabilized Ag and Au nanoparticles and their catalytic application to 4-nitrophenol reduction. *Langmuir*, 26, 2885-2893.
- Salcedo, A. R. M., & Sevilla III, F. B. (2013). Citrate-capped gold nanoparticles as colorimetric reagent for copper (II) ions. *Philippines Science Letters*, 6, 90-96.
- Samal, A. K., Polavarapu, L., Rodal-Cedeira, S., Liz-Marzán, L. M., Pérez-Juste, J., & Pastoriza-Santos, I. (2013). Size Tunable Au@Ag core-shell nanoparticles: synthesis and surface-enhanced Raman scattering properties. *Langmuir*, 29, 15076-15082.
- Sanyal, U., Davis, D. T., & Jagirdar, B. R. (2013). Bimetallic core-shell nanocomposites using weak reducing agent and their transformation to alloy nanostructures. *Dalton Transactions*, 42, 7147-7157.

- Sareen, S., Mutreja, V., Pal, B., & Singh, S. (2018). Synthesis of bimetallic Au-Ag alloyed mesocomposites and their catalytic activity for the reduction of nitroaromatics. *Applied Surface Science*, 435, 552-562.
- Sarmah, P., Deka, P., & Bharali, P. (2013). Catalytic reduction of 4-nitrophenol to 4-aminophenol over CuNi alloy particles: Synthesis, characterization and application. *Bulletin of the Catalysis Society of India*, 12, 54-59.
- Seo, Y. S., Ahn, E. Y., Park, J., Kim, T. Y., Hong, J. E., Kim, K., Park, Y., & Park, Y. (2017). Catalytic reduction of 4-nitrophenol with gold nanoparticles synthesized by caffeic acid. *Nanoscale Research Letters*, 12, 7.
- Shaabani, A., Hezarkhani, Z., & Nejad, M. K. (2016). AuCu and AgCu bimetallic nanoparticles supported on guanidine-modified reduced graphene oxide nanosheets as catalysts in the reduction of nitroarenes: tandem synthesis of benzo [b][1,4] diazepine derivatives. *RSC advances*, 6, 30247-30257.
- Shankar, C., Dao, A. T., Singh, P., Higashimine, K., Mott, D. M., & Maenosono, S. (2012). Chemical stabilization of gold coated by silver core-shell nanoparticles via electron transfer. *Nanotechnology*, 23, 245704.
- Sharma, G., Kumar, A., Sharma, S., Naushad, M., Dwivedi, R. P., AlOthman, Z. A., & Mola, G. T. (2017). Novel development of nanoparticles to bimetallic nanoparticles and their composites: A review. *Journal of King Saud University-Science*.
- Shen, X., Zhu, L., Liu, G., Yu, H., & Tang, H. (2008). Enhanced photocatalytic degradation and selective removal of nitrophenols by using surface molecular imprinted titania. *Environmental Science & Technology*, 42, 1687-1692.
- Shore, M. S., Wang, J., Johnston-Peck, A. C., Oldenburg, A. L., & Tracy, J. B. (2011). Synthesis of Au (core)/Ag (shell) nanoparticles and their conversion to AuAg alloy nanoparticles. *Small*, 7, 230-234.
- Shmarakov, I., Mukha, I., Vityuk, N., Borschovetska, V., Zhyshchynska, N., Grodzyuk, G., & Eremenko, A. (2017). Antitumor activity of alloy and core-shell-type bimetallic AgAu nanoparticles. *Nanoscale research letters*, 12, 333.
- Shrestha, S., Wang, B., & Dutta, P. (2020). Nanoparticle processing: Understanding and controlling aggregation. *Advances in Colloid and Interface Science*, 102162.

- Shukri, G. N. W., Bidin, N., Islam, S., & Krishnan, G. (2018). Synthesis of Au-Ag Alloy Nanoparticles in Deionized Water by Pulsed Laser Ablation Technique. *Journal Nanoscience Nanotechnology*, 11, 4841-4851.
- Singh, P., Kim, Y. J., Zhang, D., & Yang, D. C. (2016). Biological synthesis of nanoparticles from plants and microorganisms. *Trends in biotechnology*, 34, 588-599.
- Somorjai, G. A. (1978). Active sites for hydrocarbon catalysis on metal surfaces. *Pure and Applied Chemistry*, 50, 963.
- Song, L., Mao, K., Zhou, X., & Hu, J. (2016). A novel biosensor based on Au@ Ag core-shell nanoparticles for SERS detection of arsenic (III). *Talanta*, 146, 285-290.
- Srinoi, P., Chen, Y. T., Vittur, V., Marquez, M., & Lee, T. (2018). Bimetallic nanoparticles: Enhanced magnetic and optical properties for emerging biological applications. *Applied Sciences*, 8, 1106.
- Srnova-Sloufova, I., Lednický, F., Gemperle, A., & Gemperlova, J. (2000). Core-Shell (Ag)Au bimetallic nanoparticles: Analysis of transmission electron microscopy images. *Langmuir*, 16, 9928-9935.
- Stewart, P. L. (2017). Cryo-electron microscopy and cryo-electron tomography of nanoparticles. *Wiley Interdisciplinary Reviews: Nanomedicine and Nanobiotechnology*, 9(2), e1417.
- Sudha, P. N., Sangeetha, K., Vijayalakshmi, K., & Barhoum, A. (2018). Nanomaterials history, classification, unique properties, production and market. In *Emerging Applications of Nanoparticles and Architecture Nanostructures Elsevier*, 341-384.
- Sun, J., Fu, Y., He, G., Sun, X., & Wang, X. (2014). Catalytic hydrogenation of nitrophenols and nitrotoluenes over a palladium/graphene nanocomposite. *Catalysis Science & Technology*, 4, 1742-1748.
- Sun, L., Lv, P., Li, H., Wang, F., Su, W., & Zhang, L. (2018). One-step synthesis of Au-Ag alloy nanoparticles using soluble starch and their photocatalytic performance for 4-nitrophenol degradation. *Journal of Materials Science*, 53, 15895-15906.
- Sun, Y., & Li, T. (2018). Composition-tunable hollow Au/Ag SERS nanoprobe coupled with target-catalyzed hairpin assembly for triple-amplification detection of miRNA. *Analytical chemistry*, 90, 11614-11621.

- Suwannarat, K., Thongthai, K., Ananta, S., & Srisombat, L. (2018). Synthesis of hollow trimetallic Ag/Au/Pd nanoparticles for reduction of 4-nitrophenol. *Colloids and Surfaces A: Physicochemical and Engineering Aspects*, 540, 73-80.
- Tan, N. P. B., Lee, C. H., & Li, P. (2016). Green synthesis of smart metal/polymer nanocomposite particles and their tuneable catalytic activities. *Polymers*, 8, 105.
- Tan, S. F., Chee, S. W., Lin, G., Bosman, M., Lin, M., Mirsaidov, U., & Nijhuis, C. A. (2016). Real-Time Imaging of the Formation of Au–Ag Core-Shell Nanoparticles. *Journal of the American Chemical Society*, 138, 5190-5193.
- Tang, L., Tang, J., Zeng, G., Yang, G., Xie, X., Zhou, Y., Pang, Y., Fang, Y., Wang, J., & Xiong, W. (2015). Rapid reductive degradation of aqueous p-nitrophenol using nanoscale zero-valent iron particles immobilized on mesoporous silica with enhanced antioxidation effect. *Applied Surface Science*, 333, 220-228.
- Tanori, J., Vargas-Hernández, D., Martínez-Barbosa, E., Borja-Urby, R., García-Bórquez, A., Arenas-Alatorre, J., & Maldonado, A. (2016). AuCu, AgCu and AuAg bimetallic nanoparticles: Synthesis, characterization and water remediation. *MRS Advances*, 1, 2525-2530.
- Tessier, P. M., Velev, O. D., Kalambur, A. T., Rabolt, J. F., Lenhoff, A. M., & Kaler, E. W. (2000). Assembly of gold nanostructured films templated by colloidal crystals and use in surface-enhanced Raman spectroscopy. *Journal of American Chemical Society*, 122, 9554.
- Tojo, C., & Vila-Romeu, N. (2014). Kinetic Study on the Formation of Bimetallic Core-Shell Nanoparticles via Microemulsions. *Materials*, 7, 7513-7532.
- Tsuji, M., Hikino, S., Tanabe, R., & Yamaguchi, D. (2010). Synthesis of Ag@Cu Core-Shell Nanoparticles in High Yield Using a Polyol Method. *Chemistry Letters*, 39, 334-336.
- Tsuji, M., Miyamae, N., Lim, S., Kimura, K., Zhang, X., Hikino, S., & Nishio, M. (2006). Crystal structures and growth mechanisms of Au@Ag core-shell nanoparticles prepared by the microwave-polyol method. *Crystal Growth & Design*, 6, 1801-1807.
- Tuo, Y., Liu, G., Dong, B., Yu, H., Zhou, J., Wang, J., & Jin, R. (2017). Microbial synthesis of bimetallic PdPt nanoparticles for catalytic reduction of 4-nitrophenol. *Environmental Science and Pollution Research*, 24, 5249-5258.

- Tyagi, H., Kushwaha, A., Kumar, A., & Aslam, M. (2011). pH-dependent synthesis of stabilized gold nanoparticles using ascorbic acid. *International Journal of Nanoscience*, 10, 857-860.
- Tyagi, H., Kushwaha, A., Kumar, A., & Aslam, M. (2016). A facile pH controlled citrate-based reduction method for gold nanoparticle synthesis at room temperature. *Nanoscale Research Letters*, 11, 362.
- Udapudi, B., Naik, P., Savadatti, S.T., Sharma, R., & Balgi, S., (2013). Synthesis and Characterization of Silver Nanoparticles. *International Journal of Pharmacy and Biological Sciences*, 3, 10-14.
- Valdez, J., & Gómez, I. (2016). One-Step Green Synthesis of Metallic Nanoparticles Using Sodium Alginate. *Journal of Nanomaterials*, 2016, 33.
- Wang, C., Tian, W., Ding, Y., Ma, Y.-Q., Wang, Z. L., Markovic, N. M., Stamenkovic, V. R., Daimon, H., & Sun, S. (2010). Rational synthesis of heterostructured nanoparticles with morphology control. *Journal America Chemistry Society*, 132, 6524-6529.
- Wang, Y., & Xia, Y. (2004). Bottom-up and top-down approaches to the synthesis of monodispersed spherical colloids of low melting-point metals. *Nano letters*, 4, 2047-2050.
- Wang, R., Yao, Y., Shen, M., & Wang, X. (2016). Green synthesis of Au@Ag nanostructures through a seed-mediated method and their application in SERS. *Colloids and Surfaces A: Physicochemical and Engineering Aspects*, 492, 263-272.
- Wang, Y., Zhang, P., Mao, X., Fu, W., & Liu, C. (2016). Seed-mediated growth of bimetallic nanoparticles as an effective strategy for sensitive detection of vitamin C. *Sensors and Actuators B: Chemical*, 231, 95-101.
- Wu, T., Zhang, L., Gao, J., Liu, Y., Gao, C., & J. Yan. (2013). Fabrication of graphene oxide decorated with Au-Ag alloy nanoparticles and its superior catalytic performance for the reduction of 4-nitrophenol. *Journal Materials Chemistry A*, 1, 7384-7390.
- Xia, B., He, F., & L. Li. (2013). Preparation of bimetallic nanoparticles using a facile green synthesis method and their application. *Langmuir*, 29, 4901-4907.

- Xin, J., Yin, X., Chen, S., & Wu, A. (2014). Synthesis of uniform and stable silver nanoparticles by a gold seed-mediated growth approach in a buffer system. *Journal of Experimental Nanoscience*, 9, 382-390.
- Xu, S., Zhao, B., Xu, W., & Fan, Y. (2005). Preparation of Au–Ag core shell nanoparticles and application of bimetallic sandwich in surface-enhanced Raman scattering (SERS). *Colloids and Surfaces A: Physicochemical and Engineering Aspects*, 257, 313-317.
- Yang, M. Q., Pan, X., Zhang, N., & Xu, Y. J. (2013). A facile one-step way to anchor noble metal (Au, Ag, Pd) nanoparticles on a reduced graphene oxide mat with catalytic activity for selective reduction of nitroaromatic compounds. *CrystEngComm*, 15, 6819-6828.
- Yang, Y., Matsubara, S., Nogami, M., Shi, J., & Huang, W. (2006). One-dimensional self-assembly of gold nanoparticles for tunable surface plasmon resonance properties. *Nanotechnology*, 17, 2821.
- Yang, Y., Shi, J., Kawamura, G., & Nogami, M. (2008). Preparation of Au-Ag, Ag-Au core-shell bimetallic nanoparticles for surface-enhanced Raman scattering. *ScriptaMaterialia*, 58, 862-865.
- Yaseen, T., Pu, H., & Sun, D. W. (2019). Effects of ions on core-shell bimetallic Au@Ag NPs for rapid detection of phosalone residues in peach by SERS. *Food Analytical Methods*, 12, 2094-2105.
- You, J. G., Shanmugam, C., Liu, Y. W., Yu, C. J., & Tseng, W. L. (2017). Boosting catalytic activity of metal nanoparticles for 4-nitrophenol reduction: Modification of metal nanoparticles with poly (diallyldimethylammonium chloride). *Journal of Hazardous Materials*, 324, 420-427.
- You, L., Mao, Y., & Ge, J. (2012). Synthesis of stable SiO₂@Au-nanoring colloids as recyclable catalysts: galvanic replacement taking place on the surface. *The Journal of Physical Chemistry C*, 116, 10753-10759.
- Yuan, P., Ma, R., Gao, N., Garai, M., & Xu, Q. H. (2015). Plasmon coupling-enhanced two-photon photoluminescence of Au@Ag core-shell nanoparticles and applications in the nuclease assay. *Nanoscale*, 7, 10233-10239.
- Zelekew, O. A., & Kuo, D. H. (2016). A two-oxide nanodiode system made of double-layered p-type Ag₂O@n-type TiO₂ for rapid reduction of 4-nitrophenol. *Physical Chemistry Chemical Physics*, 18, 4405-4414.

- Zeng, J., Cao, Y., Lu, C. H., Wang, X. D., Wang, Q., Wen, C. Y., Qu, J.B., Yuan, C., Yan, Z.F., & Chen, X. (2015). A colorimetric assay for measuring iodide using Au@Ag core-shell nanoparticles coupled with Cu²⁺. *Analytica chimica acta*, 891, 269-276.
- Zhang, H., Okumura, M., & Toshima, N. (2011). Stable dispersions of PVP-protected Au/Pt/Ag trimetallic nanoparticles as highly active colloidal catalysts for aerobic glucose oxidation. *The Journal of Physical Chemistry C*, 115, 14883-14891.
- Zhang, H., & Toshima, N. (2012). Fabrication of catalytically active AgAu bimetallic nanoparticles by physical mixture of small Au clusters with Ag ions. *Applied Catalysis A: General*, 447, 81-88.
- Zhang, J., Tanha, J., Hirama, T., Khieu, N. H., To, R., Tong-Sevinc, H., Stone, E., Brisson, J.R., & MacKenzie, C. R. (2004). Pentamerization of single-domain antibodies from phage libraries: a novel strategy for the rapid generation of high-avidity antibody reagents. *Journal of Molecular Biology*, 335, 49-56.
- Zhang, J., Xu, X., Yang, C., Yang, F., & Yang, X. (2011). Colorimetric iodide recognition and sensing by citrate-stabilized core/shell Cu@Au nanoparticles. *Analytical chemistry*, 83, 3911-3917.
- Zhang, L., Xie, Z., & Gong, J. (2016). Shape-controlled synthesis of Au-Pd bimetallic nanocrystals for catalytic applications. *Chemistry Society Reviews*, 45, 3916-3934.
- Zhang, N., Chen, F., Wu, X., Wang, Q., Qaseem, A., & Xia, Z. (2017). The activity origin of core-shell and alloy AgCu bimetallic nanoparticles for the oxygen reduction reaction. *Journal of Materials Chemistry A*, 5, 7043-7054.
- Zhang, Q., Xie, J., Yu, Y., Lee, J. Y. (2012). Monodispersity control in the synthesis of monometallic and bimetallic quasi-spherical gold and silver nanoparticles. *Nanoscale*, 2, 1962-1975.
- Zhang, W. S., Cao, J. T., Dong, Y. X., Wang, H., Ma, S. H., & Liu, Y. M. (2018). Enhanced chemiluminescence by Au-Ag core-shell nanoparticles: A general and practical biosensing platform for tumor marker detection. *Journal of Luminescence*, 201, 163-169.
- Zhang, Y., Deng, D., Zhu, X., Liu, S., Zhu, Y., Han, L., & Luo, L. (2018). Electrospun bimetallic Au-Ag/Co₃O₄ nanofibers for sensitive detection of hydrogen peroxide released from human cancer cells. *Analytica chimica acta*, 1042, 20-28.

- Zhang, Y., Yang, M., Portney, N. G., Cui, D., Budak, G., Ozbay, E., Ozkan, M., & Ozkan, C. S. (2008). Zeta potential: a surface electrical characteristic to probe the interaction of nanoparticles with normal and cancer human breast epithelial cells. *Biomedical Microdevices*, 10, 321-328.
- Zhao, Z., Ma, X., Wang, X., Ma, Y., Liu, C., Hang, H., Zhang, Y., Du, Y., & Ye, W. (2018). Synthesis of amorphous PdP nanoparticles supported on carbon nanospheres for 4-nitrophenol reduction in environmental applications. *Applied Surface Science*, 457, 1009-1017.
- Zhu, X. Y., Lv, Z. S., Feng, J. J., Yuan, P. X., Zhang, L., Chen, J. R., & Wang, A. J. (2018). Controlled fabrication of well-dispersed AgPd nanoclusters supported on reduced graphene oxide with highly enhanced catalytic properties towards 4-nitrophenol reduction. *Journal of colloid and interface science*, 516, 355-363.
- Zong, S., Wang, Z., Yang, J., Wang, C., Xu, S., & Cui, Y. (2012). A SERS and fluorescence dual mode cancer cell targeting probe based on silica coated Au@Ag core-shell nanorods. *Talanta*, 97, 368-375.

Internet References

<https://pubchem.ncbi.nlm.nih.gov/compound/4-Nitrophenol#section=Top>

LIST OF PUBLICATIONS

1. Nurafaliana Berahim, Wan Jeffrey Basirun, Bey Fen Leo, “Synthesis of Bimetallic Gold-Silver (Au-Ag) Nanoparticles for the Catalytic Reduction of 4-Nitrophenol to 4-Aminophenol”, *Catalysts*, 8 (2018) 412.

University of Malaya